2016

Thermodynamics and Kinetics of the Three-Way Junction of Phi29 Motor pRNA and its Assembly into Nanoparticles for Therapeutic Delivery to Prostate Cancer

Daniel W. Binzel
University of Kentucky, daniel.binzel@uky.edu
Digital Object Identifier: http://dx.doi.org/10.13023/ETD.2016.051

STUDENT AGREEMENT:

I represent that my thesis or dissertation and abstract are my original work. Proper attribution has been given to all outside sources. I understand that I am solely responsible for obtaining any needed copyright permissions. I have obtained needed written permission statement(s) from the owner(s) of each third-party copyrighted matter to be included in my work, allowing electronic distribution (if such use is not permitted by the fair use doctrine) which will be submitted to UKnowledge as Additional File.

I hereby grant to The University of Kentucky and its agents the irrevocable, non-exclusive, and royalty-free license to archive and make accessible my work in whole or in part in all forms of media, now or hereafter known. I agree that the document mentioned above may be made available immediately for worldwide access unless an embargo applies.

I retain all other ownership rights to the copyright of my work. I also retain the right to use in future works (such as articles or books) all or part of my work. I understand that I am free to register the copyright to my work.

REVIEW, APPROVAL AND ACCEPTANCE

The document mentioned above has been reviewed and accepted by the student's advisor, on behalf of the advisory committee, and by the Director of Graduate Studies (DGS), on behalf of the program; we verify that this is the final, approved version of the student's thesis including all changes required by the advisory committee. The undersigned agree to abide by the statements above.

Daniel W. Binzel, Student

Dr. Peixuan Guo, Major Professor

Dr. Jim Pauly, Director of Graduate Studies

THERMODYNAMICS AND KINETICS OF THE THREE-WAY JUNCTION OF PHI29 MOTOR PRNA AND ITS ASSEMBLY INTO NANOPARTICLES FOR THERAPEUTIC DELIVERY TO PROSTATE CANCER

DISSERTATION

A dissertation submitted in partial fulfillment of the requirements for the degree of Doctor of Philosophy in the College of Pharmacy at the University of Kentucky

By

Daniel William Binzel

Lexington, Kentucky

Co-Directors: Dr. Peixuan Guo, Professor of Pharmaceutical Sciences

and Dr. Linda Dwoskin, Professor of Pharmaceutical Sciences

Lexington, Kentucky

2016

ABSTRACT OF DISSERTATION

THERMODYNAMICS AND KINETICS OF THE THREE-WAY JUNCTION OF PHI29 MOTOR PRNA AND ITS ASSEMBLY INTO NANOPARTICLES FOR THERAPEUTIC DELIVERY TO PROSTATE CANCER

The emerging field of RNA nanotechnology necessitates creation of functional RNA nanoparticles, but has been limited by particle instability. Previously, it was found the three-way junction (3WJ) of the Phi29 DNA packaging motor pRNA was found to be ultra-stable and assemble in solution without the presence of metal ions. The three-way junction is composed of three short oligo RNA strands and proven to be thermodynamically stable. Here the assembly mechanism, thermodynamic and enzymatic stabilities, and kinetics are examined in order to understand the stability behind this unique motif. Thermodynamic and kinetics studies found that the pRNA 3WJ formed out of three components at a rapid rate creating a single-step three component collision with a lack of dimer intermediate formation while being governed by entropy, instead of the commonly seen enthalpy. Furthermore, the pRNA 3WJ proved to be stable at temperatures above 50 °C, concentrations below 100 pM, and produced a free energy of formation well below other studied RNA structures and motifs. With the high stability and folding efficiency of the pRNA 3WJ, it serves as an ideal platform for multi-branched RNA nanoparticles constructed through bottom-up techniques. RNA nanoparticles were constructed for the specific targeting of prostate cancer cells expressing Prostate Specific Membrane Antigen (PSMA) by receptor mediated endocytosis through the addition of an RNA aptamer; and the delivery of anti-miRNA sequences for gene regulation. The resulting nanoparticles remained stable while showing highly specific binding and entry in PSMA positive cells through cell surface receptor endocytosis. Furthermore, the entry of the nanoparticles allowed for the knockdown of against onco-miRNAs. Nanoparticles harboring anti-miRNAs led to the upregulation of tumor suppressor genes, and signaling of apoptotic pathways. These findings display RNA nanotechnology can result in the production of stable nanoparticles and result in the specific treatment of cancers, specifically prostate cancer.

KEYWORDS: RNA Nanotechnology, Phi29 Packaging Motor, Thermodynamics, Kinetics, Prostate Cancer

Daniel William Binzel
Student's Signature

Date

THERMODYNAMICS AND KINETICS OF THE THREE-WAY JUNCTION OF PHI29 MOTOR PRNA AND ITS ASSEMBLY INTO NANOPARTICLES FOR THERAPEUTIC DELIVERY TO PROSTATE CANCER

By

Daniel William Binzel

Dr. Peixuan Guo
Director of Dissertation

Dr. Linda Dwoskin
Co-Director of Dissertation

Dr. James Pauly
Director of Graduate Studies

Date

To my parents and family for their continued support

ACKNOWLEDGMENTS

Firstly, I would like to thank my thesis advisor, Dr. Peixuan Guo, for his continual support and guidance throughout my PhD studies. I would like to thank Dr. Guo for providing the opportunity to study in such a well-developed laboratory, working in the intriguing research. Secondly, I sincerely appreciate Dr. Guo's mentoring through my research, and providing invaluable advice, experience, and guidance.

Additionally, I would like to thank my committee members, Dr. Linda Dwoskin, Dr. Jurgen Rohr, and Dr. Kimberly Anderson. Their advice, help and assistance through my research, qualifying exam, and dissertation defense. Their instruction through my graduate studies proved indispensable in all aspects of my graduate work.

Furthermore, I would like to thank the Cancer Nanotechnology Training Center at the University of Kentucky for the opportunity to participate in the center and gain valuable knowledge and insight in my cancer related research. Special thanks to Dr. William St. Clair, Dr. Brad Anderson, Dr. Thomas Dziubla, and Dr. Robert Yokel for their insight into my research project and Tonya Vance for her help throughout my traineeship. As part of the CNTC, I gained experience and knowledge that would otherwise not have be available to my research and scientific career.

I would like to thank the members, past and present, of the Peixuan Guo laboratory, as their willingness to share their experience and knowledge in the field proved to be fundamental developing my research and scientific career. I would like to give special thanks to Dr. Farzin Haque, Dr. Yi Shu, Dr. Randall Reif, Dr. Emil Khisamutdinov and Dr. Mario Vieweger for their training and valuable insight in my experiments and data throughout my research. I would have not made it through this endeavor without their assistance and kindness. Additionally, I would like to thank all past and present members

of the Guo laboratory; Dr. Dan Shu, Dr. Hui Zhang, Dr. Ashwani Sharma, Dr. Mario Vieweger, Dr. Taek Lee, Dr. Mathieu Cinier, Dr. Zhanxi Hao, Dr. Peng Jing, Dr. Chad Schwartz, Dr. Gian Marco De Donatis, Dr. Mehdi Rajabi, Dr. Reza Zadegan, Dr. Jia Geng, Dr. Huaming Feng, Shaoying Wang, Fengmei Pi, Hui Li, Zhengyi Zhao, Danny Jasinski, Erfu Yan, Yanxi Xie, Zhouxiang Ji, Concong Xu, Hongran Yin, Sijin Guo, Zhefeng Li, Le Zhang, and Wei Li. I truly believe my success would not have happened without the strong team work present in the Guo laboratory.

I appreciate and would like to acknowledge all other faculty and staff members throughout my graduate career, especially graduate coordinator Catina Rossol and director of graduate studies Dr. Jim Pauly at the College of Pharmacy at University of Kentucky. I thank them for their assistance in my transition from the University of Cincinnati and move to a new city. Additionally I would like to thank them for organizing class schedules, and facilitating my graduate studies.

Finally, I would like to thank and show my appreciation to my parents Doug Binzel and Mary Binzel, my sisters Katie Binzel and Abby Binzel, and my close friends Dr. Chad Schwartz, Danny Jasinski, Ryan Hughes, along with many others for their continued love, encouragement, and support through my everyday struggles. They have meant the world to me through this process and continue to play essential roles in who I am today.

The work in the thesis dissertation was supported by the National Institute of Health under grants EB003730 and CA151648 to Peixuan Guo and NIH grant R25CA153954 to Brad Anderson.

TABLE OF CONTENTS

LIST OF TABLES

LIST OF FIGURES

LIST OF ABBREVIATIONS

2’-F	2’-Fluoro RNA Modification
3WJ	Three Way Junction
$3WJ_{2'-F}$	pRNA-3WJ Composed of 2’-F modified RNA
$3WJ_a$	A strand of the pRNA-3WJ
$3WJ_b$	B Strand of the pRNA-3WJ
$3WJ_c$	C Strand of the pRNA-3WJ
$3WJ_{DNA}$	pRNA-3WJ Composed of Deoxy Nucleic Acids
$3WJ_{RNA}$	pRNA-3WJ Composed of Ribonucleic Acids
AFM	Atomic Force Microscopy
C_t	Total Concentration
DNA	Deoxy Nucleic Acid
dsDNA	Double Stranded Deoxy Ribonucleic Acid
EB	Ethidium bromide
EMSA	Electrophoresis Mobility Shift Assay
FACS	Fluorescence-Activated Cell Sorting
FBS	Fetal Bovine Serum
k_a	Forward Reaction Rate Constant
K_A	Association Constant
K_a’	Association Reaction Rate
K_D	Dissociation Constant
k_d	Reverse Reaction Rate Constant
MG	Malachite Green
miRNA	Micro Ribonucleic Acid
mRNA	Messenger Ribonucleic Acid
PAGE	Polyacrylamide Gel Electrophoresis
PBS	137 mM NaCl, 2.7 mM KCl, 100 mM Na_2HPO_4, 2 mM KH_2PO_4, pH 7.4
PCR	Polymerase Chain Reaction
pRNA	Packaging Ribonucleic Acid
PSMA	Prostate Specific Membrane Antigen
RISC	RNA-Induced Silencing Complex
RNA	Ribonucleic Acid
RNAi	Ribonucleic Acid Interference
RNase	Ribonuclease
rtPCR	Real Time Polymerase Chain Reaction
siRNA	Small Interfering Ribonucleic Acid
SPR	Surface Plasmon Resonance
STM	Scanning Tunnel Microscopy
T_a	Association Temperature
TBE	89 mM Tris-borate, 2 mM EDTA

TBM	89 mM Tris, 200 mM Borate Acid, 5 mM $MgCl_2$
TEM	Transmission Electron Microscopy
TGGE	Temperature Gradient Gel Electrophoresis
T_m	Melting Temperature
TMS	50 mM Tris pH 8.0, 100 mM NaCl, 10 mM $MgCl_2$
ΔG°	Change in Gibbs Free Energy
ΔH°	Change in Enthalpy
ΔS°	Change in Entropy
ΔT	Change in Temperature
τ	Time Constant

Chapter 1: Introduction and Literature Review

BRIEF SUMMARY:

Chapter 1 begins this thesis with an overview on the creation and necessitation of RNA nanotechnology. First the promise of RNA interference technology is examined, and how RNA nanotechnology improves the delivery of RNA therapeutics for the treatment of cancers and viral diseases. Next the importance of particles stability is looked at by examining thermodynamic and kinetic properties. Finally, these parameters are discussed in the design of RNA nanoparticles.

Chapter 2 looks at the thermodynamic stability of the pRNA-3WJ. Here the stability of the RNA motif is compared to its DNA and chemically modified 2'-Fluoro RNA species in effort to stabilize the motif against nucleases and improve the thermodynamic stability and parameters. It was found the 2'-Fluoro RNA not only provides nuclease resistance, but also enhance the thermodynamic properties by increasing the melting temperature and decreasing the change in Gibbs free energy. Through these tests, it was found that the pRNA-3WJ forms through a rapid association in which no dimer intermediate could be detected and the formation of the RNA species assemble by an increased change in entropy over the DNA species, compared to the commonly seen more favorable change in enthalpy and decrease in entropy.

Chapter 3 studies the assembly mechanism of the pRNA-3WJ is examined more in-depth. Primarily using surface plasmon resonance, kinetic parameters of the pRNA-3WJ are elucidated resulting in the discovering the assembly mechanism of the pRNA-3WJ. It was found the 3WJ formed through a two-step association, forming an intermediate that then instantly resulted in the recruitment of the third RNA strand, thus

creating the pRNA-3WJ at an unobservable rate. Additionally, it was discovered the pRNA-3WJ relied on each of its helical regions for either the rapid formation or the long lasting stability. This rapid and unique assembly mechanism proves the pRNA-3WJ reactants forms into the 3WJ with a high efficiency and yield that can be translated to the production of RNA nanoparticles.

Chapter 4 takes the findings from the second and third chapters and applies them to the production of RNA nanoparticles for the targeting and treatment of prostate cancer. Stable RNA nanoparticles were constructed using the pRNA-3WJ as the central core with an RNA aptamer to target Prostate Specific Membrane Antigen (PSMA) and anti-miRNA sequences for therapeutic treatment. It was found that the resulting RNA nanoparticles were able to specifically bind and enter PSMA expressing cancer cells, delivering the anti-miRNA sequences. This specific delivery led to knockdown of the miRNAs, thus upregulating tumor suppressor genes and sensitizing cells to apoptosis. These findings demonstrates the versatility and ability of the pRNA-3WJ as RNA nanoparticles that has previously been unobtainable.

Chapter 5 briefly summarizes the major findings and advancements of RNA nanotechnology discussed in this thesis dissertation. Furthermore, the future direction of this work is described providing a prospective on research that is still needed to fully prove the benefits of RNA nanotechnology. Finally, the current state of RNA nanotechnology is discussed looking at the major hurdles that have been solved and look at how the recent advancements can propel RNA nanotechnology into the cancer therapeutic spotlight.

HYPOTHESIS:

The 3WJ motif from Phi29 bacteriophage packaging RNA (pRNA) provides a stable RNA scaffold for the construction of nanoparticles for the treatment of cancers.

INTRODUCTION:

Nanotechnology and drug delivery

First realized by Richard Feynman in 1959, the field of nanotechnology is the control of materials in design, interactions, and function at the atomic and molecular level (1). It wasn't until the 1980s when the principles of nanotechnology were put into practice by K. Eric Drexler; when he proposed the building of nanomachines capable of self-replication (2). Nanotechnology was later defined by the National Nanotechnology Initiative to be the manipulation of materials with the size range of 1 – 100 nm in size. As technologies advanced through the years, the field of nanotechnology grew as scientists were able to image and analyze the particles using techniques such as atomic force microscopy (AFM), transmission electron microscopy (TEM), and scanning tunnel microscopy (STM). Nanoparticles have since been created from a wide array of materials such as lipids (3); polymers (4); proteins and peptides (5); viruses and viral components (6); carbons (7); heavy metals, such as gold (8) and silver (9); iron oxide (10); deoxyribonucleic acid (DNA) (11); and ribonucleic acid (RNA) (12).

While the field of RNA nanotechnology has spread to a vast array of applications, a currently developing and promising application is drug delivery (13,14). The principle of nanotechnology in drug delivery is to increase the bioavailability of drugs or

therapeutic agents (15,16). As numerous drugs currently being developed have solubility (17) or toxicity issues, their practical application for the treatment of diseases are truly limited. Nanoparticles have been proven to link, uptake and attach to said drugs in hopes of increasing delivery to targeted diseases (18-23). Nanoparticle formulations have been shown to increase the solubility of difficult drugs; deliver a high dosage of therapeutics at desired sites through drug release mechanisms, such as pH sensitive binding and release particles (24-28); and provide specific targeting to cells through the use of peptide (29-31) and aptamer ligands, RNA motifs that have been specially designed and selected for binding to chemical and protein substrates such as cell surface receptors (32,33). As a result, toxicity is decreased as a smaller total drug concentration is delivered *in vivo*, all while a higher local dosage is delivered to targeted sites.

While each nanoparticle material provides its own set of advantages and disadvantages; as a whole nanotechnology is still a developing field that is still working on overcoming hurdles to produce a more perfect drug delivery vehicle and improve on current standards of pharmaceutics. Lipid based nanoparticles allow for high drug or therapeutic loading and encapsulation and allow for high delivery of payloads through membrane fusion with cells while remaining nontoxic and not producing immune responses (34,35); however, such nanoparticles have shown issues with thermodynamic stability causing release of payload prematurely (36) and issues with production reproducibility resulting in the production of inconsistent products (37). Similarly polymer based nanoparticles allow for high levels of therapeutic encapsulation (38); however, polymers display a significant increase in thermodynamic stability and can easily be functionalized on the surface for targeting abilities (39). Yet polymers still show

issues with batch reproducibility and have shown issues with solubility and bioavailability. Biologically derived nanoparticles such as viruses, viral components and proteins and peptides have issues of producing immune responses and creating certain levels of toxicity. Yet targeted delivery allows for a lower overall dose while having a high accumulation in targeted tissues (40-43). Inorganic nanoparticles such as carbon structures and metal ions can be created with high reproducibility with a lower cost than most nanoparticles. Furthermore, these particles can be functionalized through chemical modifications; however, their high accumulation in healthy organs such as kidneys, lungs, and liver result in high toxicity and limit their overall ability for therapeutic delivery. DNA nanostructures are constructed with defined shape, size, and stoichiometry (44-46) and can achieve targeted delivery with the functionalization of DNA aptamers (47,48); yet the overall low thermodynamic stability of DNA nanoparticles limits their ability for *in vivo* applications. Additionally, positively charged nanoparticles such as metal ions, some polymers, proteins have overall positive charges that allows for endosomal escape through proton sponge effect (49), yet this positive charge allows for passive binding to negatively charge cells membranes, leading to non-specific binding to healthy tissues producing toxicities.

The promises of RNA interference in therapeutics

The discovery of RNA interference (RNAi), in which RNA sequences create gene regulation by the binding and degradation of messenger RNA, by Craig Mello and Andrew Fire in 1998 lead to revolutionary work in the RNA field (50). Their discovery of RNAs in *C. elegans* proved that RNA was not simply a temporary intermediate of the production of proteins from DNA through transcription and translation, but that RNA

plays and essential role in cell functioning and processing. Additionally the discovery of functional RNA, dismissed the myth of "junk DNA and RNA." Their work discovered microRNA (miRNA), a naturally occurring RNA loop on messenger RNA (mRNA) that is processed into single stranded RNA that is then able to bind and silence several mRNAs resulting in gene regulation. Since Mello and Fire's original work, studies of miRNA and its role in gene regulation, cell functionality, and role in disease development has exploded into a large field of study. Additionally the development of small interfering RNA (siRNA) by David Baulcombe (51) in plants and in mammalian cells by Thomas Tuschl (52,53) provided a novel method of gene regulation and proposed method of controlling cell growth, gene regulation, and even apoptosis (54-57). Much like miRNA, siRNA silences mRNAs and genes however, the sequences are synthetic and designed for a single gene while miRNA targets several genes.

The discovery of RNAi has heightened interests in using the short RNA sequences for RNA therapeutics (50). Many efforts have been made in delivery RNAi therapeutics for the treatment of diseases, most notably in cancers and viral infections (54-62). However, trials of testing the delivery of naked siRNA led to disappointing results, as the short RNA sequences were either quickly degraded by commonly occurring RNases or displayed short half-lives of only 15-45 minutes by being excreted through the liver due to their small size (63-65). Nanotechnology has since gained a large interest in the delivery of RNAi therapeutics in various disease states due to the principles of nanoparticles increasing the size of the siRNA or miRNA and protecting the RNA strands from nuclease degradation (54-62). Furthermore nanoparticles have proven beneficial in delivering payloads to cancer tumors due to their ability to pass through

leaky blood vasculature creating the enhanced permeability and retention (EPR) effect, while remaining large enough to stay in circulation in the body (66-70).

Recently, a new attractive RNAi therapeutic has been developed for the treatment of cancers. miRNAs have been shown to play a large role in cancer development whether they are either overexpressed or reduced in expression (71-77). Modified locked nucleic acid (LNA) sequences have been selected and developed to bind to miRNA seed-regions (78), resulting in the inactivation and silencing of microRNAs. This can serve as potentially powerful therapeutic to target over expressed miRNA with cancers known as oncomirs. While these anti-miRNA LNAs are too small to be delivered directly, as they would be immediately be cleared from the body, efforts have been made in delivering such LNAs through the incorporation onto nanoparticles. Several technologies have encapsulated an anti-miRNA 21 strand into polymer based nanoparticles for the delivery to triple negative breast cancer (79), lipid nanoparticles to glioblastroma (80) and lung cancer (81), and a lipid-gold nanoparticle hybrid delivered to androgen independent prostate cancer (82). Additionally anti-miR21 has been placed onto RNA nanoparticles for the specific delivery and treatment of breast cancers (83). Additionally polymer nanoparticles have been used to deliver an anti-miRNA 10b sequence to breast cancer (79) and metal nanoparticles also delivered anti-miR10b to breast cancers (84). Cheng et. al. used a pH sensitive peptide nanoparticle system for the specific delivery of anti-miR155 to lymphoma without the accumulation of nanoparticles in healthy tissue (85). The wide array of research being completed on several cancer lines and several oncomirs indicated the power of the anti-miRNA LNAs and the current interest in the RNAi field.

Birth of RNA nanotechnology

The concept of RNA was first proven in 1998 (12) through the creation of a hexameric ring of packaging RNA (pRNA) on the Phi29 bacteriophage for the packaging of viral DNA into the procapsid of virus during replication. The discovery and development of inter-molecular interactions between pRNAs, deemed loop-loop interactions, proved specific control the looped sequences forming the inter-RNA interactions. These interactions allowed for the assembly of the pRNA ring and the number of pRNA copies in the ring could therefore be controlled. pRNA is a ~120 base pair (bp) RNA structure that serves as a binding sight between the Phi29 connector pore that allows for the packaging of the genome into the virus procapsid and the gp16 ATPase. RNA is an ideal platform for the creation of nanoparticles due to its beneficial characteristics listed below. RNA is primarily composed of four nucleotides, adenine(A), cytosine (C), guanine (G) and uracil (U); giving RNA the simplistic design of DNA. This concept allows for the construction of molecules with easily predictable structures with defined shapes and stoichiometry (12,86-88). However, unlike DNA, ribonucleic acids allow for non-canonical base pairing, or pairing between non-Watson-Crick pairs such as A-G, as well as RNAs contain bulges, loops, and interactions between bases on separate strands creating what is known as kissing loops (86,89,90). The diversity in base interactions found in RNA provides a wide diversity in folding and structure much to proteins (91).

Furthermore, with the diverse folding of RNAs brings a variety of functionalities and actions. Traditionally, RNA is considered as a temporary intermediate of DNA for the translation of proteins; however, it is now well understood that RNA holds many

functionalities within the body and non-coding RNAs play important roles through gene expression and cell functionality. Such examples of these RNAs are pRNA of the Phi29 bacteriophage, ribozyme (92-94), riboswitch(95,96), small interfering RNA (siRNA) (97-99), micro RNA (miRNA) (100-102), ribosomal RNA (rRNA) (103-106), small nucleolar RNAS (snoRNA) (107-109), small nuclear RNA (snRNA) (110,111), and RNA aptamer (32,33). The simplistic design, yet diverse structuring and functionality of RNA has made it attractive to many scientist for applicational uses such as the treatment of cancers and viral infections. Due to the nature of RNAs, RNA nanotechnology provides several benefits over competing nanotechnologies utilizing proteins, DNA, and polymers (91,112): 1) as stated earlier, RNA can be produced with defined shape and stoichiometry as well as high reproducibility (12,86-88). 2) RNA can target specific cell groups by targeting cell surface receptors through the use of RNA aptamers, motifs that have specifically been selected for specific binding to chemical or protein ligands, without inducing antibody production, allowing for repeated delivery and therapy (113-115). 3) RNA nanoparticles that have been produced have a size range of 10-50 nm, the perfect size to be retained within the body and pass through leaky blood vessels in cancer tumors by Enhanced Permeability and Retention (EPR), as well as cell membranes by cell surface receptor endocytosis (66-68). 4) RNA can be created to harbor multiple therapeutic elements by utilizing branch scaffolds (98,116-119) and bottom-up construction (86,97). 5) RNA is known to have a higher thermostability over DNA with a higher melting temperature and more negative Gibbs free energy of formation (120,121). 6) RNA materials have gained FDA approval due to their known exact known size and chemical makeup compared to other nanotechnologies (91).

RNA scaffolds

Since the original development of the tunable Phi29 packaging RNA (pRNA) nanoparticles several other RNA based nano-platforms have been produced. The Guo lab has continued their work on the Phi29 pRNA system, most notably with the three-way junction (3WJ) motif composed of three short oligo strands that has been proven to be thermodynamically stable (87,122). The 3WJ has since been used as a building block to produce the pRNA X-way motif (123); varying shapes including triangles, squares, and pentagons (124-127); and further 3D arrays from the resulting shapes. Additionally, Luc Jaegar first developed a building block coined as TectoRNAs that utilized looped regions between RNA strands for base pairing to build nanostructures (89). From the TectoRNAs a variety of structures have been built including tectosquares, Jigsaw puzzles, nancubes, and nanorings (88,128-131). Similarly Thomas Hermann has developed a self-assembling square composed of an RNA backbone (132) and Saito's group has created a triangle RNA scaffold (133). Recently, Paula Hammond has developed an RNA microsponge that is capable of uptaking siRNAs for delivery (38,134). These RNA nanoparticles have laid the foundation of scaffold that can be used for the inclusion of RNAi components for the treatment of diseases (38,87,123,134-142).

Elucidation and modeling of thermodynamic parameters of nucleic acids

The formation of RNA nanoparticles from multiple strands is depended on the formation of base pairing between or within singular strands. This assembly process is governed by thermodynamics, which has since been proven to be sequence dependent. Extensive studies have been completed looking at the thermodynamic contributions of each RNA and DNA sequence, which in turn developed nearest neighbor parameters.

Thermodynamic parameters during the folding and melting of RNA and DNA duplexes has been long studied using various sequences. Originally, duplex interactions of DNA was studied to derive thermodynamic parameters that lead to the modeling of nucleotide contributions in folding energy landscapes (143,144). This work resulted in the development of nearest neighbor predictions, in which thermodynamic parameters could be predicted by the sequence of DNA. RNA models were then created in a similar fashion (145-147), that then led to the studying of RNA/DNA hybrid duplexes (120). While these initial studies were very informative, the predictive models were limited to duplex structure, whereas RNA is known to fold into diverse structures with branches, bulges, and looped regions. In looking at several junctions and looped regions, Doug Turner was able to elucidate thermodynamic energies for RNA three- and four-way junctions (3WJ, 4WJ) (148).

From these fundamental studies, thermodynamic experiments were expanded to study the overall thermostability between nucleic acid species. Lesnik and Freier first compared 14 sequences ranging from 9 up to 21 base pairs in length composed of DNA and RNA, along with each of the hybrid structures (RNA/DNA duplex) (149). From their studies, it was found that 13 of the 14 RNA sequences displayed melting temperatures, T_ms, higher than the corresponding DNA sequences. In nucleic acid studies, melting temperature is defined as the temperature in which 50 % of the nucleic acid strands are assembled into motif and 50 % are in single strand states. Furthermore, the same 13 of 14 sequences displayed the more favorable, more negative Gibbs free energy (ΔG°). The ΔG° is the release (negative) or consumption (positive) of energy by the nucleic acid strands when folding into their motifs; a negative value indicated energy is being released

and is therefore spontaneous, the lower the value the more spontaneous the reaction will be. The one exception to the study was a sequence with a repeat of A-T base pairing. Several additional studies have been published on comparing thermostabilities and folding energy levels of RNA and DNA sequences (150-153). Again from each of these studies, it was concluded RNA produced a more negative ΔG° and more positive T_m over the same DNA sequence. The widespread studies of relative stability of RNA has shown it provides a more favorable folding landscape by assembling more spontaneously and displaying a higher overall stability with the increased melting temperature over DNA.

Furthermore, from the derived nearest neighbor calculations and studying known RNA motifs and structures, several computational programs have been developed to predict the folding of RNA motifs and their relative energy landscapes for both folding and denaturing. Using energy landscape predictions, programs such as mFold (154), UNAfold (155), and RNAfold (154,156) have been developed to predict the secondary structuring of RNA motif leading to predictive base pairing. Moving from secondary interactions to tertiary and quandary predictions has proven to be much more difficult. RNA structural studies have thus been conducted by Eric Westhof (157-160), Neocles Leontis (89,90,157,161-163), and David Lilley (164-167). Such studies have created databases of RNA motifs that are now used for the predictive folding and interactions of RNA sequences (168-171).

Importance of thermodynamics and kinetics in RNA nanotechnology

Due to the fact that RNA nanoparticles rely on hydrogen bonding between base pairing to keep the nanoparticle together, folding thermodynamics and kinetics are imperative for nanoparticle stability. Together kinetics and thermodynamics describe the

ability and speed of the RNA motif or nanoparticle to fold, along with its overall stability. In nanoparticles design, the folding mechanism is crucial, in that a central motif that folds rapidly and spontaneous with favorable thermodynamics is desired. Additionally one must examine the folding energies to examine the concern of side products is minimalized, in order to produce as pure of a product as possible. In nanotechnology, creating particles of defined shape and size with high reproducibility is paramount in going through FDA approval. Additionally particle thermodynamic stability is an absolute key in nanoparticle design and construction. In looking at *in vivo* applications, nanoparticles will be subjected to dilute concentrations and elevated temperatures of the body of 37 °C. These conditions will test the stability of base-paired RNA motifs in which dissociation is not only unacceptable, but a serious concern. Nanoparticles must be tested to be stable at temperatures and concentrations that will be seen *in vivo* to ensure stability of the particle and therapeutic as well as proper delivery of the therapeutic agent to the target. As shown above through the nearest neighbor modeling, thermodynamic stability of RNA duplexes and structuring is highly dependent on both the sequence and oligo length. Therefore full characterization of folding and stability of nanoparticles is necessary for the advancement of the field to *in vivo* applications.

Chapter 2: Thermodynamic Analysis of Phi29 pRNA-3WJ

This chapter was reproduced (with some modification) with permission from Binzel DW, Khisamutdinov EF, Guo P. "Entropy-Driven One-Step Formation of Phi29 pRNA 3WJ from Three RNA Fragments." *Biochemistry*, 2014. 53 (14), 2221-2231. DOI: 10.1021/bi4017022. Copyright 2014 American Chemical Society. Special thanks to Dr. Emil F. Khisamutdinov for help in preparation of data for figures 2.3, 2.5, and 2.6A and Zhengyi Zhao in preparing figure 2.1A.

INTRODUCTION:

Since the proof-of-concept in 1998 (12), RNA nanotechnology has been emerged as a popular field (86,91,128,157,159,172-175). RNA has the simplistic chemical characteristics of DNA, and the complex folding and functionality of proteins (91). These attributes make RNA an ideal candidate for creating nanoparticles with diverse functionalities for targeting and treating cancer tumors and viral infections, as well as other applications in nano devices (12,38,86,87,118,123,176-182). RNA nanotechnology in therapeutics provides many advantages over current technologies (91,112): 1) RNA can be produced with defined shape and stoichiometry as well as high reproducibility (12,86-88). There are many modified nucleosides within RNA, but it is primarily composed of only four nucleic acid bases, allowing for simplicity in structure and predictable interactions between molecules and formation of structures. 2) RNA can target specific cell groups by targeting cell surface receptors through the use of RNA aptamers that function like protein or chemical ligands (113-115). These structures do not induce antibody production, allowing for repeated delivery and therapy (113). 3) RNA

nanoparticles that have been produced have a size range of 10-50 nm (66-68), the perfect size to be retained within the body and pass through leaky blood vessels in cancer tumors (69,183), as well as cell membranes by cell surface receptor endocytosis (68). 4) RNA can be created to harbor multiple therapeutic elements by utilizing branch scaffolds (98,116-119) and bottom-up construction, the development of nanoparticles through the design of subcomponents that then are used to assemble into the final product (86,97). Even with these advantages, RNA nanotechnology has been hindered because of the instability of RNA itself, specifically *in vivo*. Dissociation of complex without covalent bonds is an intrinsic property of molecules, e.g. RNA molecules, that are thermodynamically instable in nature (120,146,149,150,184-188).

When RNA nanoparticles are delivered systemically to the body, the particles will exist in low concentrations due to dilution by circulating blood. Only those RNA particles that do not dissociate at low concentrations are feasible for therapeutic purposes that require systemic delivery. Furthermore, RNA can easily be degraded and cleaved by RNase found throughout the human body (112). Chemically modified nucleotides have been developed to combat the nuclease degradation. Specifically, 2′-F modified nucleotides have been shown to keep the original folding and functionality of the RNA molecules while significantly increasing the half-life (189). In order to overcome the instability issues and push the RNA nanotechnology field to progress further, a stable platform needs to be produced that can remain stable at low concentrations and high temperatures while resisting RNase degradation (87,123,177).

Recently, a three way junction motif (3WJ) in the packaging RNA (pRNA) of the bacteriophage Phi29 dsDNA packaging motor was found to be ultra-stable (87). The

pRNA-3WJ produced a melting curve indicative of a low Gibbs free energy (ΔG^o), the total energy that is either released or consumed by a system through a reaction or work, thus determining spontaneity of the system (190,191), as well as a high melting temperature (T_m). It has also been elucidated that the 3WJ is stable in ultra-low concentrations, as well as in 8 M urea, a common denaturing agent for nucleic acid structures. This junction serves as the central core of the pRNA and links the helical domain (192) to the interlocking looped regions (193), and allows for intermolecular interactions with other pRNA molecules (**Fig. 2.1**). The core can be formed from three individual RNA oligos with a high efficiency without the presence of metal ions, as many RNA motifs require the presence of metal ions, like Magnesium, for folding, assembly, and stabilization. Therefore, the pRNA-3WJ shows an initial sign of higher stabilization than many RNA motifs. It has been found that this junction can incorporate RNA functional moieties, such as receptor-binding aptamer (32,33), siRNA (97-99), ribozyme (92-94), miRNA (100-102), or riboswitch (95,96). Additionally, the resulting structures have the ability to keep the strong folding of the core, while retaining the functionality of the conjugated RNA moieties (87). Even with the strong stability of the 3WJ, it is still very much susceptible to degradation by RNases; therefore, chemical modifications to the RNA are required (64,186,195). The effects on the thermodynamic stability of the pRNA-3WJ core, though, are still unknown.

Previously, thermodynamics of nucleic acids and their folding properties have been studied; however, the majority of the studies have been completed on RNA and DNA duplex sequences (120,143,144,146,149-151,153). An estimation of thermodynamic parameters for RNA 3- and 4WJ have been surmised (148) from studies

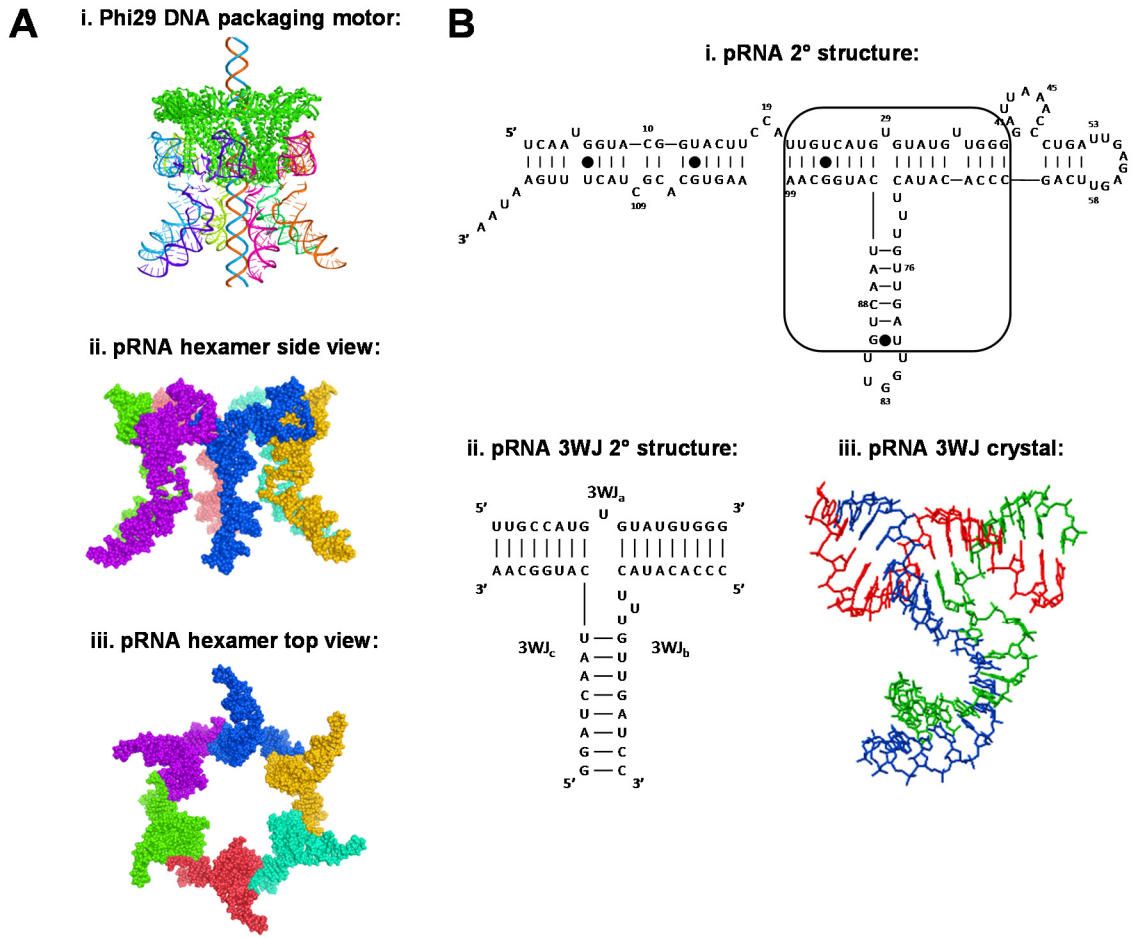

Figure 2.1. Background information for motor pRNA, pRNA three-way junction (3WJ). (a) The side-view of the hexametric structure of Phi29 DNA-packaging motor(194). Two bottom are side-view and top-view of the hexameric pRNA derived from X-ray crystallography(122). (b) Predicted secondary structure of the Phi29 packaging RNA (pRNA) with the 3WJ motif outlined and the pRNA-3WJ.

completed using two piece designs by incorporating looped regions between helical branches. A gap has remained within the thermodynamic studies of nucleic acids regarding elucidating thermodynamic characteristics of multi-branched structures, i.e., multi-stranded motifs. Additionally the understanding of chemical modifications to the RNA backbone on RNA junctions has remained a mystery, and untouched. In order to understand the thermodynamic characteristics of such structures and comprehend the governing laws of motif folding, new methods must be developed to be able to see multi-stranded interactions.

Here we report the measured thermodynamic parameters for 3WJ complexes containing DNA, RNA, and 2′-F U/C modified RNA strands (**Fig. 2.1**), as well as hybrid complexes by means of comparison of their stability using a real time Polymerase Chain Reactions (rtPCR) machine and Temperature Gradient Gel Electrophoresis (TGGE). Results concluded that use of DNA strands weakened the structure of the pRNA-3WJ, while 2′-F modifications strengthened the RNA motif by elevating the transition temperatures and lowering ΔG°. More importantly, the data appears to show the 3WJ formed in a single step without displaying presence of dimer species, showing that all three strands of the pRNA-3WJ formed together into complex rapidly with the intermediate product undetectable. The assembly was also revealed to be entropy driven.

MATERIALS AND METHODS:

Oligonucleotides and assembly of 3WJs

RNA, DNA, and oligonucleotides were obtained from Integrated DNA Technologies (IDT). RNA oligonucleotides containing 2′-F U/C modification were ordered from Trilink BioTechnologies. Assembly of 3WJs were performed by mixing

equimolar concentration of corresponding strands in TMS (50 mM TRIS pH = 8.0, 100 mM NaCl, 10 mM $MgCl_2$) buffer, heating to +80 °C, and slowly cooling to +4 °C at a rate of 2.0 °C/min for a total of 37 minutes. The 3WJ formations were assayed on a 12% native PAGE TBM running buffer (89 mM Tris, 200 mM Borate acid, and 5 mM $MgCl_2$) ran at 100 V at 4 °C for 90 min. Gels were stained with Ethidium Bromide (EB) and imaged using a Typhoon (GE).

K_D measurements

Apparent equilibrium dissociation constants (K_D) for 3WJ formations were determined by titration over a range of concentrations from 0.1 nM to 512 nM, as previously described (88,196). Concentrations of the 3WJs were calculated using the absorbance of UV light at 260 nm using a Nanodrop 2000 (Thermo Scientific) using an extinction coefficient of 40 µg/ml and 50 µg/ml for RNA and DNA, respectively. Briefly, fixed amounts of [^{32}P] ATP 5′-end labeled $3WJ_b$ strands of RNA, DNA, and 2′-F modified RNA (0.1 nM final) were mixed with variable amounts of unlabeled $3WJ_a$ and $3WJ_c$ strands RNA to make the indicated final concentration (0.1 nM to 512 nM) of each. The resulting 3WJs were then heated to 80 °C for 3 min in TMS buffer and slowly cooled to 4 °C. The resulting gel shifts were measured using Image J software and interpreted with the program Origin 8.0. The fractions (f) for each trimer forming complex was calculated by dividing the corresponding quantified values for trimers by the total sum of values for all complexes (monomer, dimer, and trimer) presented in the corresponding lane. The combined data from several independent measurements were subjected to non-linear curve fitting using the equation:

$$K_D = \frac{\left[\left(\frac{C_t}{3}\right)^2 \times (1-f)^3\right]}{f^1} \qquad (2.1)$$

where C_t is the total concentration of RNA strands in each lane and f is the fraction of 3WJ complex to total concentration.

In calculating the C_t, the concentration of the labeled $3WJ_b$ strand was not included, as it was in trace amounts and negligible to the concentrations of $3WJ_a$ and $3WJ_c$. The C_t at equilibrium was calculated by interpolation of the fraction (f) at 50%. These values were then in turn used to calculate the equilibrium K_{DS}s (191). Marky et al. described this calculation using changing temperature to reach equilibrium, thus requiring equal concentrations of each strand; however, equilibrium was reached here by varying concentrations, as previous performed (88,196), thus not requiring equal concentrations of each strand.

Real time PCR annealing curves of 3WJ complexes

Each synthesized pRNA-3WJ strand ($3WJ_a$, $3WJ_b$, $3WJ_c$) was mixed at equimolar concentrations in the presence of 1x SYBR Green II dye (Invitrogen) at equal molar ratios of 10 μM to create a $3WJ_{RNA}$, $3WJ_{DNA}$, and $3WJ_{2'\text{-}F}$. SYBR Green II dye is a reporter dye with higher specificity for RNA, but shows binding to both DNA and RNA bases (197). Using a Roche Lightcycler 480 real time PCR machine, with accurate readings of temperatures to ± >0.25 °C, samples were heated to 95 °C for 5 min for an initial denaturing period and then slowly cooled at a rate of 0.11 °C/sec until 20 °C. The Roche Lightcycler 480 was able to detect the fluorescence levels, thus monitor the formation of the 3WJ cores. All samples were completed in triplicate to ensure accuracy of the annealing temperatures and profiles. Samples were then subjected to electrophoresis on a 12% polyacrylamide gel to ensure the formation of the 3WJs. All

hybrid structures of the pRNA-3WJ core were created using a mix of RNA/DNA, RNA/2′-F RNA, or DNA/2′-F RNA in the same method described as above.

TGGE and thermodynamic parameters

All 3WJ hybrids were assembled as described above. The Temperature Gradient Gel Electrophoresis (TGGE) system from BiometraHmbGh, Germany was used in this study. Temperature was varied perpendicular or parallel to the electrical current. All experiments were performed in TMS running buffer. The RNA bands were detected in native 15% gel by total RNA stain using Ethidium bromide (EB). The concentrations of 3WJs were typically 10 μM. All varieties were run a minimum of three times to ensure accuracy of measurement.

Various concentrations of preassembled pRNA-3WJs covering 1,000 fold dilutions from 10 μM to 0.016 μM were subjected to the perpendicular TGGE for thermodynamic parameter calculations. 3WJ bands were detected with radiolabeled $3WJ_c$ strands at the 5′-end using γ-32P ATP (Perkin Elmer). A linear temperature gradient of $\Delta T = 44$ °C was applied perpendicular to the electric field. The gels were run for 1 hr at constant 80 V, dried, and exposed to phosphoroimaging screen overnight. Gels were then visualized on a Typhoon (GE), and Image J software was used to quantify the area of bands on each lane by plotting intensity of each band intensity and integrating the area under the curve for each band. Background signal of each lane immediately surrounding the band of interest from the gel was subtracted and removed from the band intensity and not included in calculations. The fraction of 3WJ bands were obtained by subtracting the area of melted bands from the trimer band. Melting temperatures were then calculated

from a plot of 3WJ fraction (f) vs. temperature, with f = 0.5 (50%) corresponding to the T_m.

Calculation of Thermodynamic parameters

T_m values at different concentration of 3WJs were used to calculate thermodynamic parameters. van't Hoff plots were generated by plotting the T_m versus the concentrations of non-self complementary three molecular strands according to a previous method (191):

$$\frac{1}{T_m} = \frac{2R}{\Delta H^\circ} \ln C_t + \frac{\Delta S^\circ - 2R \ln 6}{\Delta H^\circ} \quad (2.2)$$

where R is the gas constant 1.987 cal mol-1 K-1 , C_t is the total concentration of each 3WJs, and ΔH° and ΔS° are enthalpy and entropy changes, respectively. Under this method of calculation, the assumption is made that the heat capacity remains unchanged throughout the entire melting profile.

Fluorescence of pRNA-3WJ-MG aptamer

The assembled unmodified and 2′-F A/C modified 3WJs (1 μM) were mixed with Malachite green triphenylmethane (2 μM), a non-fluorescent dye that only fluoresces when bound to the Malachite green binding aptamer, in binding buffer containing 100 mM KCl, 5 mM $MgCl_2$, and 10 mM HEPES (pH 7.4) and incubated at room temperature for 30 min. The fluorescence was measured using a fluorospectrometer (Horiba Jobin Yvon; SPEX Fluolog-3), excited at 615 nm, and scanning from 625 to 800 nm for emission (198).

RESULTS AND DISCUSSION:

Assembly of the three-way junctions

pRNA three way junctions composed of RNA ($3WJ_{RNA}$), DNA ($3WJ_{DNA}$), and 2′-F U/C modified RNA ($3WJ_{2'\text{-}F}$) were assembled using equimolar concentrations of each strand of the 3WJ. The formation of the pRNA-3WJs in each of the species was confirmed by 12% native PAGE (**Fig. 2.2**). A step-wise assembly through the polyacrylamide gel was observed between the monomer to dimer, and finally to the fully assembled trimer band indicating the formation of 3WJs. The assembled RNA, DNA, and 2′-F 3WJs products resulted in high yield (> 90%). Any side product is assumed to be contributed to slight mismatch in strand concentrations loaded during assembly, preventing all nucleic acid strands from forming into the 3WJ complex. The data are in agreement with previously reported results of RNA-3WJ assembly (87).

Dissociation constants (K_D) measurements of the 3WJs

The K_D values of nucleic acids formation are directly related to their stabilities as more stable complexes require lower concentrations of the components for self-assembly resulting in a lower K_D value. We measured the apparent dissociation equilibrium constants for RNA, DNA and 2′-F modified RNA 3WJ complexes (**Fig. 2.3**). For the $3WJ_{RNA}$ and $3WJ_{2'\text{-}F}$ the K_D values were found to be 11.4 and 4.5 nM, respectively. For the $3WJ_{DNA}$ complex this value was about five times higher (47.7 nM). This indicates that $3WJ_{2'\text{-}F}$ and $3WJ_{RNA}$ were the most stable complexes, and the least stable was $3WJ_{DNA}$. These results demonstrated that the incorporation of enzymatically resistant DNA or 2′-F modified RNA strands into the RNA 3WJ motif could increase the resistance of the complex to RNases. However, while the DNA strands incorporation decreases the

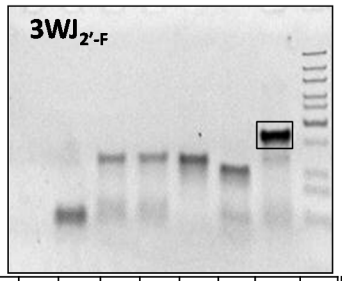

	1	2	3	4	5	6	7	8
$a_{2'-F}$	+			+		+	+	
$b_{2'-F}$		+		+	+		+	
$c_{2'-F}$			+		+	+	+	

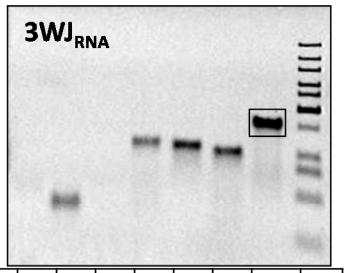

	1	2	3	4	5	6	7	8
a_{RNA}	+			+		+	+	
b_{RNA}		+		+	+		+	
c_{RNA}			+		+	+	+	

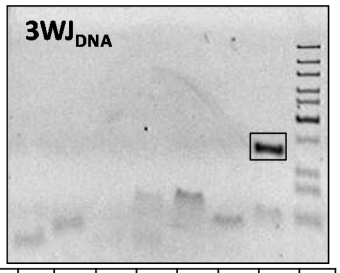

	1	2	3	4	5	6	7	8
a_{DNA}	+			+		+	+	
b_{DNA}		+		+	+		+	
c_{DNA}			+		+	+	+	

Figure 2.2. Assembly of pRNA-3WJ core structures. 12% polyacrylamide gels in native conditions displaying the stepwise assembly of the $3WJ_{2'-F}$, $3WJ_{RNA}$, and $3WJ_{DNA}$.

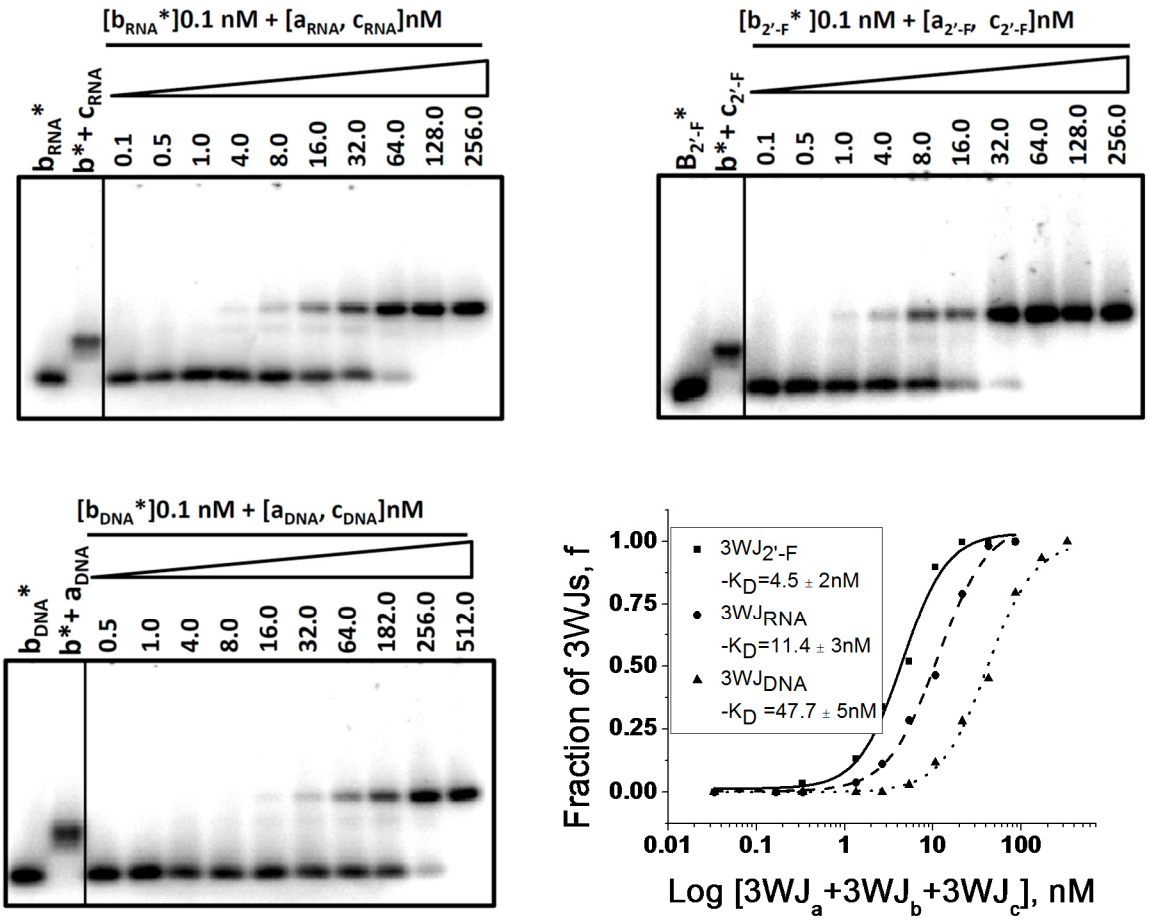

Figure 2.3. Dissociation constant measurements. Electrophoeretic Mobility Shift Assay (EMSA) of ^{32}P-labeled 3WJ$_b$ (constant concentration) assembling with increasing concentrations of 3WJ$_a$ and 3WJ$_c$ for RNA, 2′-F RNA, and DNA on 12% polyacrylamide gels in native conditions. Plot of percentage of 3WJ formed vs. total concentration to solve for K_D of each 3WJ.

stability, the 2′-F modified RNA increases the stabilization of the 3WJ complex, as shown by the lower dissociation constant compared to the $3WJ_{RNA}$. Therefore, if a nanoparticle were needed to be constructed with an alternative melting temperature than the native $3WJ_{RNA}$, the stability and properties of $3WJ_{RNA}$ motif can be tuned by alternating the ratio of 2′-F modified RNA and DNA strands to either increase or decrease the stability, respectively.

Determination of the formation of complex and T_a of DNA, RNA, and 2'-F RNA-3WJs by rtPCR machine

The thermostability of 3WJs complexes were compared by measuring their fluorescence intensities as a function of temperature in the presence of SYBR Green II dye on a Roche 480 Lightcycler to obtain T_a (87). The annealing transitions in **Fig. 2.4A-C** show that the mixture of three strands ($3WJ_a$, $3WJ_b$, and $3WJ_c$) produced the highest annealing temperature compared to any monomer or dimer formation. Within the assembling profile, the slope of the transitions directly correlates with ΔG°, as the steeper slope results in a more negative ΔG° values (190,191). These results showed that the assembly of the 3WJ was preferred over any dimer formation of any two strands in each of the three species: RNA, DNA, and 2′-F modified RNA.

From each of the transitions obtained by the Roche 480 Lightcycler, the curves of the each of the completed 3WJ structures were compared (**Fig. 2.4D**). The $3WJ_{2'-F}$ was the most stable with T_a = 69.8 °C, the $3WJ_{RNA}$ was the next stable at 59.3 °C, and the $3WJ_{DNA}$ had the lowest where T_a = 48.9 °C. These results correlated with literature reported values of overall thermostability for nucleic acids, and followed the order of stability: 2′-F RNA > RNA > DNA (150,151,199). Surprisingly, from the assembly profiles of the pRNA-3WJ species, a single annealing temperature was seen, not two.

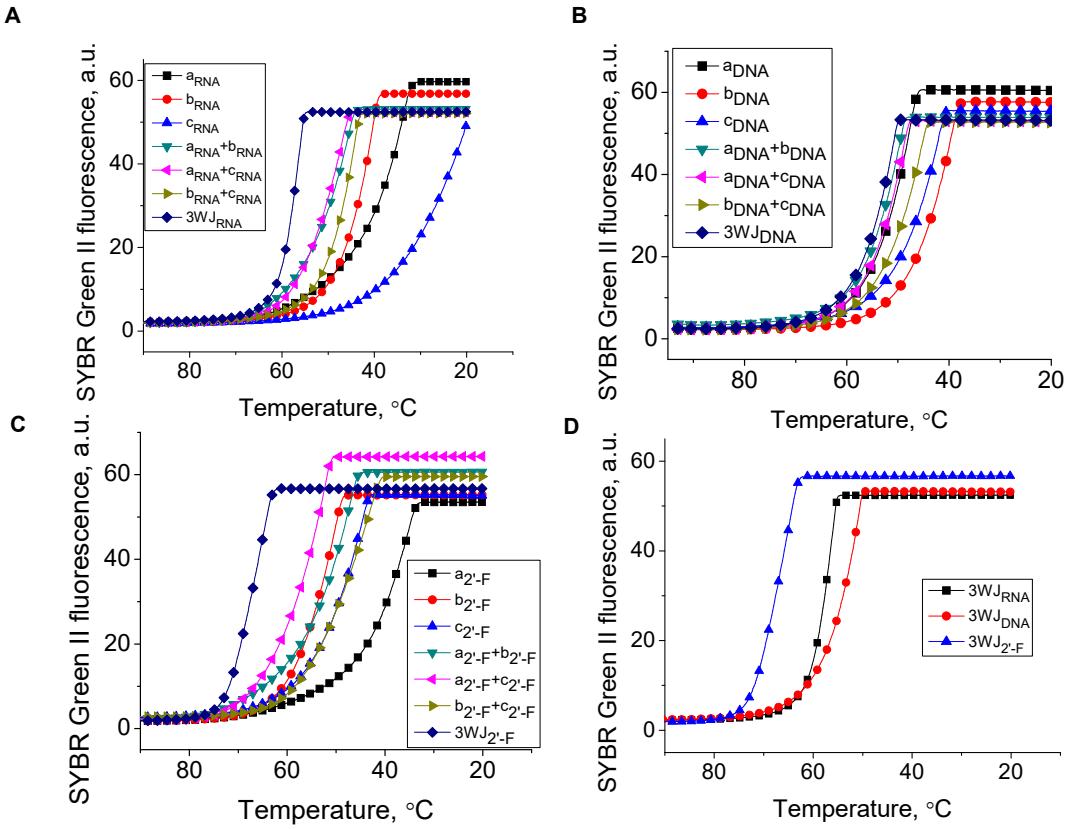

Figure 2.4. Assembly curves produced from the Roche 480 Lightcycler using SYBR green II reporter dye. (a) $3WJ_{RNA}$, (b) $3WJ_{DNA}$, (c) $3WJ_{2'-F}$, and each of the components of the 3WJs. (d) The three 3WJ species directly compared, showing the differences in melting temperatures (T_a).

This is evidenced by the single slope to the transition profile and hinting that the 3WJ is forming rapidly with all three strands producing no by-products; whereas, a two-step association would display a plateau within the melting curve itself or two individual sloped regions, resulting in two annealing temperatures. These results show the three stranded motif forming together, and a dimer species was undetectable due to the rapid 3WJ formation. This rapid formation from three fragments to form the pRNA-3WJ is highly beneficial due to the fact that it allows a high yield of assembly, while permitting for the construction and assembly of RNA nanoparticles without creating side products as a result of the dimer formation.

Comparison of stability between DNA, RNA, and 2'-F RNA-3WJs by TGGE

TGGE is common technique to measure T_m of large and complex nucleic acids (88,200,201). This approach has an advantage over the real time PCR in that it can be applied to directly measure the T_m of RNA complexes as fractions of RNA versus temperature with no intercalation dye required.

Melting temperatures of 3WJ complexes were determined by measuring the decrease in the yield of 3WJs versus temperature (**Fig. 2.5**). A temperature gradient was applied perpendicular to the electrical current, with an increasing temperature that resulted in the melting of the structures in the later lanes. Here, the percent 3WJ complex was compared to dimer and monomer formations. T_m were determined as 50% of 3WJ remaining. Any remaining dimers were not considered as a complex, as it was not complete 3WJ formations. From the resulting gels, melting temperatures were derived for the $3WJ_{2'\text{-}F}$, $3WJ_{RNA}$, and $3WJ_{DNA}$ as 66.5 °C, 57 °C, and 35.2 °C, respectively. The melting temperatures for the two RNA species were within the range of error from the T_m

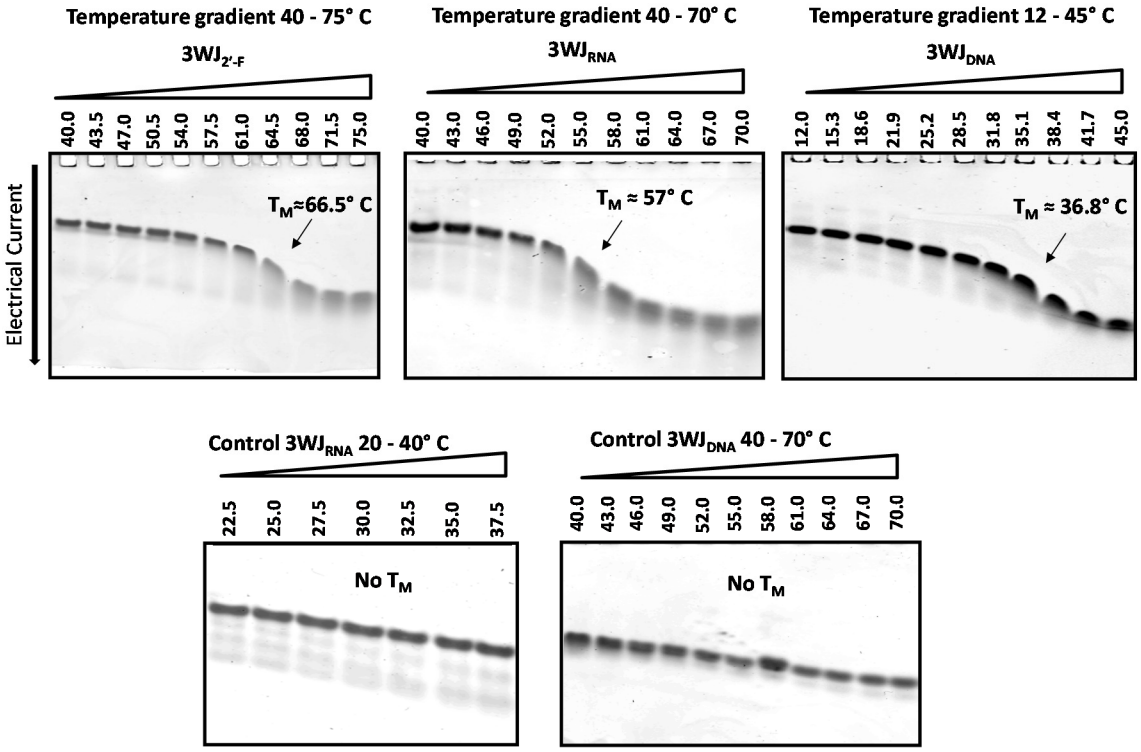

Figure 2.5. Representative 15% native TGGE with temperature gradient perpendicular of the electrical current. (a) $3WJ_{2'\text{-}F}$, (b) $3WJ_{RNA}$, and (c) $3WJ_{DNA}$; total 3WJ concentration in each lane = 10 μM. (d) and (e) are control gels showing migration of $3WJ_{RNA}$ (d) before reaching its T_m in the temperature range of 20-40°C and migration of $3WJ_{DNA}$ (e) in the temperature range of 40-70 °C that is over its T_m. The 3WJ bands were detected by total nucleic acid stain with EB.

found by the fluorescence melting curves, but there was a large difference in T_m between the two methods for the $3WJ_{DNA}$. This difference between these two methods was presumably due to differing affinities of SYBR Green II to DNA and RNA stacking bases (197). Nevertheless, both methodologies produced data that allowed direct comparison of the stability among 3WJ complexes, and demonstrated the trend that 2′-F RNA had a higher melting temperature than RNA, and RNA had a higher T_m than DNA.

Within the TGGE melting gels, the dimer species were again undetected in the melting curves in the 2′-F RNA and RNA 3WJ species, further pointing to the possibility of the unusual assembly pathway. However, the $3WJ_{DNA}$ seemed to display a dimer intermediate, which was previously not seen from the PCR melting profiles. We believe that this difference between the two temperatures is due to the fact that the TGGE showed the melting profile, while the PCR curves showed the association of the molecules. Therefore the TGGE system of the DNA species was dissociation down to a dimer then monomer, possibly due to the fact that DNA was not the natural species of the pRNA-3WJ and forced the motif into an unnatural conformation. Furthermore, any dimer species that is seen in radiolabeled gel analysis can be attributed a slight concentration mismatch between unlabeled individual strands, and were therefore ignored.

Thermodynamic parameters for 3WJs formation

Non-self complementary nucleic acids usually exhibit a linear correlation T_m and RNA concentration, as the T_m increased with the increase in nucleic acid strands concentration (146,148,202). The TGGE approach was further applied to measure T_m of 3WJ species as a function of concentration using ~1,000 fold dilution of the $3WJ_{RNA}$, $3WJ_{2'-F}$, and $3WJ_{DNA}$ complexes from 10 μM to 0.016 μM (**Fig. 2.6A**). T_ms were

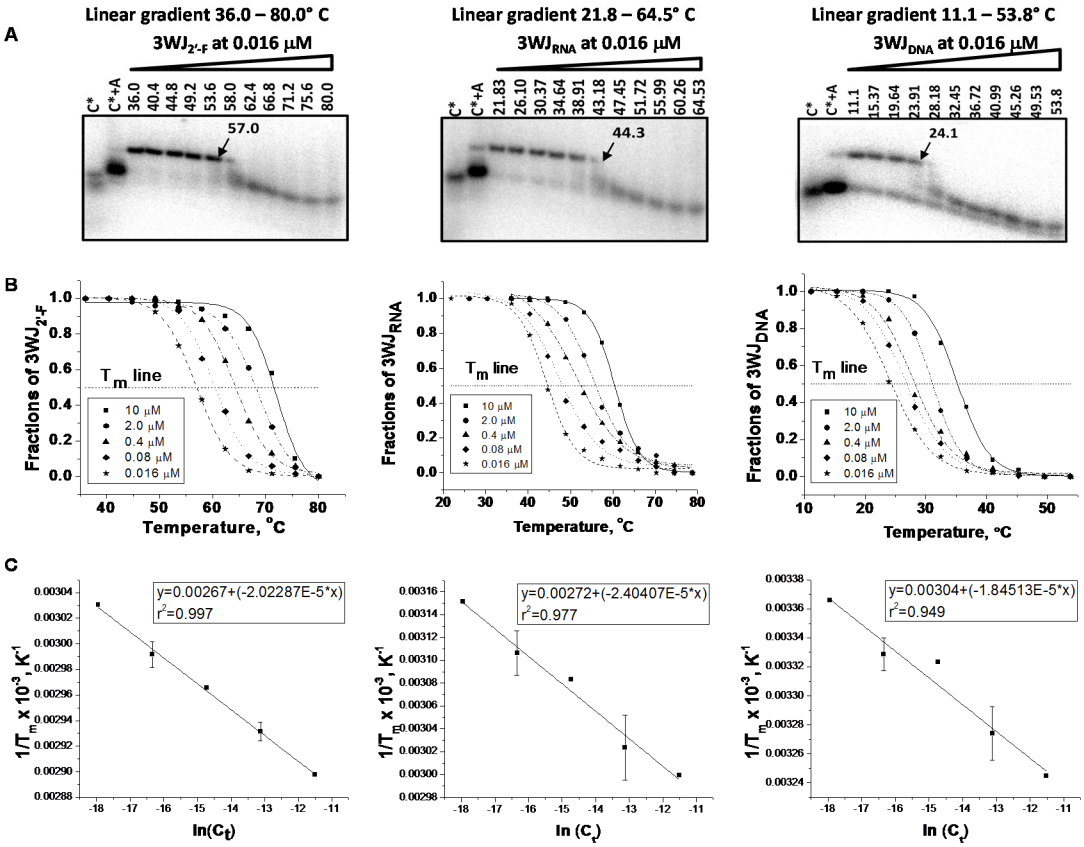

Figure 2.6. Calculation of thermodynamic parameter for 3WJs formation. (a) Representation of native 15 % TGGE for the 3WJ complexes at the lowest concentration (0.016 μM in each lane). The radiolabeled C strand of corresponding 3WJ complexes indicated with asterisk '*'. Lanes $3WJ_c$* and $3WJ_c$*+$3WJ_a$ served as controls for monomer and dimer location. (b) Melting temperature profiles of RNA, 2′-F RNA, and DNA 3WJs obtained after quantification of the corresponding band from the perpendicular TGGE at various concentrations. (c) Plots of T_m vs. 3WJ concentrations (van't Hoff analysis) evaluated from melting curves of the 3WJ complexes obtained at different strand concentrations.

calculated by finding the temperature at which 50% of the nucleic acids were in trimer formation compared to the total concentration of the bands observed. 3WJ T_ms were used to calculate thermodynamic parameters for three components of non-self complementary sequences, according to Marky et al. (191). The typical van't Hoff plots for $3WJ_{2'\text{-}F}$, $3WJ_{RNA}$, and $3WJ_{DNA}$ are represented in **figure 2.6C**. From the obtained ΔH° and ΔS° parameters the $\Delta G°_{37}$ was calculated using equation 2.3:

$$\Delta G^{\circ}_{37} = \Delta H^{\circ} - (310.15K)\Delta S^{\circ} \qquad (2.3)$$

where ΔH° and ΔS° are enthalpy and entropy, respectively, and K is the abbreviation for Kelvin. All thermodynamic parameters are summarized in **table 2.1**. Here the data produced a near linear trend lines with r^2 values very near 1.00. Due to this little error is seen in calculating melting temperatures, samples were repeated in a selective fashion due to the high number of gels that would be needed. The repeated experiments allowed for calculation of error in the thermodynamic parameters which remained low. The results indicated that the most thermodynamically stable was the $3WJ_{2'\text{-}F}$ ($\Delta G°_{37}$ = -36 kcal/mol) complex, followed by $3WJ_{RNA}$, ($\Delta G°_{37}$ = -28 kcal/mol), and the $3WJ_{DNA}$ ($\Delta G°_{37}$ = -15 kcal/mol). Based on the parameters of free energy change for RNA and 2′-F RNA-3WJ assemblies, it can be determined that the energy for these complexes were favored two-fold compared to the $3WJ_{DNA}$. The $3WJ_{DNA}$ displayed a more favorable decreased enthalpy value of ΔH° = -220 kcal/mol, compared to $3WJ_{2'\text{-}F}$ (ΔH° = -200 kcal/mol), and $3WJ_{RNA}$ (ΔH° = -170 kcal/mol). However, the comparison of entropy parameters resulted in a significant increase for the RNA and 2′-F RNA complexes. The two RNA species resulted in more negative free energy changes, yet had higher enthalpies when compared to DNA. This data combined with the increased entropy

Table 2.1. Thermodynamic parameters for 3WJs formation.[a]

3WJs	$1/T_m$ vs Log (C_t)			
	$\Delta G°_{37}$ (kcal/mol)	**$\Delta H°$ (kcal/mol)**	**$\Delta S°_{37}$ (e.u.)**	**T_m[b] (°C)**
2'-F RNA	-36 ± 0.45	-200 ± 5.7	-520 ± 17	72.1
RNA	-28 ± 0.58	-170 ± 13	-440 ± 39	60.4
DNA	-15 ± 0.71	-220 ± 25	-650 ± 83	35.2

[a]Parameters derived from 15% native TGGE.

[b]T_m values for 3WJ strand concentrations of 10^{-6} M

values of the RNA species indicated that the thermodynamic stabilities of the $3WJ_{RNA}$ and $3WJ_{2'\text{-}F}$ were entropy-driven (**Table 2.1**).

The findings of more negative ΔG° values for 2′-F RNA and RNA are consistent with other studies comparing helical DNA, RNA, and 2′-F RNA (150,151,153,199,203). However, the notion that was RNA entropically driven, compared to DNA in helical structures appeared less unanimous as the majority report RNAs to be less entropically favored and that folding is normally driven by a lower enthalpy value (150,151,153,203). Here it is believed that the $3WJ_{DNA}$ provided a more rigid structure, producing a lower internal energy or ΔH compared to the RNAs; however, the flexibility of the RNAs provided more disorder, thus giving strong stability, ease of folding, and a more negative ΔG°. This entropy driven assembly combined with the one step assembly expresses the unusual thermodynamic characteristics of the pRNA-3WJ.

Analysis of 3WJ hybrid formations and thermostability

The hybrid composition (2′-F RNA/RNA; RNA/DNA; DNA/2′-F RNA) within the RNA 3WJs are of great interest due to their ability to maintain the diverse functionality of structured RNA molecules, while incorporating the chemical stability of 2′-F RNA and DNA. To test for hybrid 3WJ viability, the 2′-F RNA/RNA; RNA/DNA; DNA/2′-F RNA hybrids of the 3WJs complexes were characterized by parallel TGGE and fluorescence melting temperature experiments. Using the TGGE, a temperature gradient was applied in parallel to the electrical current (**Fig 2.7**). As the samples migrated through the gel, the temperature increased from 20 °C to 70 °C; therefore, melting the hybrid structures as they migrated further into the gel. A less stable 3WJ complex migrates further as the elevated temperature melts the structure to smaller single

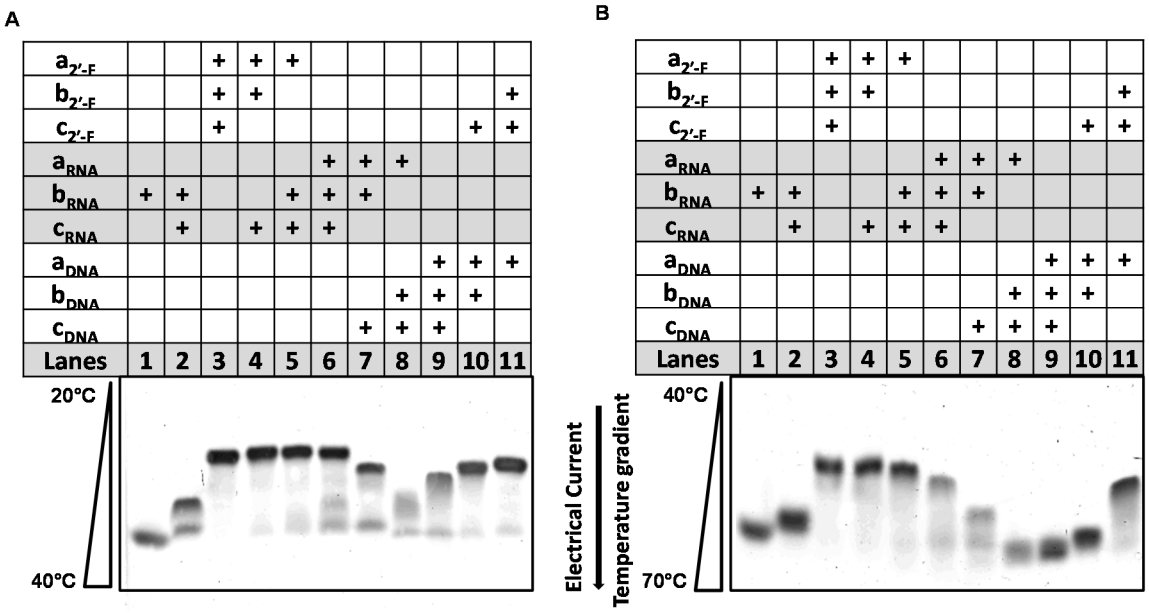

Figure 2.7. Native 15% TGGE of some hybrid 3WJs with temperature gradient in parallel of the electrical current. As the 3WJs migrated into the gels, weaker structures melted due to the elevating temperatures, resulting in a more rapid migration; stable structures migrated at slower rates. Concentration of hybrids in each lane = 10 μM, the bands were detected by total nucleic acid stain with EB. (a) Hybrids analyzed in linear temperature gradient of 20 – 40 °C and (b) the same samples but the temperature range was 40-70 °C.

strands, thus causing an increased rate of migration and separating the stable hybrids from unstable hybrids.

The TGGE analysis demonstrates that each hybrid structure forms correctly and is stable at lower temperature ranges 20-40 °C (**Fig. 2.7A**). However, at a higher range of 40-70 °C the RNA/DNA and DNA/2′-F RNA-3WJ hybrid structures melted, resulting in a more rapid migration rate compare to 2′-F RNA/RNA hybrids (**Fig. 2.7B**). This direct comparison between hybrid stability demonstrates weakness in the thermostability of hybrids involving DNA strands. In addition, the 3WJs hybrids followed the general trend that more strands with 2′-F modifications equate to a higher stability overall. These results were further confirmed by the melting temperatures produced for each hybrid on the Roche 480 Lightcycler as shown in **figure 2.8** and **table 2.2**. Combining the TGGE gels along with the annealing temperatures provided from the fluorescence melting curves, the data further supports the findings that 2′-F modifications strengthen the thermostability of the pRNA-3WJ while DNA substitutions only weaken the 3WJ complex. In this case, even limited modifications lead to a difference in the thermostability.

MG-aptamer functionality assay and stability

In order to ensure that the added stability of the 2′-F modifications to the pRNA-3WJ was true for a functional, more complex RNA nanoparticle, a fluorescence assay was performed. The pRNA-3WJ used in this study harbored the Malachite Green (MG) RNA aptamer that binds to Malachite green triphenylmethane dye causing the chemical to fluoresce (204). Malachite green itself emits very low fluorescence; therefore, a change

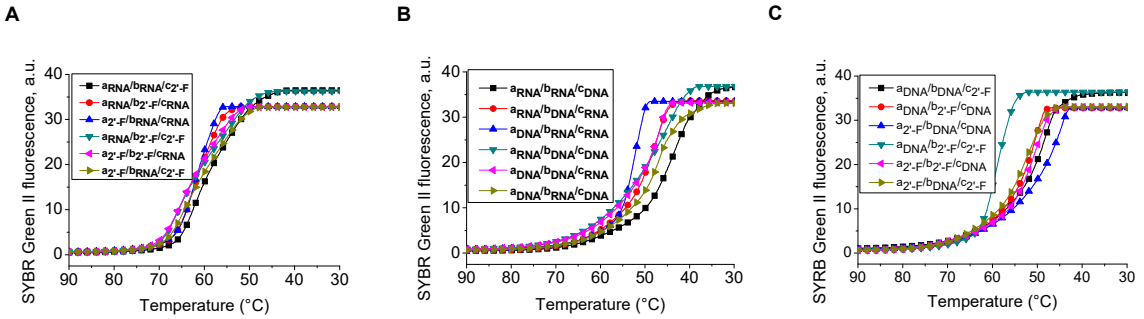

Figure 2.8. Comparison of pRNA-3WJ hybrid structures. Assembly curves produced from the Roche 480 Lightcycler of the pRNA-3WJ (a) RNA/DNA hybrids, (b) RNA/2′-F RNA hybrids, and c) DNA/2′-F RNA hyrbids.

Table 2.2. Annealing temperature for 3WJ hybrid formation.[a]

2′-F RNA to RNA	T_a (°C)	RNA to DNA	T_a (°C)	DNA to 2′-F RNA	T_a (°C)
$a_{2'\text{-}F}/b_{2'\text{-}F}/c_{2'\text{-}F}$	69.8±2.0	$a_{RNA}/b_{RNA}/c_{RNA}$	59.3±1.7	$a_{DNA}/b_{DNA}/c_{DNA}$	48.9±3.2
$a_{2'\text{-}F}/b_{2'\text{-}F}/c_{RNA}$	65.4±0.1	$a_{RNA}/b_{RNA}/c_{DNA}$	42.6±2.2	$a_{DNA}/b_{DNA}/c_{2'\text{-}F}$	48.4±1.6
$a_{2'\text{-}F}/b_{RNA}/c_{2'\text{-}F}$	64.1±0.2	$a_{RNA}/b_{DNA}/c_{RNA}$	48.6±1.5	$a_{DNA}/b_{2'\text{-}F}/c_{DNA}$	51.6±0.4
$a_{RNA}/b_{2'\text{-}F}/c_{2'\text{-}F}$	65.5±0.2	$a_{DNA}/b_{RNA}/c_{RNA}$	53.1±0.1	$a_{2'\text{-}F}/b_{DNA}/c_{DNA}$	47.2±1.5
$a_{2'\text{-}F}/b_{RNA}/c_{RNA}$	62.1±0.1	$a_{RNA}/b_{DNA}/c_{DNA}$	44.5±2.6	$a_{DNA}/b_{2'\text{-}F}/c_{2'\text{-}F}$	59.5±0.2
$a_{RNA}/b_{2'\text{-}F}/c_{RNA}$	62.7±0.2	$a_{DNA}/b_{RNA}/c_{DNA}$	45.9±2.4	$a_{2'\text{-}F}/b_{DNA}/c_{2'\text{-}F}$	52.4±0.6
$a_{RNA}/b_{RNA}/c_{2'\text{-}F}$	61.9±0.4	$a_{DNA}/b_{DNA}/c_{RNA}$	47.3±0.4	$a_{2'\text{-}F}/b_{2'\text{-}F}/c_{DNA}$	51.2±1.8

[a] Annealing temperatures calculated at 10 μM total strand concentration in TMS buffer.

in the fluorescence can be used to confirm binding and complexation between the RNA aptamer and chemical (69,198,204,205).

It has been previously shown that the MG aptamer remains active in binding when nucleotides remain unmodified, as well as when using 2′-F cytosine and adenine modified nucleotides (198). Therefore we constructed the pRNA-3WJ-MG using unmodified RNA strands and 2′-F A/C modified RNA strands (see **Fig. 2.9A** for 2D structure). The resulting particles were then tested for binding to the MG to show the folding and functionality of the MG aptamer by measuring its fluorescence emissions (**Fig. 2.9B**). Both nanoparticles showed almost identical fluorescence values indicating the formation of correctly folded structures.

Further we used real time PCR to measure the T_a of pRNA-3WJ-MG and 3WJ-$MG_{2'\text{-}F}$ constructs (**Fig. 2.9C**). The annealing curves show that the 2′-F A/C modified 3WJ resulted in the annealing temperature of 69.7 °C, higher than unmodified RNA variant with T_a value of 62.8 °C. This is consistent with the trend of increased RNA 3WJ stability using 2′-F modifications. Thus, the data demonstrate the effectiveness of the fluorine modifications regardless of the complexity of the structure, while retaining the functional conformation of the pRNA-3WJ.

CONCLUSIONS:

In this chapter we obtained thermodynamic parameters for the pRNA-3WJ using real time PCR and TGGE approaches. It was seen that the three fragments existed either in 3WJ complex or as monomers, with the intermediate of dimers almost undetectable. It seems that the three fragment can lead to the formation of 3WJ complex efficiently within a rapid time. It is also found that the formation of the three-component complex

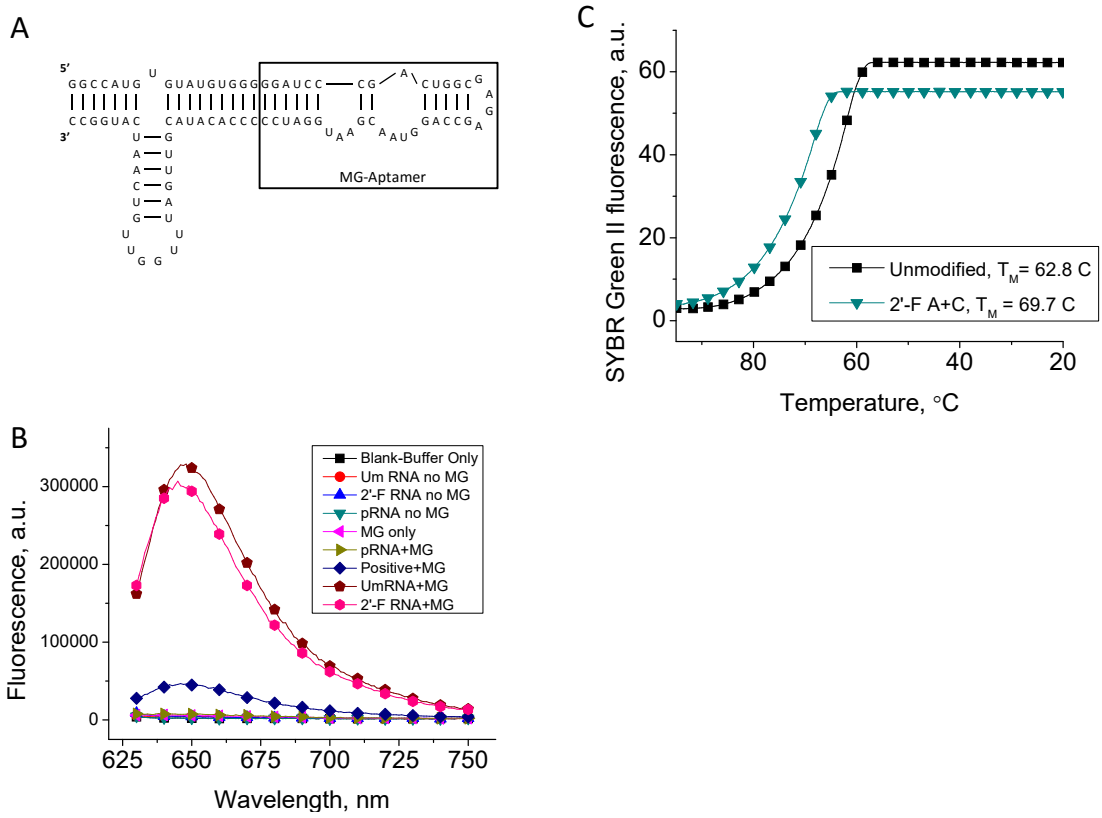

Figure 2.9. Thermo-stability of functional pRNA-3WJ nanoparticle. (a) Secondary structure and sequence of the 3WJ-MG aptamer. (b) Fluorescence emission of 3WJ-MG aptamer, demonstrating binding of the nanoparticle to MG in both RNA and 2′-F species. (c) Melting curves for the 3WJ-MG and 2′-F A/C RNA-3WJ.

was governed by entropy, instead of enthalpy, as usually found in RNA complexes. By combining this beneficial assembly with the improved thermodynamic characteristics by 2′-Fluoro modifications to the pRNA-3WJ stable RNA nanoparticles can be constructed with a high yield of over 90%for the treatment of cancers and viral infections.

ACKNOWLEDGMENT:

The authors would like to thank Jeannie Haak for help in preparing this manuscript and Zhengyi Zhao for help in preparing figures.

FUNDING SOURCE:

This research was supported by NIH grants EB003730 and CA151648 to P.G. The content is solely the responsibility of the authors and does not necessarily represent the official views of NIH. Funding to Peixuan Guo's Endowed Chair in Nanobiotechnology position is by the William Fairish Endowment Fund. P. Guo is a co-founder of Kylin Therapeutics, Inc., and Biomotor and RNA Nanotechnology Development Corp. Ltd.

Chapter 3: Kinetic Evaluation of pRNA-3WJ Folding

This chapter (with some modification) is in submission at *Journal of Biological Chemistry*. Special thanks to Dr. Janice Ortega for help and assistance in preparation of data for figures 3.2, 3.3, 3.5 and Dr. Emil F. Khisamutdinov for help in preparation of data for figure 3.4.

INTRODUCTION:

The field of RNA nanotechnology has recently undergone rapid expansion mainly due to the fact that RNA has the simplicity characteristic of DNA yet the versatile functionality of proteins (86,91,128,157,159,172-175). With the combination of the advantage of these two materials, RNA can easily be designed and constructed through bottom-up construction and plays diverse roles (86,97). The wide-ranging functionalities of RNA makes it a prime candidate for applications in sensing operates (206), logic gate computional parts (207-214), imaging reagents (215-218), nano-electro-mechanical devices (219), and therapeutics including the delivery, specific targeting, and treatment of cancer and viral infections (12,38,86,87,118,123,176-182). The use of RNA as a delivery vehicle provides several benefits over other systems and technologies. Firstly, RNA nanoparticles can be produced with known stoichiometry and high reproducibility (12,86-88,124-126), as RNA is composed of simple building blocks with predictable secondary structure. RNA aptamers can be employed for specific targeting of cell groups through binding to cell surface receptors much like a protein ligand or antibody (113-115). Furthermore the replacement of protein targeting reagents with nucleic acids prevents the induction of antibody (113), allowing for repeated administration. RNA nanoparticles are

typically between 10 and 50 nanometers in size meaning they are retained in the human body, yet are small enough to pass through cell membranes through endocytosis (66-68,68,69,125,126,183). In *in vivo* testing RNA nanoparticles have shown favorable pharmacokinetic and biodistribution properties, as they are able to avoid accumulation in healthy organs and tissues with efficient retention in tumors (87,123), which is further expanded upon in Chapter 4. Additionally, RNA possesses unique *in vivo* attributes such as transcription, termination, splicing and processing allow for *in vivo* RNA production; riboswitches (95,96) and ribozymes (92-94) result in *in vivo* processing and possible assembly into nanoparticles in cell for special function such as intracellular computation (207-214)}; RNA can self-assemble without external forces (208); and RNA is stable in acidic environments allowing for survival in endosome (112). Even with these advantages, RNA nanotechnology still has many hurdles that it must overcome in order to be employed in therapeutics. Most notably, RNA is known to have stability issue and is prone to degradation by RNase that has since been solved through backbone modifications, such as 2'-Fluoro (189,220), 2'-OMethyl (221), or Locked nucleotides (222). The dissociation of the self-assembled RNA nanoparticles at low concentrations and elevated temperatures at *in vivo* environments makes it obligatory to address the dynamic and kinetics issues in RNA nanoparticle assembly (120,146,149,150,184-188).

Recently a novel ultra-stable RNA motif was found in the packaging RNA (pRNA) of the Phi29 dsDNA packaging motor (**Fig. 3.1**), that has since diminished the concerns of RNA nanoparticles dissociating at low concentrations found *in vivo* because of its unusually high thermostability (87). This motif is a three way junction (3WJ) that serves as the central core structure of the pRNA and connects the helical domain (192)

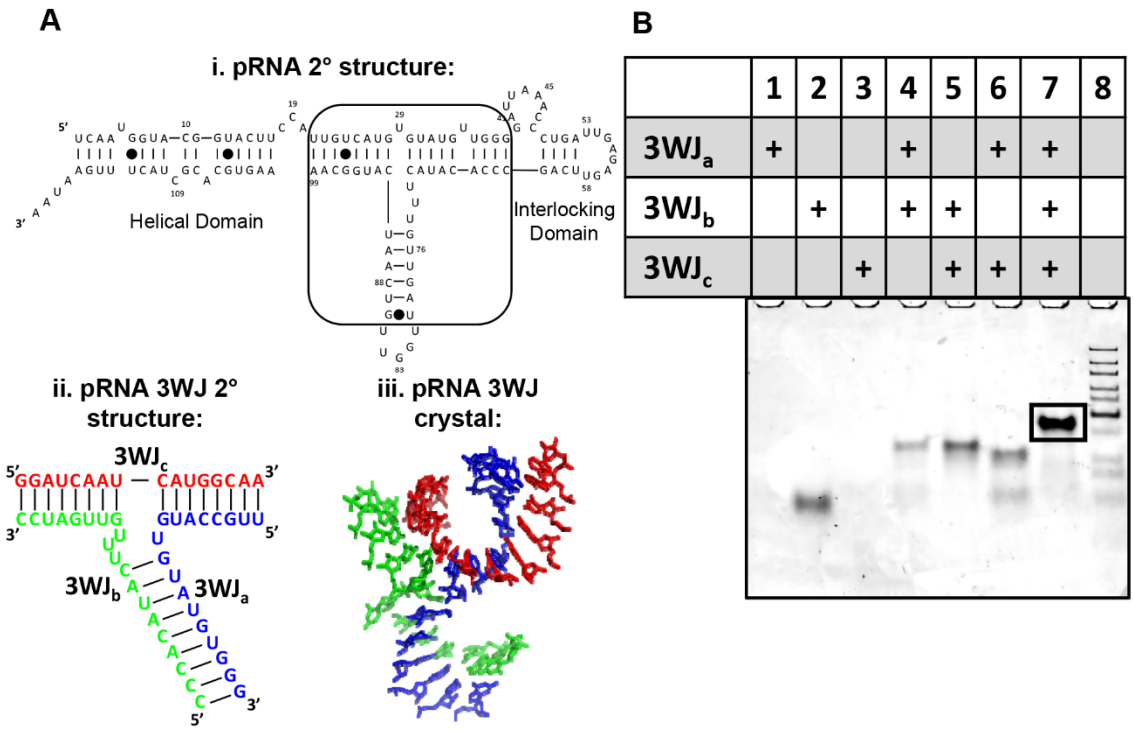

Figure 3.1: Overview of the Phi29 pRNA and the three-way junction (3WJ). (A) i) Secondary structure of the Phi29 pRNA monomer with the pRNA-3WJ outlined by the box which connects the helical domain to the interlocking procapsid binding domains. ii) Secondary structure and sequence of the pRNA-3WJ and the iii) crystal structure of the pRNA-3WJ. (B) Assembly gel of the pRNA-3WJ from the three short RNA oligo strand on 12% Native PAGE. The 3WJ (lane 7) shows efficiency of folding and particle homogeneity before purification.

with the two interlocking looped regions of the pRNA (193). It has been determined that the 3WJ serves as the central folding domain and provides the overall high stability seen in pRNA (87,122). The motif can be formed from three individual RNA oligos at a high yield even in the absence of metal ions (87). The novelty behind this structure is in the ease of formation and the produced melting curve with a remarkably low Gibbs free energy (ΔG) of -28 kcal/mol and a high melting temperature (T_m) of 59.3 °C (223). Furthermore it has been proven that the pRNA 3WJ allows the inclusion of RNA functional moieties such as receptor-binding aptamer, siRNA, ribozyme, miRNA or riboswitch, resulting in the production of functional nanoparticles (87,137,139). The addition of functional groups did not interfere with the proper folding of the 3WJ or the added functional moieties (87). Previously, attempts have been made to elucidate the mechanism for the kinetic stability of the pRNA-3WJ, yet the 3WJ was found to be too stable to detect its dissociation by the current technology of radioactive chasing (87).

The understanding of the mechanism of assembly of the pRNA-3WJ and the interaction of the RNA strands is of fundamental importance, but the study of three component collisions have not been well-studied in chemistry, biology, or material sciences. Here, we investigated the kinetic properties of the pRNA-3WJ using Surface Plasmon Resonance (SPR) to study its association and disassociation using bottom-up construction RNA nanotechniques. We provided real-time examination of three component collision of the pRNA-3WJ. Through these studies, the pRNA-3WJ proves to be ultra-stable and only disassociate at extremely low concentration that are atypical to other well-studied double-stranded RNA or dimeric macromolecules. Furthermore, the

pRNA central motif relies heavily on each of the three strands for rapid folding and slow dissociation rates.

MATERIALS AND METHODS:

Oligonucleotides and Assembly of 3WJs

The pRNA-3WJ was constructed from three RNA oligo fragments. RNA strands were produced by Integrated DNA Technologies (IDT). Assembly of the pRNA-3WJ was completed by mixing each of the three RNA strands ($3WJ_a$, $3WJ_b$, $3WJ_c$) at equal molar concentrations at room temperature in TMS buffer (50 mM Tris pH = 8.0, 100 mM NaCl, 10 mM $MgCl_2$). Samples were then ran on a 12% native polyacrylamide gel at 100 V for 2 hrs at 4 °C in TBM running buffer (89 mM Tris, 200 mM Borate acid, and 5 mM $MgCl_2$) to ensure pRNA-3WJ proper size folding.

Surface Plasmon Resonance (SPR) Studies of the pRNA 3WJ

The BioRad ProteOn XPR36 was used to complete real time interaction studies of the pRNA-3WJ motif. A neutravidin coated HLC chip (BioRad) was used to immobilize one of the three 3WJ strands with a 5' biotin labeled strand of the 3WJ. Several studies were completed by immobilizing the $3WJ_a$ and $3WJ_c$ strand to the chip surface, followed by injection and interaction of the remaining two 3WJ strands. All studies were conducted at room temperature and in TMS buffer (50 mM Tris pH = 8.0, 100 mM NaCl, 10 mM $MgCl_2$) with added 0.1% Tween. RNA strands were injected at a concentration ranging from 20.0 μM to 78.0 nM at a constant flow rate of 25 μL/min for a total of 660 sec, making the analyte RNAs in high excess as an association phase followed by injection of blank TMS buffer for 2700 sec at 25 μL/min as a dissociation

phase. Real time association and disassociation was observed and displayed into a histograph of total response (relationship on mass on chip surface) and time.

SPR studies of the pRNA 3WJ dimers

Utilizing a similar approach as the pRNA-3WJ, the formation and dissociation of dimers from the pRNA-3WJ were analyzed. In order to remain consistent in the studies, the same concentration gradients were used to examine the formation of two of the three strands coming together within the three way junction.

Kinetic modeling of Surface Plasmon Data

Data were extracted from the BioRad ProteOn XPR36 and modeled using Igor Pro 6.37. The association periods of the SPR plots were modeled using a Langmuir pseudo first-order model consisting of two and three components using the equation 3.1 and 3.2, respectively. The dissociation of all RNA motifs were modeled using a Langmuir zero-order reaction as shown in equation 3.3.

$$R = \frac{k_a[3WJ_a]_o R_{max}}{k_a[3WJ_a]_o + k_d}\left(1 - e^{-(k_a[3WJ_a]_o + k_d)(t - t_o)}\right) \quad (3.1)$$

$$R = \frac{k_a[3WJ_a]_o^2 R_{max}}{k_a[3WJ_a]_o^2 + k_d}\left(1 - e^{-(k_a[3WJ_a]_o^2 + k_d)(t - t_o)}\right) \quad (3.2)$$

$$R = R_o e^{-k_d(t - t_o)} \quad (3.3)$$

Where R is the response of the SPR in terms of t, time in sec. These kinetic models are derived in Appendix 1. In fitting the data, the global fitting package was used in linking the association and dissociation of each sample through the k_d and R_{max} and R_o.

Calculation of time constant (τ) for complex assembly of pRNA-3WJ$_a$, 3WJ$_b$, and 3WJ$_c$

The time constant (τ) of the pRNA-3WJ core strand was studied through Electrophoresis Mobility Shift Assays (EMSA). Single strand of the pRNA-3WJ fragments was radio labeled using 5′-end using γ-32P ATP (Perkin Elmer), denoted with an asterisk, as previously described (223). The radio labeled oligo was then held at a constant concentration of 10 nM and incubated over varying time points ranging from 0 – 720 min with completed pRNA-3WJ structure at 100 nM concentrations. Samples were snap frozen on dry ice and then ran in a 12% polyacrylamide native gel at 100 V for 2 hr at 4 °C in TBM running buffer. The gel was then imaged by transferring the radio signal to a phosphor screen for 12 hr at -80 °C and visualized using a Typhoon 7000 (GE). Band quantification was completed using OriginPro 8.5. The ratio of single strand to 3WJ was then calculated and plotted against time. The curve was fitted using equation 3.4 below:

$$[3WJ_x] = [3WJ_x]_o \cdot e^{-t/\tau} \tag{3.4}$$

Where t is the time in seconds and τ is the time constant at which 50% of the labeled 3WJ strand was in single strand state and 50% had replaced unlabeled strand in the 3WJ complex (196).

RESULTS AND DISCUSSION:

Determination of Kinetic Parameters of the pRNA-3WJ

The BioRad ProteOn XPR36 allows for real time monitoring and analysis of molecule association and disassociations. Through the real time analysis, we are able to calculate the disassociation constant (defined as K_D) by measuring the rates of the chemical reactions moving toward the completed 3WJ and the disassociation to single RNA strands.

Through classic definitions of kinetics, all chemical reactions are viewed to reach equilibrium where there is a balance in the production of products and reactants. In the case of the pRNA three way junction, a single step chemical reaction is described as the equation below:

$$3WJ_a + 3WJ_b + 3WJ_c \underset{k_d}{\overset{k_a}{\rightleftharpoons}} 3WJ \tag{3.5}$$

and the rate of reaction forming pRNA-3WJ can be written as:

$$\frac{d[3WJ]}{dt} = k_a[3WJ_a][3WJ_b][3WJ_c] - k_d[3WJ] \tag{3.6}$$

Where k_a is the rate constant of the reaction moving toward the formation of the pRNA-3WJ and the k_d is the rate constant of the reaction moving toward the reactants or individual strands of RNA expressed as $M^{-2}s^{-1}$ and s^{-1}, respectively. At equilibrium these rates of reactions forward and backward are equal to each other, creating a balance between the formation of the pRNA-3WJ and single stranded RNA. Together the two rate constants can be combined to define the disassociation and association constant.

$$K_D = \frac{k_d}{k_a} \text{ and } K_A = \frac{k_a}{k_d} \tag{3.7}$$

Based on previous experiments it was believed that the pRNA-3WJ was undergoing a single association and dissociation step following what is seen in equation 3.5 (87,223). Using SPR, association and disassociation of the pRNA-3WJ was examined by binding the $3WJ_a$ strand to the chip surface acting as the ligand followed by co-injecting $3WJ_b$ and $3WJ_c$ strands acting as analytes. A single transition is seen in the association over a range of concentrations from 20 μM to 78 nM. As a result the data was fit with a Langmuir three component pseudo-first order model, solving for the reaction

rate constants (**Fig. 3.2A-B**). In these experiments a relatively constant dissociation averaging to $4.52x10^{-05}$ s^{-1}; this value is within what is expected values of biological samples. However, it was seen that the association rate of the pRNA-3WJ was seen constant across tested concentrations of 20 to 0.078 μM, thus leading to varying k_a values. This clearly negates first-order chemical reactions and indicates error in the assembly kinetic parameters.

Calculation of K_D of the pRNA-3WJ dimers

In order to confirm RNA/RNA interactions on the SPR chip, dimers of the pRNA-3WJ were tested and assembled (**Fig. 3.3, Table 3.1**). In each of the dimer interactions ($3WJ_{ab}$, $3WJ_{ac}$, and $3WJ_{bc}$) Proper association and dissociation periods were produced. Furthermore, once the data was fit with a pseudo-first order Langmuir model, it was seen that each of the produced k_as and k_ds produced were constant and concentration independent. This means the pRNA-3WJ dimers were forming properly on the chip surface. Interestingly, in comparing the association rate constants of each of the dimer species, the $3WJ_{bc}$ dimer produced the most rapid on rate with a k_a of ~$1.35x10^{05}$ $M^{-1}s^{-1}$, this is nearly an order of magnitude higher than either the $3WJ_{ab}$ or $3WJ_{ac}$ dimers. Furthermore, one would predict the $3WJ_{ab}$ dimer to produce the most rapid association rate as the dimer helix consists of 9 base pairs compared to the 8 base pairs seen in the $3WJ_{bc}$ dimer (**Fig. 3.1A**). In comparing the dissociation rate constants (k_d) of the dimers, the $3WJ_{ab}$ dimer is seen to be the most stable (~$6.78x10^{-05}$ s^{-1}) followed by $3WJ_{ac}$ with a k_d of ~$6.33x10^{-04}$ s^{-1} and finally the weakest dimer being the $3WJ_{bc}$ (~$3.95x10^{-03}$ s^{-1}). This indicates the $3WJ_{bc}$ dimer not only would form the quickest by also dissociate the most rapidly.

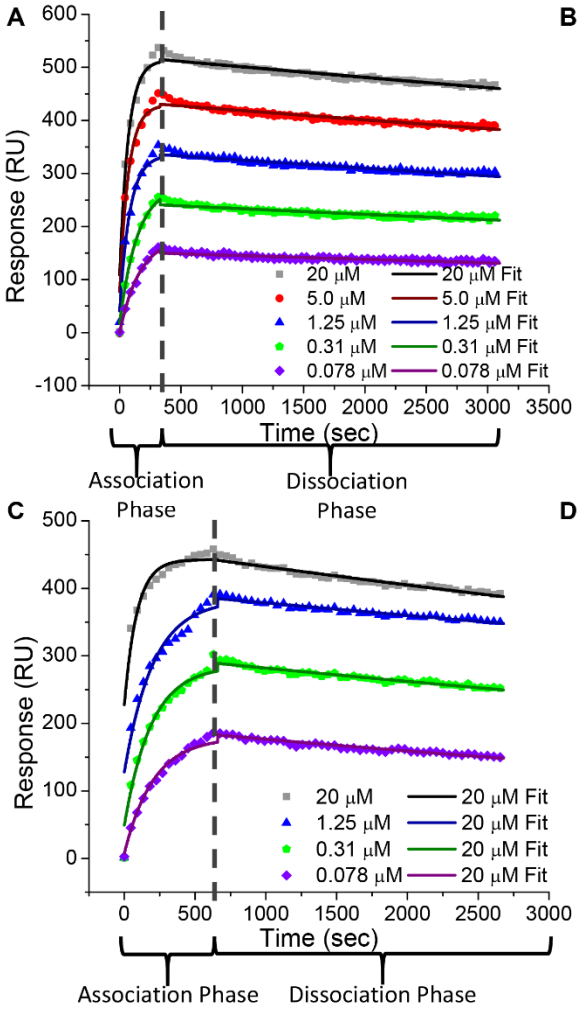

B

	k_a ($M^{-2}s^{-1}$)	k_a Error	k_d (s^{-1})	k_d Error	K_D (M^2)	K_A (M^{-2})
	3.58E+07	1.87E+05	4.07E-05	2.18E-07	1.14E-12	8.79E+11
	5.52E+08	2.17E+06	4.24E-05	2.35E-07	7.67E-14	1.30E+13
	7.75E+09	1.14E+07	4.77E-05	2.37E-07	6.15E-15	1.63E+14
	7.13E+10	6.64E+08	4.61E-05	4.73E-07	6.46E-16	1.55E+15
	9.96E+11	1.67E+10	4.91E-04	4.04E-07	4.29E-17	2.03E+16

D

	k_a ($M^{-}s^{-1}$)	k_a Error	k_d (s^{-1})	k_d Error	K_D (M)	K_A (M^{-1})
	5.59E+02	9.02E+00	6.46E-05	8.54E-07	1.16E-07	8.65E+06
	3.88E+03	5.63E+01	5.00E-05	8.54E-07	1.29E-08	7.77E+07
	1.67E+04	8.66E+01	7.23E-05	7.18E-07	4.33E-09	2.31E+08
	4.11E+04	3.91E+02	9.66E-05	6.48E-07	2.35E-09	2.15E+08

Figure 3.2: Surface Plasmon Resonance (SPR) of the pRNA-3WJ. A) Assembly of the 3WJ of three component strands. 5'-Biotin labeled $3WJ_a$ was first immobilized to the SPR chip surface. $3WJ_b$ and $3WJ_c$ strands were mixed at equal, varying concentrations, ranging from 20 μM to 78 nM, and injected across the chip surface for 330 sec (association phase). Following the interaction of the 3WJ strands, blank TMS buffer was injected across the chip surface for 2700 sec (dissociation phase). The association and dissociation curves were fit using a A) three-component pseudo-first order model. B) Calculated Kinetic parameters from SPR curve following a three component pseudo-first order kinetic model. C) SPR assay for pRNA-3WJ under assumption of previous dimer

formation data. 5'-Biotin labeled $3WJ_a$ was first bound to the SPR chip surface. $3WJ_b$ and $3WJ_c$ strands were mixed at equal, varying concentrations, ranging from 20 μM to 78 nM, were injected across the chip surface for 660 sec followed by blank TMS buffer for 2700 sec. Association and dissociation curves were fit using a two component pseudo-first order model. D) Kinetic parameters from SPR curves following a two-component pseudo-first order kinetic model.

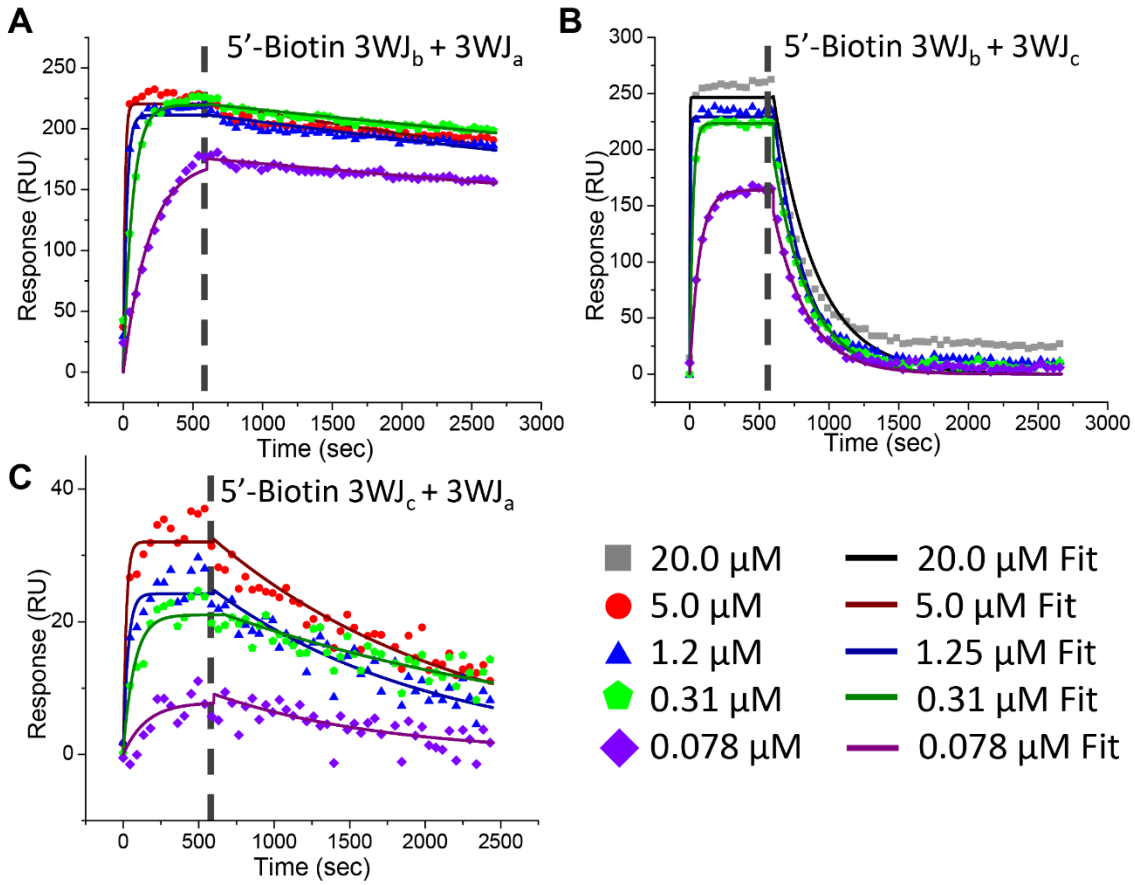

Figure 3.3: SPR assay for pRNA-3WJ dimers. Dimer species that make up the pRNA-3WJ were examined through SPR at varying concentrations ranging from 20 µM to 78 nM. The injected RNA strand was injected for 660 sec (association phase) followed by blank TMS buffer for 2700 sec (dissociation phase). The histographs were then fit using a two-component pseudo-first order Langmuir model for A) bound 5'-Biotin 3WJ$_b$ and 3WJ$_a$, B) bound 5'-Biotin 3WJ$_b$ and 3WJ$_c$, C) bound 5'-Biotin 3WJ$_c$ and 3WJ$_a$.

Table 3.1: Kinetic parameters of pRNA-3WJ dimer species

Ligand	Analyte	k_a ($M^{-1}s^{-1}$)	k_a Error	k_d (s^{-1})	k_d Error	K_D (M)	K_A (M^{-1})
$3WJ_b$	$3WJ_a$	4.18E+04	2.55E+02	6.78E-05	2.71E-07	2.30E-09	6.73E+08
$3WJ_c$	$3WJ_a$	3.59E+04	1.37E+03	6.34E-04	8.86E-06	2.71E-08	6.17E+07
$3WJ_b$	$3WJ_c$	1.37E+05	6.31E+03	3.95E-03	1.95E-05	2.88E-08	3.49E+07

Next in hopes of gaining insight in the assembly mechanism of the pRNA-3WJ, the association rates of the dimer species were compared to the association rate of the tested three component one step reaction of the pRNA-3WJ. This was completed by calculating association rates (k_a') by taking the fitted rate constants and multiplying by the concentration of the studied interaction resulting in an s^{-1} unit (**Table 3.2**). It is important to note that the pRNA-3WJ was multiplied by a concentration squared value while dimers only by concentration due to the difference in units of the k_as. Surprisingly, it is seen that the pRNA-3WJ produces a rates of reaction on average an order of magnitude below the $3WJ_{bc}$ dimer. This would indicate the formation of the dimer species is occurring before the formation of the pRNA-3WJ, thus creating an intermediate step that was previously not seen through thermodynamic studies (223).

Determination of time constants of each pRNA-3WJ strand

To further gain insight on the formation of a dimer species and the unusual formation of the shorter 8 base helix between the $3WJ_b$ and $3WJ_c$ strands, kinetic studies were completed on each of the individual pRNA-3WJ strands. Using a time based strand replacement EMSA, time constants were calculated for each of the RNA strands in order to examine which, if any of the strands, provides the stability to the 3WJ core. The results show that the $3WJ_a$ and $3WJ_b$ strands produce a similar τ of 38.89 min and 35.93 min, respectively, while the $3WJ_c$ showed a τ of only 11.81 min (**Fig. 3.4**). The longer times for 50% strand replacement of the $3WJ_a$ and $3WJ_b$ strands suggests that the structure and property of $3WJ_c$ strand is special and unique. Using Ethidium bromide or SYBR Green staining within gels, the $3WJ_c$ is undetectable while both $3WJ_a$ and $3WJ_b$ are detected (87). From these studies, it was determined the $3WJ_a$ and $3WJ_b$ strands were essential for

Table 3.2: Association and dissociation rates of pRNA-3WJ and its components

		k_a' (s^{-1})				k_d (s^{-1}) (x10^{-3})			
	Ligand	**$3WJ_b$**	**$3WJ_c$**	**$3WJ_b$**	**$3WJ_a$**	**$3WJ_b$**	**$3WJ_c$**	**$3WJ_b$**	**$3WJ_a$**
	Analyte	**$3WJ_a$**	**$3WJ_a$**	**$3WJ_c$**	**$3WJ_b$+$3WJ_c$**	**$3WJ_a$**	**$3WJ_a$**	**$3WJ_b$**	**$3WJ_b$+$3WJ_c$**
Concentration	5.00E-06	.0846	.0502	.650	.0138	.0850	.601	3.25	.0424
	1.25E-06	.0415	.0312	.185	.0121	.0715	.679	4.45	.0477
	3.10E-07	.01.52	.0129	.0414	.00685	.0550	.378	3.99	.0461
	7.80E-08	.00533	.00567	.0105	.00606	.0598	.879	4.11	.0491

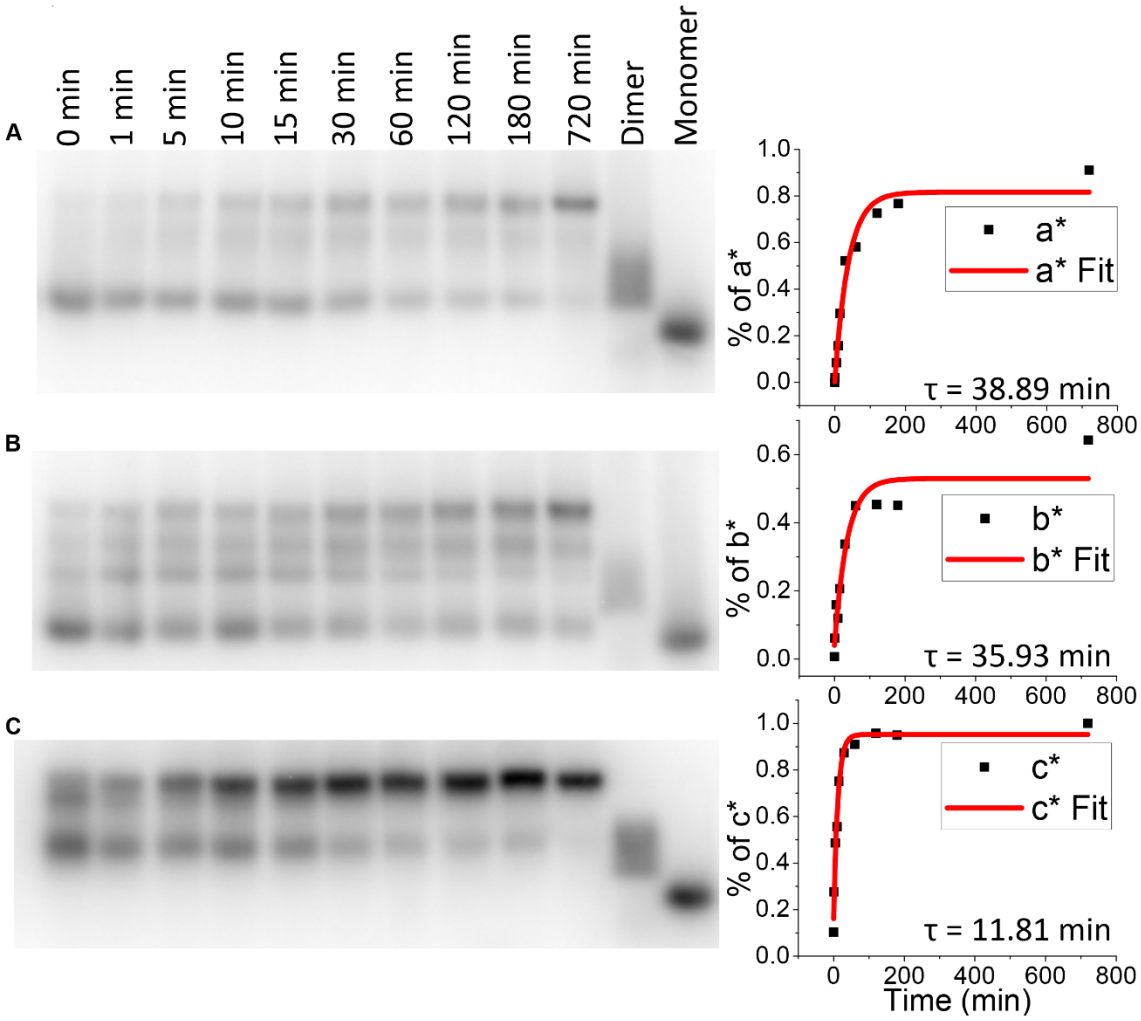

Figure 3.4: Time Constants of 3WJ strands by Electrophoretic Mobility Shift Assays (EMSA). The half-life of each 3WJ strand in the pRNA-3WJ were calculated by EMSA using ^{32}P labeled free strands, replacing unlabeled strands on assembled pRNA-3WJ. The transition of monomer to 3WJ was then plotted and the data was fitted to calculate τ. A) $3WJ_a$, B) $3WJ_b$, C) $3WJ_c$.

the strong stability of the pRNA-3WJ motif; however, the high reactivity of the $3WJ_c$ strand allows for the rapid association seen in the SPR studies and previous thermodynamic studies.

Association mechanism of the pRNA-3WJ

Previous studies on the pRNA-3WJ showed that the three RNA fragments associated very rapidly and the formation of a dimer intermediate was undetected. While the idea of a one-step association between the three strands seemed highly unlikely it was believed that the pRNA-3WJ was formed through the initiation by the folding of a dimer with a very rapid addition of the third RNA strand. Here we have found that in fact the $3WJ_b$ and $3WJ_c$ strands form a dimer species at a rapid rate, and above what was seen in the testing all three strands together. Thus we assume and believe that the two analytes ($3WJ_b$ and $3WJ_c$) were forming into dimer complex and at equilibrium before being able to interact with the $3WJ_a$ ligand strand on the chip surface. With this idea the pRNA-3WJ data was re-analyzed to follow a pseudo-first order reaction that would result in an assembly mechanism of $3WJ_b + 3WJ_c \leftrightarrow 3WJ_{bc} + 3WJ_a \leftrightarrow 3WJ_{abc}$ (**Fig. 3.2B**). Here the same dissociation rates were seen as when modeled as a three component system. Additionally the rates of association were independent of concentrations tested leading to varying rate constant values. The only reasonable explanation for this occurring is the real association rate constant is many orders of magnitude below the observed k_a and working concentrations. This means the rate of the reaction for the $3WJ_{bc} + 3WJ_a \leftrightarrow 3WJ_{abc}$ is occurring so quickly that it cannot be sensed on the SPR due to concentration restrictions.

Therefore, it is proposed that the pRNA-3WJ undergoes a two-step reaction, in which the second reaction takes place immediately following the first at a rate that is too fast to currently quantify (**Fig. 3.5**). This high reaction rate is due to the fact that upon the initiation of the $3WJ_{bc}$ formation the affinity for the $3WJ_a$ strand increases significantly due to the presence of 17 bases for pairing between the two strands, rather than 8 or 9 base pairs of a single strand. This second high speed reaction is therefore rate limited to the first reaction of forming the $3WJ_{bc}$ dimer, thus in examining the formation of the pRNA-3WJ a singular step is seen as without the evidence of an intermediate forming. Furthermore, each strand and helical region of the pRNA-3WJ plays an important role in the rapid formation and high stability. As discussed earlier from the τ values, we know the $3WJ_c$ strand is highly reactive, this causes results in the highest k_a of the $3WJ_{bc}$ dimer. While the dimer between the $3WJ_b$ and $3WJ_c$ strands form the quickest, it also displays the shortest dissociation rate showing that the pRNA-3WJ stability is provided through other base pairing. The $3WJ_a$ and $3WJ_c$ strands provide the high stability of the 3WJ as shown in their long half-lives and the slow k_d seen in SPR studies of the $3WJ_{ab}$. However, while the pRNA-3WJ relies heavily on the $3WJ_{ab}$ helix region for its stability, the pRNA-3WJ itself is the most stable motif as shown in having the slowest off rate (k_d) (**Table 3.2**). This can be attributed to the fact that if one helical region of the pRNA-3WJ breaks, the local concentration of the strand is very high compared to what would be seen in solution, thus initiating an immediate refolding of that helical region as the second half of the strand is still attached to the pRNA-3WJ. As a result of these kinetic studies, the high association rate and slow dissociation rate of the pRNA-3WJ results from contributions of each of the RNA strands resulting in a three component collision.

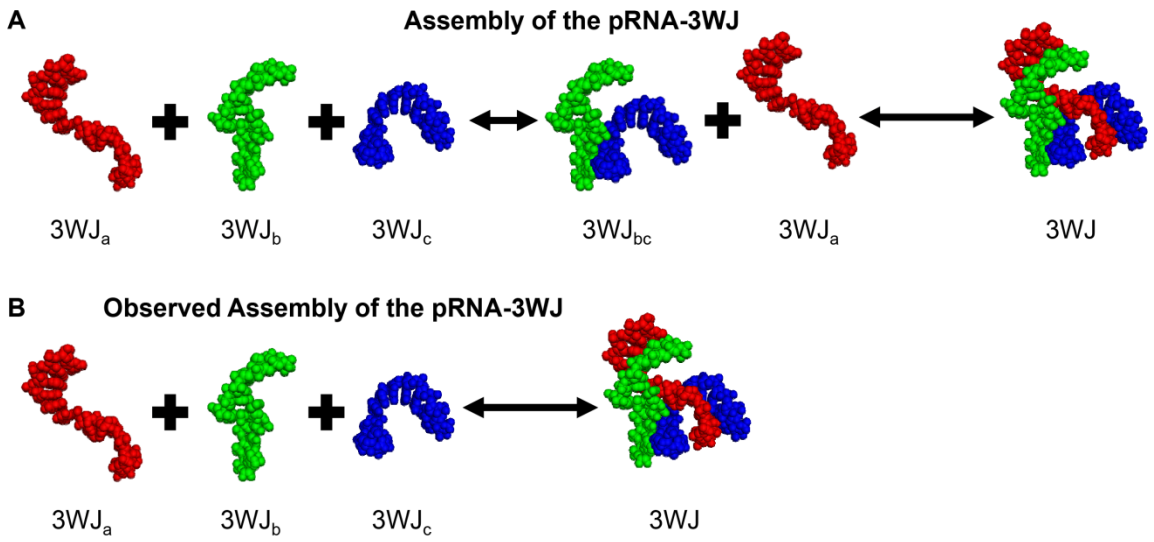

Figure 3.5: Proposed Assembly Mechanism of the pRNA-3WJ. A) The pRNA-3WJ assembles in a two-step mechanism of $3WJ_b + 3WJ_c \leftrightarrow 3WJ_{bc} + 3WJ_a \leftrightarrow 3WJ_{abc}$, in which the first assembly of the $3WJ_{bc}$ dimer is rate limiting. As the dimer is formed it immediately folds into the complete pRNA-3WJ due to the increased base pairing presented for the $3WJ_a$ strand. The second step occurs at an unobservable step, making the assembly appear as a B) one-step assembly mechanism.

CONCLUSIONS:

The pRNA-3WJ forms under a two-step assembly mechanism through the $3WJ_b + 3WJ_c \leftrightarrow 3WJ_{bc} + 3WJ_a \leftrightarrow 3WJ_{abc}$ mechanism, in which the $3WJ_{bc}$ dimer formation occurs at a rate constant of $\sim 1x10^5$ $M^{-1}s^{-1}$ and the formation of the pRNA-3WJ at a rate that was unobservable. The resulting motif is more stable than any of its dimers, while each RNA strand plays an important role in either the association or dissociation of the 3WJ. The pRNA-3WJ show extra-ordinary stability, and ease of formation without an observable intermediate, resulting in a stable branched motif that can be used for the construction of RNA nanoparticles.

ACKNOWLEDGMENT:

This research was supported by NIH grants EB003730 and CA151648 to P.G and NIH grant R25CA153954 to Brad Anderson. The content is solely the responsibility of the authors and does not necessarily represent the official views of NIH. Funding to Peixuan Guo's Endowed Chair in Nanobiotechnology position is by the William Fairish Endowment Fund. P. Guo. is a co-founder of Biomotor and RNA Nanotechnology Development Corp. Ltd.

Chapter 4: Development of RNA Nanoparticles for Prostate Cancer

This chapter was reproduced (with some modification) with permission from Binzel DW, Shu Y, Li H, Sun M, Zhang Q, Shu D, Guo B, Guo P. "Specific Delivery of miRNA for High Efficient Inhibition of Prostate Cancer by RNA Nanotechnology." *Molecular Therapy*. 2016 In Press. Special thanks to Dr. Yi Shu and Dr. Dan Shu for help and assistance in preparation of data for figures 4.5, Hui Li for assistance with figures 4.7A, C, and Dr. Bin Guo and his students Meiyan Sun and Qunshu Zhang for assistance with figure 4.7B.

INTRODUCTION:

Functionality of living organisms is made up by a wide variety of molecules consisting of DNA, RNA, and proteins. In the past, DNA has been used for its simplistic and defined structure in biomaterials (224-227), while proteins have extensively been utilized for their diverse structure and functionalities (228). RNA brings together the characteristics of the simplicity of DNA and the wide variety of folding structures and functions of proteins, making it an attractive candidate for use in nanobiotechnology (91,229). Utilizing RNA in therapies provides several advantages over other technologies, including: known stoichiometry and defined folding of nanoparticles, thereby decreasing the possibility of side effects and toxicity (12,86-88). Multiple RNA moieties can be incorporated such as receptor-binding aptamer (32,33), siRNA (97-99), ribozyme (92-94), miRNA (100-102), and riboswitch (95,96) through the use of bottom up self-assembly (86,97). RNA nanoparticles normally are in the 10-50 nm size range, which is the optimal to pass through cell membranes through cell surface receptor

mediated endocytosis while still being retained by the body (66-68). Finally, RNA nanoparticles can prevent antibody detection by being protein free, but maintain their selectivity using receptor-binding aptamers (113-115). The previous problem of instability of RNA nanoparticles once hindered the field of RNA nanotechnology (112); but 2'-Fluoro (2'-F) modifications to uracil and cytosine backbones not only improves the thermodynamic stability but makes the resulting RNA resistant to RNase degradation (189,199). With these benefits, a stable RNA nanoparticle would prove to be a beneficial therapeutic delivery vehicle that could be used in the specific targeting and treatment of cancers and viral diseases.

Affecting one in every six men and being the second deadliest cancer in men (behind lung cancer), prostate cancer is a severe disease that affects a wide population. There are roughly 250,000 new cases of prostate cancer diagnosed each year with 30,000 deaths (American Cancer Society statistics). LNCaP cells are a class of prostate cancer cells known for being hormone dependent and androgen sensitive for growth (230-232). Extensive work on prostate cancer therapies has previously been done using LNCaP cells as they are normally considered a less aggressive cancer (215,233-235). It is beneficial to use the early stage cancer cells as a target for therapies, as the tumor has not had time to develop into an aggressive state, is still hormonal dependent, and overall easier to manage than an hormone independent tumor. This allows for a contained treatment and a higher chance of successful removal of the disease. Furthermore, it has been shown that LNCaP tumor cells over express Prostate Specific Membrane Antigen (PSMA) (232,236-238), making it an even more attractive target as it can be easily identified from healthy

prostate cells allowing for a specific targeting and delivery of therapeutics while having low toxicity effects on normally functioning prostate cells.

Within cancers, it has been found that many microRNA (miRNA) are either down regulated or over-expressed (239-241). The differences in expression from healthy tissues have shown adverse downstream effects on many protein expressions, most notably leading to down-regulation of tumor suppressors and increased anti-apoptotic genes. LNCaP-FGC prostate cancer cells are known to have miR17 and miR21 play important roles (242,243), two common miRNAs that have been shown to be directly related to cancer progression and growth. These two microRNAs lead to the down-regulation of tumor suppressors such as *PTEN* and *PDCD4* and up-regulation of anti-apoptotic genes (243-248). The regulation of these important oncogenes could correct the hindered tumor suppression and sensitize the cells to apoptosis. Recently anti-miRNA LNA sequences have been developed for miR17 and miR21, resulting in the silencing of their respective miRNAs (78). However, due to their small size, they display poor biodistribution characteristics and are easily cleared from the body. Furthermore, the anti-miRNA sequences naturally lack any targeting ability to specifically deliver to cancer cells.

Previously, a thermodynamically and chemically stable RNA three-way junction (3WJ) was discovered within the packaging RNA (pRNA) of the phi29 bacteriophage DNA packaging motor (87). pRNA forms into a hexameric ring on the packaging connector and consists of two domains, the helical domain and central domain containing two interlocking loops) (249-252). The two domains are connected together through a 3WJ that has been shown to form from three short RNA oligo strands in the absence of metal ions (87). The junction also has the ability to harbor RNA moieties off each branch

while still retaining the central folding structure of the 3WJ as well as the functionality of the RNA extensions (87). This ultra-stable platform has proven to be a viable scaffold to carry RNA functionalities for the use in therapeutics in cancers and viral diseases (87,123,137,139).

Using the pRNA-3WJ, we propose to create a RNA molecule with specific targeting ability to prostate cancer cells to carry miRNA LNAs (78). Here we report the use of the pRNA-3WJ for the construction of RNA nanoparticles for the specific targeting of prostate cancer tumor cells. LNCaP-FGC cells were used as *in vitro* cell model and the over-expression of the PSMA in LNCaP-FGC cells was used as a specific target. Targeting was achieved through the use of the PSMA A9g RNA aptamer that has been previously developed (253,254), and conjugated onto the pRNA-3WJ through bottom-up construction. Furthermore, we have conjugated anti-miRNA LNAs as well as fluorescent tags onto the remaining two branches of the three way junction for monitoring the binding and entry into the tumor cells. Nanoparticles were successfully constructed with defined stoichiometry and size that maintained the folding structures of both the pRNA-3WJ and A9g PSMA aptamer, keeping the functionality of the aptamer. The molecules further showed specific targeting to LNCaP-FGC cells *in vitro* through flow cytometry, cell confocal microscopy, and dual luciferase assays. Dual luciferase assays and qRT-PCR reported specific knockdown of miR21 and miR17 in LNCaP cells. Through these studies, we have proven that the combination of the A9g PSMA aptamer with anti-miRNA LNAs through the pRNA-3WJ into therapeutic nanoparticles, selective targeting to prostate cancer, specifically LNCaP-FGC cells, can be accomplished,

providing a vehicle for therapeutical elements like siRNAs, miRNAs, or chemotherapies for tumor treatments.

MATERIALS AND METHODS:

Design and construction of pRNA-3WJ nanoparticles harboring PSMA binding aptamer and anti-miRNA LNA

RNA nanoparticles were constructed using a bottom-up approach, as previously described. Briefly, DNA oligos primers (Integrated DNA Technologies) were used to create dsDNA templates through polymerase chain reaction (PCR) for each RNA strand. RNA strands were then transcribed by T7 polymerase *in vitro*. Additionally 2'-fluoro (2'-F) modified cytosine and uracil were used in transcriptions along with an Y639F mutant T7 polymerase, giving nuclease stability to the RNA strands. The anti-micro RNA LNAs were synthesized by Exiqon.

Transcribed RNA strands were purified on 8% polyacrylamide gels containing 8 M Urea ran at 120 V for 1.5 hours on TBE running buffer (89 mM Tris-borate, 2 mM EDTA). RNA bands of interest were excised from the gel using UV shadow on thin layer chromatography plates and eluted from gel in elution buffer (0.5 M Ammonium Acetate, 0.1 mM EDTA, 0.1% SDS) at 37 °C for a minimum of 3 hours and then precipitated by ethanol.

RNA nanoparticles were assembled by mixing strands at equal molar concentrations in TMS buffer (50 mM Tris pH 8.0, 100 mM NaCl, 10 mM $MgCl_2$) and heated to 80 °C for 5 minutes and slowly cooled over 40 minutes to 4 °C. Assembled RNA nanoparticles were then purified on 8% polyacrylamide gels at 100 V for 2 hours

on TBM running buffer (89 mM Tris, 200 mM borate acid, and 5 mM MgCl2) and at 4 °C. Samples were then excised and eluted as described above.

Temperature Gradient Gel Electrophoresis (TGGE) assay for studying thermodynamic stability of RNA nanoparticles

For TGGE analysis, the experimental setup was adjusted to have a linear temperature gradient perpendicular to the electric field (BiometraHmbGh). The temperature gradient was set from 36.0 °C to 80.0 °C. RNA sample (500 nM) was combined with 6× gel loading buffer and run on 8% native PAGE at 100 V for 1 h. 10 mM $MgCl_2$ was present in both gel and electrophoresis buffer. The nanoparticles contained a Cy5 fluorophore on the $3WJ_b$ strand for monitoring melting and imaged by Typhoon FLA 7000 (GE Healthcare). The pRNA-3WJ constructs within the total RNA was analyzed by ImageJ, and the melting curve of the construct was fitted using nonlinear Sigmoidal fitting. Melting temperatures (T_m) were calculated where 50% of total RNA concentration was at ssRNA and 50% was in complexed 3WJ form.

Serum stability assay for studying chemical stability of RNA nanoparticles

400 ng of pRNA-3WJ nanoparticle was incubated in TMS buffer containing fetal bovine serum (FBS, final concentration is 10%). The total volume was 10 µl. Samples were taken at multiple time points, including 0, 0.25, 0.5, 1, 2, 6, 12, and 24 hours after incubation at 37 °C. 8% Native TBM PAGE gel electrophoresis was applied to visualize RNA. After running for 1.5 hr at 4 °C, the gel was stained by ethidium bromide. Images were taken by Typhoon FLA 7000 (GE Healthcare).

Dynamic light scattering and Zeta potential measurement of RNA nanoparticles

Apparent hydrodynamic sizes and zeta potential of pre-assembled A9g-3WJ-anti-miR21 LNA and A9g-3WJ nanoparticles were measured by a Zetasizer nano-ZS (Malvern Instrument, LTD). All RNA samples were measures at 2 μM in DEPC H_2O and PBS buffer (137 mM NaCl, 2.7 mM KCl, 100 mM Na_2HPO_4, 2 mM KH_2PO_4, pH 7.4) at 25 °C.

Cell Culture

Human prostate cancer cell lines LNCaP-FGC, LNCaP C4-2 and PC-3 (American Type Culture Collection, ATCC) were grown and cultured in RPMI 1640 medium (Invitrogen) containing both 10% fetal bovine serum (FBS) and penicillin/streptomycin in a 37 °C incubator with a 5% CO_2 and a humidified atmosphere.

Flow Cytometry assay of PSMA pRNA-3WJ nanoparticles binding to LNCaP-FGC cells

LNCaP-FGC and PC-3 cells were trypsinized and rinsed with blank RPMI-1640 medium. 100 nM Cy5 labeled A9g-3WJ and the control pRNA-3WJ were each incubated with 2×10^5 LNCaP-FGC or PC-3 cells at 37 °C for 2 hr. After washing with PBS (137 mM NaCl, 2.7 mM KCl, 100 mM Na_2HPO_4, 2 mM KH_2PO_4, pH 7.4), the cells were resuspended in PBS buffer. Flow Cytometry was performed by the UK Flow Cytometry & Cell Sorting core facility to observe the cell binding efficacy of the Cy-5 A9g-3WJ nanoparticles. Analysis was completed using Flowing Software v2.5 (Turku Centre for Biotechnology).

Confocal Microscopy imaging analyzing RNA nanoparticle binding and entry into LNCaP-FGC cells

LNCaP-FGC and PC-3 cells were grown on glass coverslides in RPMI-1640 medium overnight. 100 nM concentration $Alexa_{647}$ labeled A9g-3WJ and the control pRNA-3WJ were each incubated with the cells at 37 °C for 2 hr. After washing with PBS, the cells were fixed by 4% paraformaldehyde and stained by Alexa Fluor® 488 phalloidin (Invitrogen) for cytoskeleton and TO-PRO®-3 iodide (642⁄661) (Invitrogen) for nucleus. The cells were then assayed for binding and cell entry by Zeiss LSM 510 laser scanning confocal microscope.

Dual Luciferase Assay to analyze delivery of anti-miRNA by pRNA-3WJ nanoparticles

LNCaP-FGC and PC-3 cells were grown on 24-well plates in RPMI-1640 medium until reaching ~80-90% confluency. 100 nM and 50 nM A9g-3WJ-anti miRNA LNA and the control RNAs including pRNA-3WJ/anti-miRNA-(17 or 21) LNA and A9g-3WJ were incubated with cells in opti-MEM at 37 °C for 3 hr. As a positive control, anti-miRNA LNA transfected by RNAi MAX (following standard protocol by Invitrogen) into cells, while complete nanoparticles were merely incubated with cells. After incubation with the RNA, cells were washed once with blank RPMI-1640 medium and then transfected with psi-Check 2 plasmid (Promega) which contains an oncogenic miRNA targeting sequences at the 3'-UTR region of Renilla Luciferase gene using Lipofectamine 2000 (Life Technologies). Dual-luciferase assay (Promega) was used to evaluate the anti-miRNA LNA effects 24 hr post-transfection upon manufacture's instruction. Briefly, cells were washed once with PBS and lysed with passive lysis buffer. The plates were shaken for 30 minutes at room temperature. 20 µL of the lysate were added to 50 µL of luciferase assay reagent (LAR II) in a luminometer tube and firefly luciferase activity was measured. Upon addition of 50 µL of Stop & Glo Reagent, control

measurements of Renilla luciferase activity were then obtained. The Renilla luciferase activity obtained was then normalized with respect to the Firefly luciferase activity for determining the average ratio of Renilla to Firefly luciferase activity over several trials. Results were statistically analyze by an ANOVA two-way test in comparing Renilla expression to the cell only control and between PC-3 and LNCaP cell lines among each concentration.

qRT-PCR assay

Two A9g-pRNA-anti-miRNA LNA constructs were assayed for the subsequent gene up-regulation effects: one harboring anti-miR21 LNA; and, the other harboring anti-miR17 LNA.

LNCaP-FGC cells were incubated with 10 and 100 nM of the individual A9g-3WJ-anti-miRNA LNA and control RNAs as described above. After 72 hr treatment, cells were collected and target gene up-regulation effects were assessed by qRT-PCR. PC-3 cells were used as negative control cell line.

Cells were processed for total RNA using Trizol RNA extraction reagent following manufacture's instruction (Life Technologies). The first cDNA strand was synthesized on total RNA (1 μg) from cells with the various RNAs treatment using SuperScript^{TM} III First-Strand Synthesis System (Invitrogen). Real-time PCR was performed using Taqman Assay. All reactions were carried out in a final volume of 20 μL using Taqman Fast Universal PCR Master Mix and assayed in triplicate. Primers/probe set for human *PTEN* and *18S* were purchased from Life Technologies. PCR was performed on Step-One Plus real time PCR system (Applied Biosystem). The data was analyzed by the comparative C_T Method ($\Delta\Delta C_T$ Method). Data was statistically

analyzed by an ANOVA one-way test in comparing values with the cell only control in each concentration and gene.

Caspase III assay for studying cell viability upon pRNA-3WJ nanoparticle treatment

LNCaP-FGC cells were plated in 24-well plate and incubated with 100 nM A9g-3WJ-anti miRNA LNA constructs and control RNAs as described above at 37 °C for 24 hr. A positive control of incubating cells with 5 μM Campothecin for 4 hr at 37 °C was used. Caspase III signaling was then assayed using Caspase III Assay Kit (BD Pharmigen) following the standard protocol. Cells were washed in 1× PBS buffer followed by incubated in 200 μL Cell Lysate Buffer for 30 min on ice. 100 μL of cell lysate was then incubated with 1 mL of 1× HEPES Buffer and 15 μl Ac-DEVD-AMC fluorescent substrate and incubated at 37 °C for 1 hr. Fluorescence was the measured from 420 to 460 nm with an excitation of 380 nm on fluorospectrometer (Horiba Jobin Yvon; SPEX Fluolog-3). A peak fluorescence at 440 nm was used to analyze Caspase III signaling.

In vivo biodistribution and tumor targeting of RNA nanoparticles

LNCaP C4-2 cells were cultured *in vitro* and subcutaneously injected under the skin of 4 week old male nude mice. A total of 2×10^6 cells were injected in solution with Matrigel (Corning) as a 50/50 % blend. Tumors were grown for 4 weeks until tumors reached a volume of 200 mm^3. Mice were then administered PBS (blank control), pRNA-3WJ (negative control), and A9g-3WJ each with $Alexa_{647}$ labels as naked oligos at a dose of 2 μM at 100 μL through the tail vein. Mice were imaged for whole body fluorescence at time points 0, 1, 2, 3, 4, and 8 hours with an IVIS imager (Caliper Life Sciences). Upon the completion of the study, mice were sacrificed, and tumors, hearts, kidneys,

livers, and brains were collected and imaged by the whole body imager for $Alexa_{647}$ signal. Additionally, tumors were frozen at –80 °C, and sectioned for confocal microscopy as described above.

Furthermore, tumors were fixed in 4% paraformaldehyde with 10% sucrose in 1x PBS buffer at 4 °C overnight. Tumor samples were then placed in Tissue-Tek O.C.T. compound (Sakura Finetek USA, Inc.) for frozen sectioning (10 μm thick). Sectioned tissue were then stained with DAPI and mounted with ProLong Gold Anti-fade Reagent (Life Technologies) overnight. Slides were then fluorescently imaged by FluoView FV1000-Filter Confocal Microscope System (Olympus).

In vivo tumor reduction by anti-miRNA LNA pRNA-3WJ nanoparticles

LNCaP C4-2 cells were grown and subcutaneously injected into 4 week old male nude mice. 2×10^6 cells were injected as a 50% cell, 50% Matrigel (Corning) blend into the flank of the mice with a total of 5 mice hosting 2 tumors each. Xenograft tumors were monitored until they reached roughly 200 mm^3 in volume. Naked RNA nanoparticles harboring the PSMA A9g aptamer and anti-miRNA LNAs were injected through the tail vein of mice at a concentration of 20 μM at 100 μL on days 7, 10, 13, 17 and 20 while monitoring tumor volume and total mouse weight up to day 29.

Western blot of miRNA downstream genes of xenograft tumors

Upon the completion of tumor reduction experiments, mice were sacrificed and tumors were harvested. LNCaP C4-2 tumors were homogenized in RIPA buffer containing Protease (ThermoFisher). Total protein concentration was measured by BCA protein assay (ThermoFisher) against protein standards. 100 μg of total protein from the tumor was loaded onto TDX FastCast SDS PAGE gels (BioRad) and ran at 100 V for 2

hr. Gels were transferred onto membranes and stained with *PTEN*, *PDCD4*, and *β-Actin* antibodies (Cell Signaling) and imaged. *β-Actin* was used as an internal control and *PTEN* and *PDCD4* are expressed as a ratio with *β-Actin*.

RESULTS AND DISCUSSION

Construction of pRNA-3WJ nanoparticles harboring PSMA binding aptamer

An RNA aptamer using 2'-Fluoro modified nucleotides was generated through SELEX (Systematic evolution of ligands by exponential enrichment) for specific targeting of PSMA by Lupold et al (253). Furthermore, Rockey et al. rationally truncated the A9 PSMA aptamer shortening the overall length while keeping the high specificity to PSMA (254). It is well known that prostate specific membrane antigen is overexpressed in LNCaP-FGC prostate cancer cells (231,232,255-258). PSMA is an important target since it is overexpressed in primary prostate tumors as well as metastases in the lymph nodes (259). Furthermore, PSMA has been shown to be upregulated in tumors after patients have been treated with common androgen-deprivation therapies (257,260). The truncated PSMA A9g aptamer was placed onto the pRNA-3WJ, creating a branched RNA motif to specifically target prostate cancer cells. RNA 3WJs were created with the PSMA aptamer attached to the $3WJ_a$/$3WJ_c$ branch in three different orientations (**Figs. 4.1, 4.3**) in order to test if there is any variation in the aptamer folding once placed on the pRNA-3WJ. Each of the three variants of the A9g-3WJ displayed proper folding and sizing on polyacrylamide gels ran in native conditions.

Next the prostate targeting 3WJs were tested for nuclease and thermodynamic stability. First each of the 2'-F modified A9g-3WJs were incubated with 10% fetal bovine serum over 24 hours (**Fig. 4.2A**). Samples were then ran on polyacrylamide gels, where

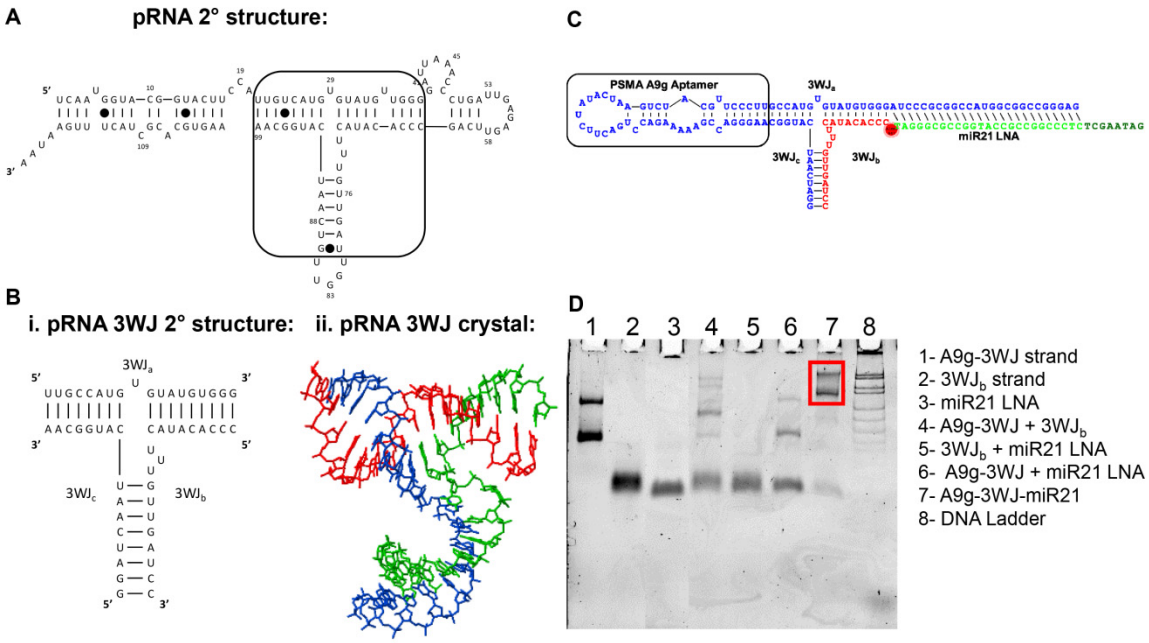

Figure 4.1. Design and construction of pRNA-3WJ nanoparticles harboring PSMA binding aptamer and anti-miRNA LNA. A) The sequence and secondary structure of bacteriophage phi29 packaging RNA (pRNA). B) 3WJ core of pRNA. C) Design of pRNA-3WJ nanoparticles harboring PSMA binding aptamer and anti-miRNA LNA. D) 10% native TBM PAGE of A9g-3WJ-anti-miR21 nanoparticle.

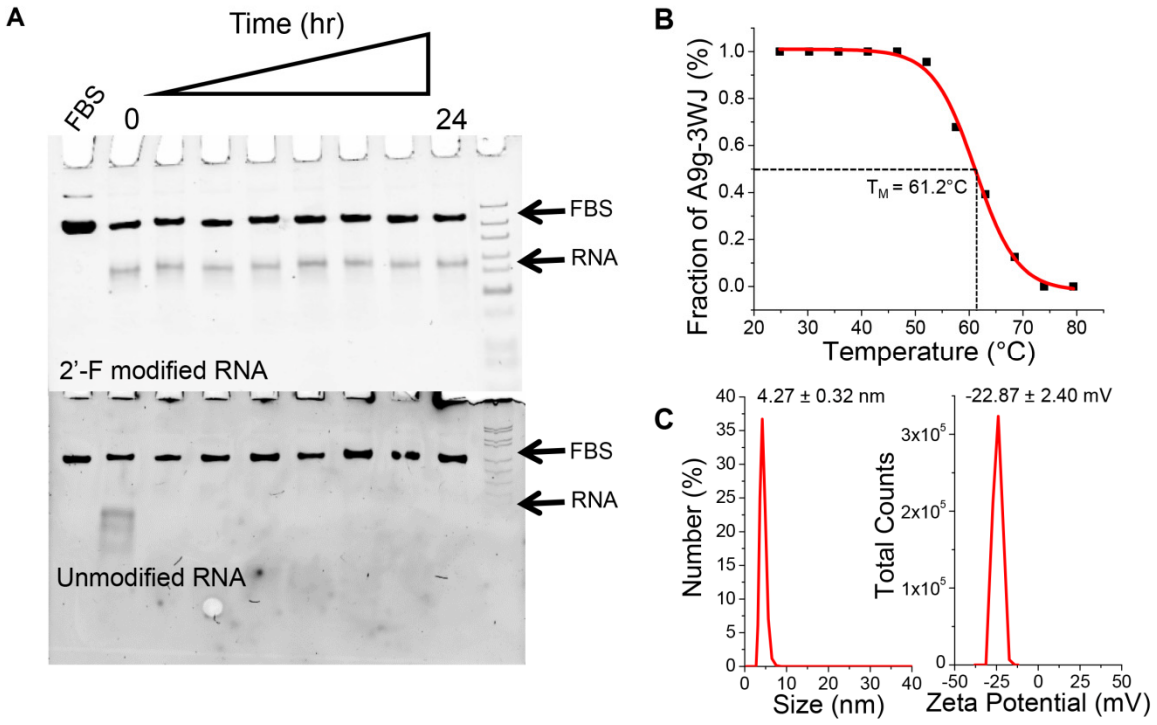

Figure 4.2. The stability and characterization of assembled pRNA-3WJ nanoparticles harboring PSMA binding aptamer and anti-miRNA LNA. A) Assessment of chemical stability of A9g-3WJ-anti-miRNA LNA treated with 10% serum contained cell culture medium in 8% TBM native PAGE. B) Assessment of thermodynamic stability of A9g-3WJ-anti-miRNA LNA by TGGE assay. Melting profile of nanoparticle derived from PAGE with sigmoidal fitting of data to find melting temperature. C) Hydrodynamic sizing and zeta potential measurements of the A9g-3WJ-anti-miR21 nanoparticle using a Zetasizer nano-ZS.

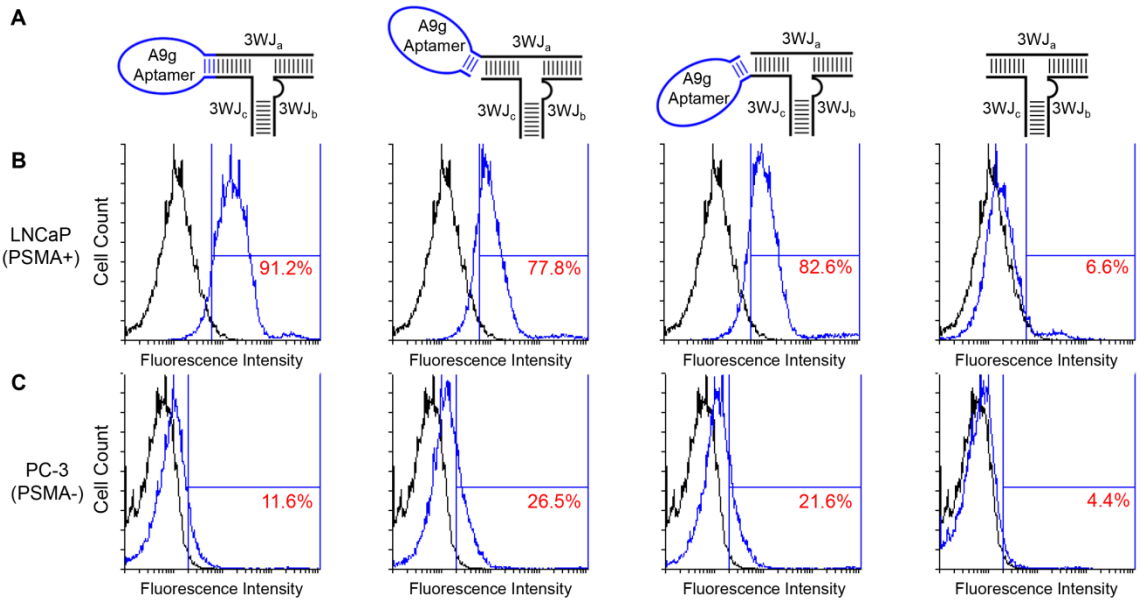

Figure 4.3. Flow Cytometry assay for studying specific binding of pRNA-3WJ nanoparticles on prostate cancer cells. A) Illustration of various design of conjugating PSMA binding A9g aptamer onto the pRNA-3WJ core. Alexa$_{647}$ labelled A9g-3WJ RNA nanoparticles were incubated with B) PSMA+ LNCaP-FGC cells and C) PSMA- PC-3 cells. Nanoparticles indicated positive binding of nanoparticles to LNCaP cells while avoiding non-specific binding to PC-3 cells.

the band corresponding to the assembled RNA nanoparticles remained stable throughout all time points. This data shows the RNA nanoparticles will remain stable during *in vivo* applications as RNases are not able to recognize and degrade the fluoro modified nucleic acids. Furthermore, the thermodynamic stability of the PSMA targeting 3WJ was assayed using temperature gradient gel electrophoresis. Temperature gradient was applied perpendicular to the electrical current in order to find the melting temperature of the 3WJ harboring the aptamer (**Fig. 4.2B**). Previously the melting temperature (T_m) of 2'-F modified pRNA-3WJ core was found to be 69.8 °C (223). From the TGGE melting curve, the melting temperature of the A9g-3WJ was found to be 61.2 °C. Although the T_m of the aptamer-3WJ complex is less than the 3WJ itself, the still rather high melting temperature of the nanoparticle indicates the PSMA A9 aptamer does not significantly hinder the stability of the pRNA-3WJ core, and in fact the 3WJ actually provides added stability to the PSMA aptamer.

After establishing that A9g-3WJ displayed the high stability previously seen in the pRNA-3WJ, the targeting 3WJ was expanded to harbor anti-miRNA LNAs for testing the delivery of therapeutics to LNCaP-FGC cells (**Fig. 4.1C**). The extended helical regions off of the unoccupied branch of the 3WJ posed no problem in folding of the RNA strands, as all completed nanoparticles were assayed on polyacrylamide gels ran in native conditions (**Fig. 4.1D**). Assembly gels showed high yield of the folded RNA nanoparticle, without any side product bands being contributed to mismatch in RNA concentrations during assembly. Within the assembly gel, two bands were seen from the A9g-3WJ strand and the A9g-3WJ-anti-miRNA samples, this was attributed to formation of a self-dimer of the A9g aptamer. Furthermore assembled nanoparticles, A9g-3WJ and

A9g-3WJ-anti-miR21 LNA, were tested for zeta potential and hydrodynamic size (**Fig. 4.2C**). Here it was found that the size of the nanoparticles were 3.77 ± 0.59 nm and 4.27 ± 0.32 nm, with a zeta potential of -18.0 ± 1.45 mV and -22.87 ± 2.40 mV, respectively. These values are in line with predictions and previously published results of other RNA nanoparticles (83,125,126).

Targeting of pRNA-3WJ nanoparticles to LNCaP-FGC cells

In order to test the targeting of the pRNA-3WJ, either a fluorescent $Alexa_{647}$ or whole chain labeling with Cy5 fluorophore was placed on the $3WJ_b$ strand to allow for tracking of the RNA nanoparticles created and described above. The A9g-3WJ nanoparticles were incubated with LNCaP-FGC cells, as well as PC-3 cells (PSMA–) as a negative control. Following the RNA incubation and washing steps cells were analyzed by flow cytometry to confirm the binding of each of the three A9g-3WJs. FACS data showed each of the designs showed strong binding (>75%) to LNCaP-FGC cells while the aptamer negative pRNA-3WJ displayed only 6.59% binding (**Fig. 4.3**). However, with this high binding it was found that the two designs with hinging aptamers produced an increased and undesired non-specific binding to PC-3 cells. Therefore connecting the A9g PSMA aptamer to the pRNA-3WJ directly to the two helical regions of the $3WJ_a$/$3WJ_c$ branch provided the highest binding to LNCaP-FGC (91.22 %), while having low non-specific binding to PSMA- PC-3 cell line (11.60 %) (**Table 4.1**). Flow cytometry data displayed that the addition of the pRNA-3WJ to the end of the PSMA A9g aptamer did not interrupt cell binding, and provided a branched scaffold for the addition of therapeutic elements such as siRNAs, miRNAs, and anti-miRNAs.

Table 4.1. Summary of flow cytometery binding data

Sample (100nM)	LNCaP	PC-3
3WJ (negative)	6.6%	4.4%
A9-3WJ version 1	91.2%	11.6%
A9-3WJ version 2	77.8%	26.6%
A9-3WJ version 3	82.6%	21.6%
Aptamer (positive)	87.6%	9.2%

Next, endocytosis entry of the RNA nanoparticles harboring the PSMA A9g aptamer into LNCaP-FGC cells was examined. In order for proper delivery of therapeutics and RNA nanoparticles to act as anti-cancer agents, entry into the cells are required for proper release of therapeutic agents. $Alexa_{647}$ labeled A9g-3WJ nanoparticles were incubated with LNCaP-FGC and PC-3 cells, cells were then fixed and the nuclei and cytoplasm were stained. Confocal microscopy images shows proper binding of the A9g aptamer to LNCaP cells with very little signal seen on PC-3 cells. Furthermore, confocal imaging along with Z-axis stacking imaging (**Fig. 4.4**) confirmed $Alexa_{647}$ signal within LNCaP-FGC cells on A9g positive nanoparticles. Additionally, little $Alexa_{647}$ signal was seen around cells samples without the PSMA aptamer and the signal was only seen accumulating around the LNCaP cells and not within. This data displays that PSMA A9g aptamer is not only specifically binding to PSMA+ cells, but entering through receptor mediated endocytosis as expected. Additionally, cell binding assays were completed using VCaP (PSMA+) and Jurkat (PSMA-) cell lines to further test the specificity of the A9g-3WJ nanoparticles (data not shown). Here very similar binding profiles were seen as with LNCaP and PC-3 cells further confirming the targeting of the A9g aptamer. With positive detection of nanoparticles in the LNCaP-FGC cells, it is possible to deliver therapeutics in hopes of leading to apoptosis of LNCaP cells through RNA interference (RNAi).

Delivery of anti-miRNA LNA to LNCaP-FGC cells

Upon confirmation of PSMA targeting nanoparticles entering into LNCaP-FGC cells, experiments were expanded to test the delivery of therapeutic components. LNCaP-FGC cells are known to overexpress miR17 and express miR21, two common oncomirs

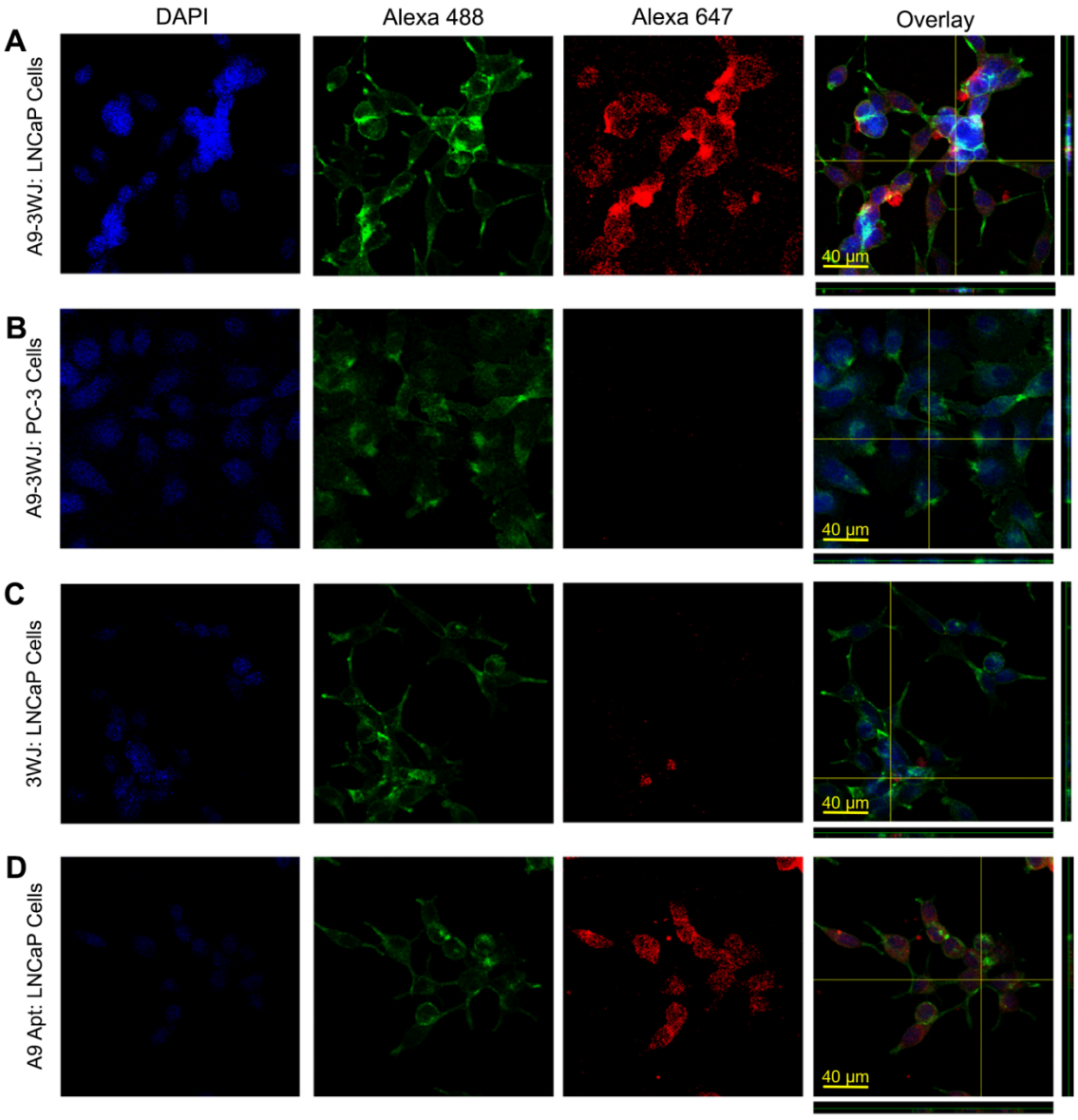

Figure 4.4. Confocal Microscopy for assaying the binding and internalization of pRNA-3WJ nanoparticles via PSMA binding aptamer A9g. RNA nanoparticles were incubated with cell groups then fixed and stained for fluorescent imaging. A) A9g-3WJ to LNCaP cells. B) A9g-3WJ to PC-3 cells. C) 3WJ control to LNCaP cells. D) A9g aptamer control to LNCaP cells. Blue: DAPI stained nucleus. Green: Phalloidin-Alexa 488 stained cytoplasm. Red: Alexa 647 labeled RNA nanoparticles. Overlay of 3 signals with z-axis scanning.

that are seen in cancers (242,243). These two microRNAs lead to the down-regulation of tumor suppressors such as *PTEN* and *PDCD4* and up-regulation of anti-apoptotic genes (243-248). Additionally miR-21 has been shown to promote hormone independency prostate cancers (261) and enhances the invasiveness of LNCaP cells (262); while miR17 has been proven to promote tumor growth and invasiveness in prostate cancer cells (263). Therefore, silencing miR17 and miR21 could lead to the sensitization of the LNCaP-FGC cells leading to apoptosis. Anti-miRNA sequences have been developed to target, and bind miR17 and miR21, thus blocking their gene silencing roles (78).

These anti-miRNAs were placed onto the PSMA A9g-3WJ by a DNA linker strand for delivery into LNCaP-FGC cells (83). Incubation studies of the RNA nanoparticles harboring the PSMA RNA aptamer with the miR17 and miR21 were completed testing the delivery using Promega's psi-check2 dual luciferase plasmid. The transfected plasmid contained sequences for Firefly and Renilla luciferase plasmids with each plasmid containing the microRNA targeting sequences at the 3'-UTR region of Renilla luciferase, respectively. Therefore in the native cells, the Renilla expression would be knocked-out, as the miRNA would bind to plasmid, preventing the translation of Renilla luciferase proteins, but Firefly expression would remain unaffected. As anti-miRNA LNA sequences are delivered to the cells, miR17 and miR21 are knocked-down, thus resulting in an increased expression of Renilla in the dual luciferase assay.

By incubating RNA nanoparticles with LNCaP and PC-3 cells, miR17 and miR21 knock-down was assayed by the described dual luciferase assay. Data in LNCaP-FGC cells shows significant increase in Renilla expression in the A9g-3WJ-anti-miRNA LNA and anti-miRNA LNA transfected samples; however, little effect seen from PSMA

aptamer negative samples for both miR17 and miR21 (**Fig. 4.5A-B**). This shows the anti-miRNA sequences are being properly delivered to LNCaP-FGC cells by the PSMA A9g aptamer and processed by RISC. Additionally, studies completed in PC-3 cells showed significantly less increase in Renilla expression from the A9g-3WJ-anti-miRNA LNA samples, indicating RNA nanoparticles were selectively targeting LNCaP cells through PSMA binding, indicating a low toxicity to PSMA- cell lines. Furthermore, due to the fact that the aptamer sequence is on a different strand from the anti-miRNA sequences, these studies indicate that the RNA nanoparticles are remaining stable and intact through the pRNA-3WJ core throughout the studies.

To further confirm the delivery of anti-miRNA LNA sequences into LNCaP-FGC cells and the ability for the LNAs to effect downstream gene expressions quantitative real time PCR was completed, examining the expression of *PTEN* and *PDCD4*, known downstream genes of both miR17 and miR21. *18S* was used as an internal control during these experiments to standardize the expressions of *PTEN* and *PDCD4* mRNA. q-rtPCR results show significant increase of *PTEN* at only a 10 nM concentration of RNA nanoparticles in the A9g-3WJ-anti-miR21 samples over the negative controls (**Fig. 4.5C**). Additionally it was seen that the RNA nanoparticles were able to slightly increase the *PDCD4* expression slightly over negative controls and the cell only samples. These data further prove the delivery of anti-miRNA LNAs to LNCaP-FGC cells through the A9g-3WJ complex. Furthermore, the increase of tumor suppressor genes not only shows a true knockdown of the miRNAs, but displays the RNA nanoparticles' ability to correct errors in gene expressions caused by the prostate cancer.

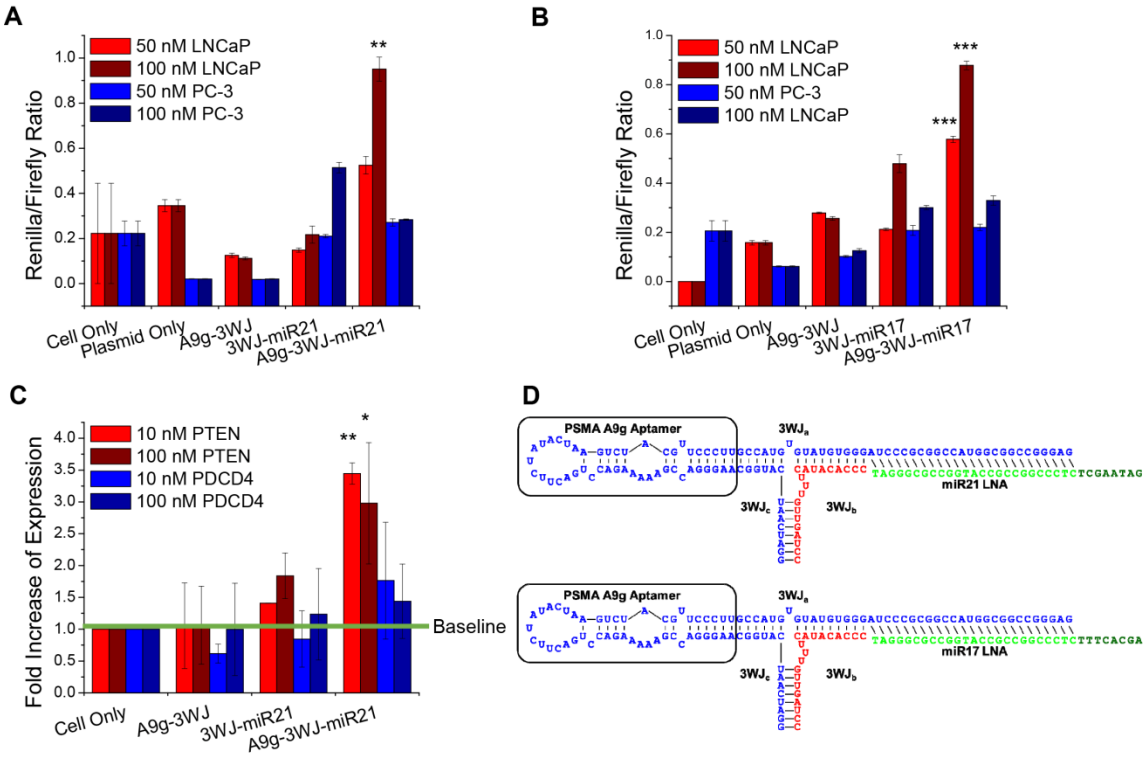

Figure 4.5. Assay for miRNA knockdown and downstream gene regulation effects of pRNA-3WJ nanoparticles harboring PSMA binding aptamer and anti-oncogenic miRNA LNA. A) Dual-luciferase assay for evaluating delivered anti-miR21 LNA and B) anti-miR17 LNA effects on prostate cancer cells from incubation of RNA nanoparticles. Knockdown of miRNAs led to spiked increase of reporter Renilla expression. C) qPCR results of downstream genes *PTEN* and *PDCD4* expression as a result of miR21 knockdown in LNCaP cells 72 hours post incubation with A9-3WJ-anti-miR21 LNA nanoparticles. D) Design of A9g-3WJ-anti miR21 LNA and -anti-miR17 LNA nanoparticles. In all plots *p<0.1, **p<0.01, ***p<0.001.

From the confirmed up-regulation of tumor suppressor genes by delivery of miRNA LNAs by the 3WJ, testing of apoptotic effects were completed through assaying Caspase III signaling on LNCaP-FGC and PC-3 cells after incubation with A9g-3WJ-anti-miRNAs along with negative nanoparticle controls described before (**Fig. 4.6**). The PC-3 cells and negative RNA nanoparticles with LNCaP cells were used to show the RNA nanoparticles were not toxic to the cells and apoptosis only occurred through specific delivery of the anti-miRNA LNAs. A spike in Caspase III signaling was seen in LNCaP cells treated with A9g-3WJ-anti-miR17 and transfected by RNAi Max anti-miRNA LNAs (**Fig. 4.6**). This indicates that the silencing of miRNA was able to successfully lead to the death of LNCaP cells. Here apoptosis caused by the decreased expression of miR17 shows the important role of the miRNA in LNCaP cells and the ability to control the cell growth and death through its expressions.

Through this data, the prostate cancer targeting RNA nanoparticles delivering the anti-miRNA LNAs shows the vast possibility of RNA nanoparticles. Here, we show constructed nanoparticles using the pRNA-3WJ were stable in FBS, being resistant to RNases and stable at temperatures well above the 37 °C needed for *in vivo* applications. Furthermore, the 3WJ harboring the PSMA aptamer and anti-miRNA LNAs and positive functionality of each shows the versatility of the pRNA-3WJ to harbor RNA moieties while keeping the original functionality of each of the RNA groups; i.e. the targeting and binding of the PSMA aptamer and the silencing ability of the anti-miRNA LNAs. Through these experiments, we have shown that stable RNA nanoparticles can be constructed for the specific targeting and treatment of cancers, and past hurdles that have held back the field of RNA nanotechnology are no longer a concern.

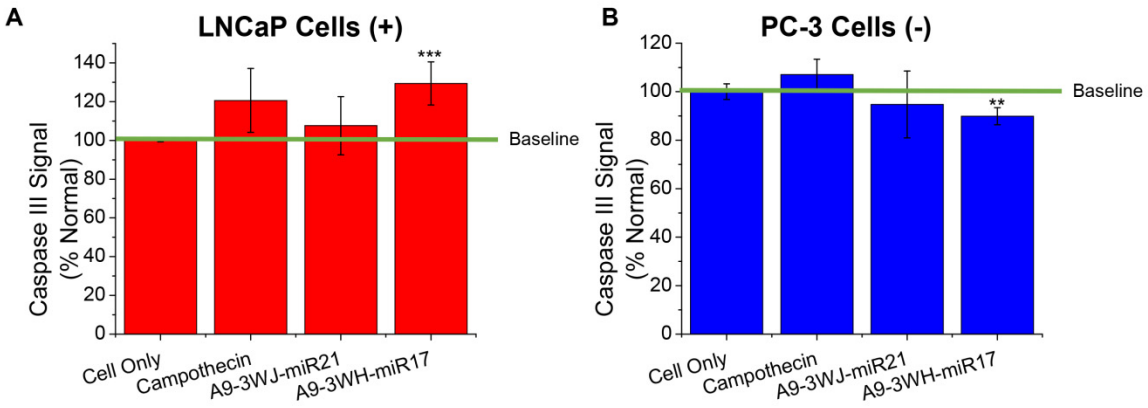

Figure 4.6. Caspase III signaling assay for apoptosis effects of 3WJ-pRNA nanoparticles harboring PSMA binding aptamer and anti-oncogenic miRNA LNA. RNA nanoparticles with anti-miR21 and -miR17 LNA were incubated with A) LNCaP and B) PC-3 cells cells for 24 hours. Caspase III signaling was assayed by fluorescent reporter with peak fluorescent of 440 nm as a reporter of cell apoptosis as a result of RNA nanoparticle delivery of anti-miRNA sequences. 5 μM Campothecin was used as a positive control and benchmark of apoptosis (**$p<0.01$, ***$p<0.001$).

In vivo delivery of anti-miRNA LNA to LNCaP

Subcutaneous xenograft tumors were developed in male nude mice with LNCaP C4-2 cells. Once tumors were fully developed (2 weeks) with cardio vasculature, 100 μL of 20 μM solution of pRNA-3WJ nanoparticle harboring the PSMA A9g aptamer along with an $Alexa_{647}$ fluorescent tag were administered to the mice through tail-vein injection. For all *in vivo* studies, nanoparticles were injected and delivered as bare oligos without the aid of any additives. Through a series of time points, mice were whole body imaged to examine the biodistribution of nanoparticles, along with the accumulation in tumors as well as healthy organs. Initially $Alexa_{647}$ was detected throughout the whole body of the mice indicating nanoparticles successfully circulated through the mice. Through early time points, $Alexa_{647}$ concentrated in the tumor, liver, and bladder of the mice; indicating the excess nanoparticles were excreted through the urine. After 8 hours, fluorescence signal was undetectable in all healthy organs was remaining strong in the xenograft tumor (**Fig. 4.7A)**. Additionally tumors were sectioned and imaged for fluorescent imaging (**Fig. 4.7C**). Confocal imaging shows specific targeting and accumulation of the A9g-3WJ nanoparticles to the LNCaP xenograft tumor. This indicates nanoparticles have no lasting accumulation in the liver or kidneys, thus having low toxicity profiles.

Furthermore the therapeutic effects of the A9g-3WJ-anti-miRNA nanoparticles were tested *in vivo* on LNCaP C4-2 subcutaneous xenografts. After tumors were developed to a volume of ~200 mm^3, nanoparticles harboring the anti-miR17 and –miR21 LNAs were administered to the mice through a series of five tail vein injections. Tumor volume and total weight of the mice were monitored throughout this experiment.

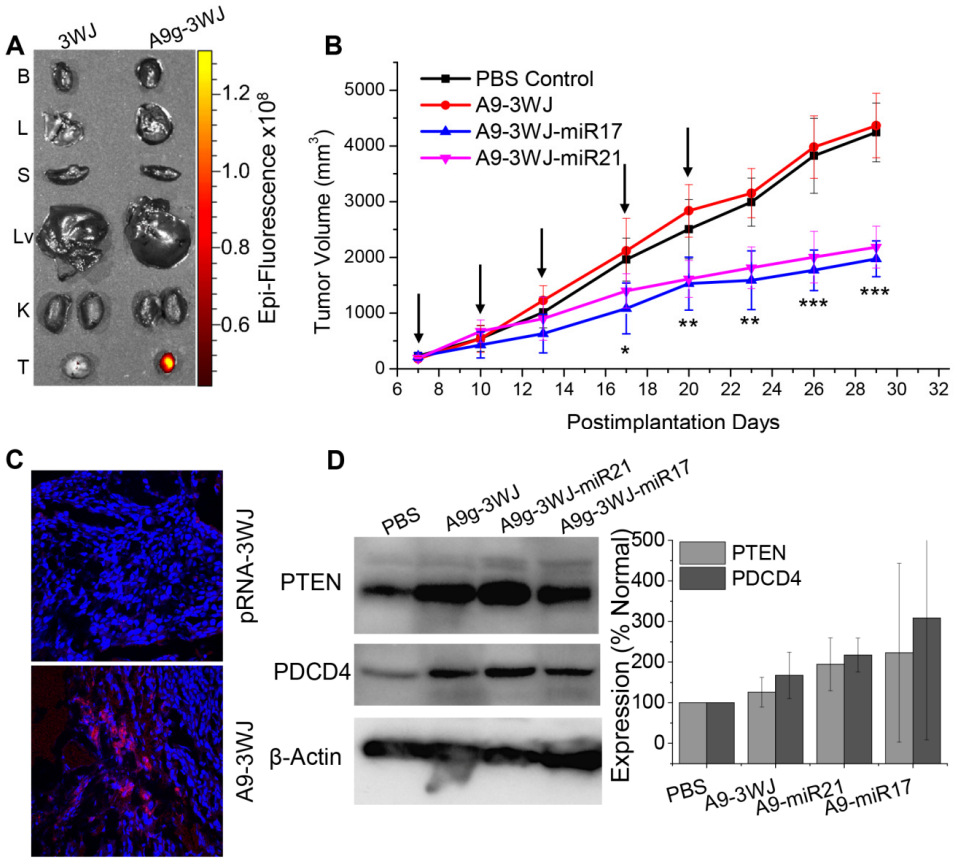

Figure 4.7. *In vivo* delivery of 3WJ-pRNA nanoparticles harboring PSMA binding aptamer and anti-miRNA LNA. RNA nanoparticles were delivered as bare oligos to LNCaP C4-2 subcutaneous xenografts in nude mice. A) Biodistribution of A9g-3WJ-Alexa$_{647}$ through nude mice. B: Brain, L: Lung, S: Spleen, Lv: Liver, K: Kidney, T: Tumor. B) Tumor bearing nude mice were administered nanoparticles through a series of five injections through the tail vein of 20 μM solution at 100 μL (indicated by arrows), while tumor volume (mm^3) and total mouse weight (g) were monitored (*P<0.05, **P<0.01, ***P<0.0001). C) Fluorescent confocal microscopy of tumor samples 8 hr post i.v. administration of RNA nanoparticles. DAPI (Blue) is cell nucleus, Alexa$_{647}$ (red) is RNA nanoparticle. D) Western blot examining downstream expression of *PTEN* and *PDCD4* from silencing of miR17 and miR21 using *β-Actin* as an internal control.

From the tumor volume data (**Fig. 4.7B**), it can clearly be seen that the A9-3WJ-anti-miRNA samples led to a stunted tumor growth and proliferation compared to negative controls, thus indicating the anti-miRNA oligos had a profound effect on the tumor environment and cell growth. Even after post-administration of the nanoparticles, a lack of growth in the tumors was seen for several days compared to non-treated tumors. Furthermore, there was no significant change in the mice weights over the observed RNA nanoparticle delivery indicating no toxicity in the mice and the tumor reduction was as a result of specific delivery to the tumors.

At the conclusion of *in vivo* delivery of the pRNA-3WJ nanoparticles, mice were sacrificed and tumors were harvested. *PTEN* and *PDCD4* expressions were measured in the tumors, using *β-Actin* as an internal control. Western blots (**Fig. 4.7D**) show an increase in *PTEN* and *PDCD4* in the pRNA-3WJ nanoparticles harboring the anti-miRNA LNAs. These results display the same ability of the 3WJ-pRNA nanoparticles as seen *in vitro* with the LNCaP cells, as the anti-miRNA sequences led to the increase of expression tumor suppressor genes as a result of decreased miR21 and miR17 expressions. On average an increase was seen in the A9g-3WJ sample over the control but less than A9g-3WJ-anti-miRNA groups. This may have been due to the repeated dosage of the RNA to the tumor cell in the animal trials, the larger volume of the nanoparticle may have had an effect on the gene expression within the tumor; however, the change in gene expression was not enough to create a change in tumor growth as shown in **Fig. 4.7B**. Here we demonstrate not only the ability of the RNA nanoparticles to accumulate and target the tumor specifically with high affinity, but deliver anti-oncogenic RNA sequences to regulate tumor growth and development of tumors.

CONCLUSIONS

Here we created RNA nanoparticles using the pRNA-3WJ core from the phi29 packaging motor for specific targeting and treatment of prostate cancer cells. RNA nanoparticles were proven to remain chemically and thermodynamically stable after the addition of functional groups off each branch. The LNCaP prostate cancer specific nanoparticles produces excellent binding profiles, displaying binding at over 90% at 100 nM RNA concentrations and later proved to provide specific delivery of anti-miRNA sequences for the knockdown of miR17 and miR21, two common oncogenes. Significant knockdown of miR17 and miR21 and up-regulation of *PTEN* indicated the positive and specific delivery by the pRNA-3WJ RNA nanoparticles in *in vitro* and *in vivo*. Through these studies, RNA nanoparticles have been developed that have the capability to target tumors primary and metastatic tumors as well tumors after hormone deprivation treatments. Furthermore, anti-miRNA sequences have been shown to control tumor growth and proliferation, while having the possibility to prevent PSMA tumors from transitioning to hormonal independent states.

AKNOWLEDGEMENTS:

The authors would like to thank the UK Flow Cytometry & Cell Sorting core facility for their assistance in FACS experiments. The UK Flow Cytometry & Cell Sorting core facility is supported in part by the Office of the Vice President for Research, the Markey Cancer Center and an NCI Center Core Support Grant (P30 CA177558) to the University of Kentucky Markey Cancer Center. This research was supported by NIH grants R01EB003730 and U01CA151648 to Peixuan Guo, R01CA186100 to Bin Guo and R25CA153954 to Brad Anderson. The content is solely the responsibility of the

authors and does not necessarily represent the official views of NIH. Funding to Peixuan Guo's Endowed Chair in Nanobiotechnology position is by the William Fairish Endowment Fund and Pharmaceutics and Drug Delivery System is by the Sylvan G. Frank Endowment Fund. Peixuan Guo is a co-founder of Kylin Therapeutics, Inc., and Biomotor and RNA Nanotechnology Development Corp. Ltd.

Chapter 5: Future Direction and Current State of the Field

CONCLUSIONS AND FUTURE DIRECTION:

In this thesis work is described for the advancement of the RNA nanotechnology field. In the past RNA nanoparticles have been limited due to their lack of stability to nucleases found in the body and their thermodynamic stability. As a result the promises of RNAi technologies have been ignored and the once strong interest has disappeared. Here in Chapter 2 and Chapter 3 of this dissertation, the instability of RNA has been overcome. By using previously developed 2-Fluoro modifications RNAs are now resistant to nucleases that are found *in vivo*. From the data here the pRNA-3WJ has proven to be a thermodynamically stable branched motif allowing for the conjugation of up to three functional groups. The novel assembly of the pRNA-3WJ of three RNA strands assembling in a one-step assembly that is entropically favored results in a ultra-stable RNA molecule stable to 29.5 pM and 69.8 °C. These findings were then translated into developing RNA nanoparticles for the specific targeting and delivery of anti-miRNA therapeutics to LNCaP prostate cancer cells. The pRNA-3WJ produced stable RNA nanoparticles that resulted in the knock-down of miRNA-21 and -17, ultimately leading to the apoptosis of the LNCaP cells, while displaying no toxic effects to PSMA- cells. Here the pRNA-3WJ has proven to be a stable, versatile RNA motif that revives the previous excitement behind RNAi therapeutics by overcoming previous roadblocks of instability.

However, in order to fully prove the potential of the pRNA-3WJ and RNA nanotechnology for the treatment of prostate cancer, future work is need. While it is

proven that the pRNA-3WJ based nanoparticles can target and treat prostate cancer cells *in vitro* and in subcutaneous xenograft tumors, and similar nanoparticles have been tested on other cancer models *in vivo* in mice; the PSMA-3WJ-anti-miRNA-21 and -17 need to be tested in a further tested more extensive mouse models to make proper conclusions for the applications in humans. It is generally accepted that pRNA-3WJ nanoparticles do not display any toxic effects or have long lasting accumulation in healthy organs; characterization of prostate cancer targeting and treatment of a solid prostate cancer tumor is needed. While a subcutaneous xenograft is a simple animal model to create, orthotopical models of prostate cancer would provide a more representative tumor model within mice. This would allow for a more hormonal dependent environment for proper tumor growth. In testing the RNA nanoparticles should be assayed for targeting and honing to the tumor developed in the mice as well as monitoring the tumor growth after treatment of the RNA nanoparticles. Futhermore, it is thought that the targeted miRNA-21 and -17 play roles in metastasis of prostate cancer and the created RNA nanoparticles may be able to control this action. If this is to be true extended studies in mice with a metastasis model treated with A9g-3WJ-anti-miRNA nanoparticles is to be tested. Furthermore, it should be confirmed that the RNA nanoparticles do not have any toxic effects or accumulations in healthy organs within the mice. If the future *in vivo* testing of the PSMA-3WJ-anti-miRNA nanoparticles remains as promising as presented here, further development into clinical trials should be considered.

CURRENT STATE OF THE FIELD:

Since the development of RNA nanotechnology in 1998 (12), the field has come a long way covering several hurdles that once blocked its progress. With the current growth

and findings of the most recent research, RNA nanotechnology has a possibility of bringing the initial promise of RNAi therapeutics to fruition. Previously RNA nanotechnology was not thought of for the treatment of cancers and viral infections due to several limitations of RNA, most notably the cost of production, susceptibility to RNases found in throughout the body, thermodynamic stability and dissociation of the RNA strands. Progress through the field has overcome most of these limitations.

As described in this dissertation, RNAs have now been proven to remain stable both against nucleases and dissociation. Chemical modifications to the carbon ring of RNA has shown to produce nucleic acid structures that are stable against nucleases (189) and are stable *in vivo* as shown in mice (87,123,137,139). Additionally these modifications have also been shown to increase the thermodynamic stability of the RNA structure (223). The Phi29 pRNA three-way junction motif has been tested and proven to remain stable at ultra-low concentrations and does not dissociation when placed into mice. Furthermore, several other RNA nanoparticles have been constructed and shown to be stable during *in vivo* testing (264-266). These recent results have shown the RNA nanotechnology has overcome two previous hurdles blocking the field from growing.

Previously, one of the major limitations of RNA nanotechnology was the cost of production and limitations to the size of production. RNA is typically produced through *in vitro* transcription with T7 RNA polymerase (177,267) or through chemical synthesis. *In vitro* transcription of RNAs provides a relatively low cost of production; however, not only is the process time consuming, the batch size of production is normally limited to a small scale that is far too small to be used for human dosing. Additionally the production of RNA through T7 polymerase created some level of error in both the length and

sequence created, requiring purification of RNA strands to remove off-target, undesired strands. On the opposite spectrum chemical synthesis provides very specific RNA products. However, the cost of production of RNA through chemical synthesis was cost prohibitive in order to produce RNA on a scale needed for clinical testing. Additionally, the chemical synthesis was limited to synthesizing RNA to sizes below 60 base pairs. The limitations behind each of the methods thus limited the large scale production of RNAs needed for clinical trials. However, recent work and efforts have targeted the production of RNA to lower the cost and increase the scale of production. Chemical synthesis of RNAs have now increased the length able to be produced and continues to grow. Additionally large scale production has now been produced to reach up to gram scale synthesis, while lowering the cost of production. Furthermore, techniques have been developed for large scale purification of RNAs (268). As technologies advance the production of RNA for *in vivo* testing and moving to translational work will only advance, making RNA nanoparticles a viable product as the cost will continue to decrease and become more reasonable.

While the field of RNA nanotechnology is considered relatively young compared to other nanotechnology fields, it has recently proven to be a promising area of research for the treatment of cancers and viral infections. RNA nanoparticles are now to the point that they have proven to work and function properly and at a non-toxic level *in vitro* and *in vivo* in animal testing; and are approaching the point in which they will undergo clinical testing. Methods in large scale production of RNA is now possible to provide the demand of large amounts of RNA that will be needed for delivery into humans. After close to two decades of growth, the field of RNA nanotechnology has reached a point in

which the hurdles that were once limiting the growth have been overcome and now research and testing of the particles can move forward unhindered.

APPENDICES

APPENDIX 1: DERRIVATION OF KINETICS MODELS

Association Phase:

In the reaction: $3WJ_a + 3WJ_b + 3WJ_c \underset{k_d}{\overset{k_a}{\rightleftarrows}} 3WJ$ the rate equation will be as below

$$\frac{d[3WJ]}{dt} = k_a[3WJ_a][3WJ_b][3WJ_c] - k_d[3WJ]$$

In solving this reaction it will be assumed that $3WJ_c$ is the ligand strand bound to the SPR chip surface and $3WJ_a$ and $3WJ_b$ strands are the analyte strands flowing over the chip surface. In this case, the $[3WJ_a]$ and $[3WJ_b]$ are at a much higher concentration than $[3WJ_c]$ and the formation of 3WJ will result in no noticeable change in the concentrations of $[3WJ_a]$ or $[3WJ_b]$ therefore:

$[3WJ_a] = [3WJ_a]_o$

and

$$[3WJ_b] = [3WJ_b]_o$$

additionally

$$[3WJ_a]_o = [3WJ_b]_o$$

To solve the differential rate equation, x will be the $[3WJ_c]$ that has been converted to $[3WJ]$. Therefore

$$[3WJ_c]_t = [3WJ_c]_o - x$$

and

$$[3WJ]_t = [3WJ]_o + x$$

This gives a new differential equation of

$$\frac{dx}{dt} = k_a[3WJ_a]_o[3WJ_b]_o([3WJ_c]_o - x) - k_d([3WJ]_o - x)$$

Or

$$\frac{dx}{dt} = k_a[3WJ_a]_o^2([3WJ_c]_0 - x) - k_d([3WJ]_o - x)$$

Next, at equilibrium the reaction forward forming 3WJ is at the same rate as the reverse reaction forming ssRNAs; the following equations are true

$$[3WJ_c]_e = [3WJ_c]_o - x_e$$

$$[3WJ]_e = [3WJ]_o + x_e$$

$$k_a[3WJ_a]_o[3WJ_b]_o[3WJ_c]_e = k_a[3WJ_a]_o^2[3WJ_c]_e = k_d[3WJ]_e$$

These equilibrium equations can be plugged into the differential equation

$$\frac{dx}{dt} = k_a[3WJ_a]_o^2([3WJ_c]_e + x_e - x) - k_d([3WJ]_e - x_e + x)$$

Or rearranged to

$$\frac{dx}{dt} = (k_a[3WJ_a]_o^2[3WJ_c]_e - k_d[3WJ]_e) + k_a[3WJ_a]_o^2(x_e - x) + k_d(x_e - x)$$

Where the first term is equal to zero at an equilibrium state, resulting in

$$\frac{dx}{dt} = (k_a[3WJ_a]_o^2 + k_d)(x_e - x)$$

The integration of this differential leads to

$$\frac{dx}{(x_e - x)} = (k_a[3WJ_a]_o^2 + k_d)dt$$

$$-\int_0^x d\ln(x_e - x) = (k_a[3WJ_a]_o^2 + k_d)\int_{t_o}^{t} dt$$

Or

$$-\ln\frac{x_e - x}{x_e} = (k_a[3WJ_a]_o^2 + k_d)(t - t_o)$$

Exponential of both sides leads to

$$x = x_e\left(1 - e^{-\left(k_a[3WJ_a]_o^2 + k_d\right)(t - t_o)}\right)$$

Here *x* is replaced with Response from the SPR which is direct proportion to [*3WJ*], expressed as *R*

$$R = R_{eq}\left(1 - e^{-\left(k_a[3WJ_a]_o^2 + k_d\right)(t - t_o)}\right)$$

Solving for R_{eq}:

At a steady state of the reaction of ssRNA folding to the pRNA-3WJ, the change in response is expressed as

$$\frac{dR}{dt} = 0 = k_a[3WJ_a]_o^2 R_{max} - (k_a[3WJ_a]_o^2 + k_d)R$$

Where *R* is the [*3WJ*] and R_{max} is the maximum 3WJ that can be formed and is limited to [$3WJ_c$]. Therefore,

$$k_a[3WJ_a]_o^2 R_{max} = (k_a[3WJ_a]_o^2 + k_d)R$$

R is replaced with R_{eq} since the reaction is at steady state

$$R_{eq} = \frac{k_a[3WJ_a]_o^2 R_{max}}{k_a[3WJ_a]_o^2 + k_d}$$

Dissociation Phase:

The dissociation of the pRNA-3WJ is considered unimolecular and rate of reaction is expressed as

$$\frac{d[3WJ]}{dt} = -k_d[3WJ]$$

Again the [*3WJ*] is placed in terms of Response from the SPR machine and the rate differential equation id then expressed as

$$\frac{dR}{dt} = -k_d R$$

The simple differential is then solved through integration to

$$\frac{dR}{R} = -k_d dt$$

$$\int_{R_o}^{R} \frac{dR}{R} = -k_d \int_{t_o}^{t} dt$$

$$\ln R - \ln R_o = -k_d(t - t_o)$$

Taking an exponential on both sides results in

$$R = R_o e^{-k_d(t-t_o)}$$

Therefore the SPR curves can be modeled using the following equations for the association and dissociation phases, respectively.

$$R = \frac{k_a[3WJ_a]_o^2 R_{max}}{k_a[3WJ_a]_o^2 + k_d}\left(1 - e^{-\left(k_a[3WJ_a]_o^2 + k_d\right)(t-t_o)}\right)$$

$$R = R_o e^{-k_d(t-t_o)}$$

REFERENCES

1. Feynman RP (1960) There's Plenty of Room at the Bottom---An Invitation to Enter a New Field of Physics (Dec. 29, 1959 at the Ann Meet Amer Phys Soc,Ca Ins of Tech). *Caltech's Engineering and Science,* December issue:

2. K.Eric Drexler (1986) *Engines of Creation: The Coming Era of Nanotechnology*, Anchor Books, New York

3. Westesen K, Siekmann B, & Koch MHJ (1993) Investigations on the Physical State of Lipid Nanoparticles by Synchrotron-Radiation X-Ray-Diffraction. *International Journal of Pharmaceutics* 93: 189-199

4. Quintanar-Guerrero D, Allemann E, Fessi H, & Doelker E (1998) Preparation Techniques and Mechanisms of Formation of Biodegradable Nanoparticles From Preformed Polymers. *Drug Development and Industrial Pharmacy* 24: 1113-1128

5. Weber C, Coester C, Kreuter J, & Langer K (2000) Desolvation Process and Surface Characterisation of Protein Nanoparticles. *International Journal of Pharmaceutics* 194: 91-102

6. Klem MT, Willits D, Young M, & Douglas T (2003) 2-D Array Formation of Genetically Engineered Viral Cages on Au Surfaces and Imaging by Atomic Force Microscopy. *J. Am. Chem. Soc.* 125: 10806-10807

7. Wang XS, Li QQ, Xie J, Jin Z, Wang JY, Li Y, Jiang KL, & Fan SS (2009) Fabrication of Ultralong and Electrically Uniform Single-Walled Carbon Nanotubes on Clean Substrates. *Nano Letters* 9: 3137-3141

8. Eigler DM & Schweizer EK (1990) Positioning Single Atoms With A Scanning Tunneling Microscope. *Nature* 344: 524-526

9. Munro CH, Smith WE, Garner M, Clarkson J, & White PC (1995) Characterization of the Surface of A Citrate-Reduced Colloid Optimized for Use As A Substrate for Surface-Enhanced Resonance Raman-Scattering. *Langmuir* 11: 3712-3720

10. Babes L, Denizot B, Tanguy G, Le Jeune JJ, & Jallet P (1999) Synthesis of Iron Oxide Nanoparticles Used As MRI Contrast Agents: A Parametric Study. *Journal of Colloid and Interface Science* 212: 474-482

11. Kallenbach N, Ma R, & Seeman N (1983) An Immobile Nucleic Acid Junction Constructed From Oligonucleotides. *Nature* 305: 829-831

12. Guo P, Zhang C, Chen C, Trottier M, & Garver K (1998) Inter-RNA Interaction of Phage Phi29 PRNA to Form a Hexameric Complex for Viral DNA Transportation. *Mol. Cell.* 2: 149-155

13. Duncan R (2003) The Dawning Era of Polymer Therapeutics. *Nat Rev. Drug Discov.* 2: 347-360

14. Ferrari M (2005) Cancer Nanotechnology: Opportunities and Challenges. *Nat Rev. Cancer* 5: 161-171

15. Mudshinge SR, Deore AB, Patil S, & Bhalgat CM (2011) Nanoparticles: Emerging Carriers for Drug Delivery. *Saudi Pharmaceutical Journal* 19: 129-141

16. Morgen M, Bloom C, Beyerinck R, Bello A, Song W, Wilkinson K, Steenwyk R, & Shamblin S (2012) Polymeric Nanoparticles for Increased Oral Bioavailability and Rapid Absorption Using Celecoxib As a Model of a Low-Solubility, High-Permeability Drug. *Pharmaceutical Research* 29: 427-440

17. Savjani KT, Gajjar AK, & Savjani JK (2012) Drug Solubility: Importance and Enhancement Techniques. *ISRN. Pharm.* 2012: 195727

18. Mallick A, More P, Ghosh S, Chippalkatti R, Chopade BA, Lahiri M, & Basu S (2015) Dual Drug Conjugated Nanoparticle for Simultaneous Targeting of Mitochondria and Nucleus in Cancer Cells. *ACS applied materials & interfaces* 7: 7584-7598

19. Pham E, Birrer MJ, Eliasof S, Garmey EG, Lazarus D, Lee CR, Man S, Matulonis UA, Peters CG, Xu P, Krasner C, & Kerbel RS (2015) Translational Impact of Nanoparticle-Drug Conjugate CRLX101 With or Without Bevacizumab in Advanced Ovarian Cancer. *Clinical Cancer Research* 21: 808-818

20. Chu KS, Schorzman AN, Finniss MC, Bowerman CJ, Peng L, Luft JC, Madden AJ, Wang AZ, Zamboni WC, & DeSimone JM (2013) Nanoparticle Drug Loading As a Design Parameter to Improve Docetaxel Pharmacokinetics and Efficacy. *Biomaterials* 34: 8424-8429

21. De Jong WH & Borm PJA (2008) Drug Delivery and Nanoparticles: Applications and Hazards. *International Journal of Nanomedicine* 3: 133-149

22. Banerjee R, Parida S, Maiti C, Mandal M, & Dhara D (2015) PH-Degradable and Thermoresponsive Water-Soluble Core Cross-Linked Polymeric Nanoparticles As Potential Drug Delivery Vehicle for Doxorubicin. *Rsc Advances* 5: 83565-83575

23. Han HS, Thambi T, Choi KY, Son S, Ko H, Lee MC, Jo DG, Chae YS, Kang YM, Lee JY, & Park JH (2015) Bioreducible Shell-Cross-Linked Hyaluronic Acid Nanoparticles for Tumor-Targeted Drug Delivery. *Biomacromolecules* 16: 447-456

24. Bartlett RL & Panitch A (2012) Thermosensitive Nanoparticles With PH-Triggered Degradation and Release of Anti-Inflammatory Cell-Penetrating Peptides. *Biomacromolecules.* 13: 2578-2584

25. Hatakeyama H, Murata M, Sato Y, Takahashi M, Minakawa N, Matsuda A, & Harashima H (2013) The Systemic Administration of an Anti-MiRNA Oligonucleotide Encapsulated

PH-Sensitive Liposome Results in Reduced Level of Hepatic MicroRNA-122 in Mice. *J Control Release*

26. Kale AA & Torchilin VP (2007) "Smart" Drug Carriers: PEGylated TATp-Modified PH-Sensitive Liposomes. *J Liposome Res* 17: 197-203

27. Kyriakides TR, Cheung CY, Murthy N, Bornstein P, Stayton PS, & Hoffman AS (2002) PH-Sensitive Polymers That Enhance Intracellular Drug Delivery in Vivo. *J Control Release* 78: 295-303

28. Lv S, Tang Z, Zhang D, Song W, Li M, Lin J, Liu H, & Chen X (2014) Well-Defined Polymer-Drug Conjugate Engineered With Redox and PH-Sensitive Release Mechanism for Efficient Delivery of Paclitaxel. *J Control Release* 194C: 220-227

29. Lehto T, Simonson OE, Mager I, Ezzat K, Sork H, Copolovici DM, Viola JR, Zaghloul EM, Lundin P, Moreno PM, Mae M, Oskolkov N, Suhorutsenko J, Smith CI, & Andaloussi SE (2011) A Peptide-Based Vector for Efficient Gene Transfer in Vitro and in Vivo. *Mol. Ther.* 19: 1457-1467

30. Olson ES, Jiang T, Aguilera TA, Nguyen QT, Ellies LG, Scadeng M, & Tsien RY (2010) Activatable Cell Penetrating Peptides Linked to Nanoparticles As Dual Probes for in Vivo Fluorescence and MR Imaging of Proteases. *Proc. Natl. Acad. Sci. U. S. A* 107: 4311-4316

31. Schiffelers RM, Ansari A, Xu J, Zhou Q, Tang Q, Storm G, Molema G, Lu PY, Scaria PV, & Woodle MC (2004) Cancer SiRNA Therapy by Tumor Selective Delivery With Ligand-Targeted Sterically Stabilized Nanoparticle. *Nucleic Acids Res.* 32: e149

32. Ellington AD & Szostak JW (1992) Selection in Vitro of Single-Stranded DNA Molecules That Fold into Specific Ligand-Binding Structures. *Nature* 355: 850-852

33. Gold L (1995) The SELEX Process: a Surprising Source of Therapeutic and Diagnostic Compounds. *Harvey Lect.* 91: 47-57

34. Arvinte T, Wahl P, & Nicolau C (1987) Resonance Energy-Transfer and Fluorescence Intensity Studies of the Transport of Liposome-Encapsulated Molecules into Isolated Mouse Liver Nuclei. *Biochemistry* 26: 765-772

35. Gutierrez-Merino C, Bonini dR, I, Pietrasanta LI, & Barrantes FJ (1995) Preferential Distribution of the Fluorescent Phospholipid Probes NBD-Phosphatidylcholine and Rhodamine-Phosphatidylethanolamine in the Exofacial Leaflet of Acetylcholine Receptor-Rich Membranes From Torpedo Marmorata. *Biochemistry* 34: 4846-4855

36. Douglas SJ, Davis SS, & Illum L (1987) Nanoparticles in Drug Delivery. *Crit Rev. Ther. Drug Carrier Syst.* 3: 233-261

37. Moon MH & Giddings JC (1993) Size Distribution of Liposomes by Flow Field-Flow Fractionation. *J. Pharm. Biomed. Anal.* 11: 911-920

38. Lee JB, Hong J, Bonner DK, Poon Z, & Hammond PT (2012) Self-Assembled RNA Interference Microsponges for Efficient SiRNA Delivery. *Nat. Mater.* 11: 316-322

39. Duncan R (2011) Polymer Therapeutics As Nanomedicines: New Perspectives. *Curr. Opin. Biotechnol.* 22: 492-501

40. Manchester M & Singh P (2006) Virus-Based Nanoparticles (VNPs): Platform Technologies for Diagnostic Imaging. *Adv. Drug Deliv. Rev.* 58: 1505-1522

41. Rae CS, Khor IW, Wang Q, Destito G, Gonzalez MJ, Singh P, Thomas DM, Estrada MN, Powell E, Finn MG, & Manchester M (2005) Systemic Trafficking of Plant Virus Nanoparticles in Mice Via the Oral Route. *Virology* 343: 224-235

42. Weiner LM (1999) Monoclonal Antibody Therapy of Cancer. *Semin. Oncol.* 26: 43-51

43. Harrison J, Shi X, Wang L, Ma JK, & Rojanasakul Y (1994) Novel Delivery of Antioxidant Enzyme Catalase to Alveolar Macrophages by Fc Receptor-Mediated Endocytosis. *Pharm. Res* 11: 1110-1114

44. Li J, Pei H, Zhu B, Liang L, Wei M, He Y, Chen N, Li D, Huang Q, & Fan CH (2011) Self-Assembled Multivalent DNA Nanostructures for Noninvasive Intracellular Delivery of Immunostimulatory CpG Oligonucleotides. *ACS Nano* 5: 8783-8789

45. Lin C, Liu Y, Rinker S, & Yan H (2006) DNA Tile Based Self-Assembly: Building Complex Nanoarchitectures. *Chemphyschem.* 7: 1641-1647

46. Lo PK, Metera KL, & Sleiman HF (2010) Self-Assembly of Three-Dimensional DNA Nanostructures and Potential Biological Applications. *Current Opinion in Chemical Biology* 14: 597-607

47. Kang D, Wang J, Zhang W, Song Y, Li X, Zou Y, Zhu M, Zhu Z, Chen F, & Yang CJ (2012) Selection of DNA Aptamers Against Glioblastoma Cells With High Affinity and Specificity. *PLoS ONE* 7: e42731

48. Liu X, Yan H, Liu Y, & Chang Y (2011) Targeted Cell-Cell Interactions by DNA Nanoscaffold-Templated Multivalent Bispecific Aptamers. *Small* 7: 1673-1682

49. Henke E, Perk J, Vider J, de CP, Chin Y, Solit DB, Ponomarev V, Cartegni L, Manova K, Rosen N, & Benezra R (2008) Peptide-Conjugated Antisense Oligonucleotides for Targeted Inhibition of a Transcriptional Regulator in Vivo. *Nat Biotechnol.* 26: 91-100

50. Fire A, Xu S, Montgomery MK, Kostas SA, Driver SE, & Mello CC (1998) Potent and Specific Genetic Interference by Double-Stranded RNA in Caenorhabditis Elegans. *Nature* 391: 806-811

51. Hamilton AJ & Baulcombe DC (1999) A Species of Small Antisense RNA in Posttranscriptional Gene Silencing in Plants. *Science* 286: 950-952

52. Elbashir SM, Harborth J, Lendeckel W, Yalcin A, Weber K, & Tuschl T (2001) Duplexes of 21-Nucleotide RNAs Mediate RNA Interference in Cultured Mammalian Cells. *Nature* 411: 494-498

53. Elbashir SM, Lendeckel W, & Tuschl T (2001) RNA Interference Is Mediated by 21- and 22-Nucleotide RNAs. *Genes Dev.* 15: 188-200

54. Ghildiyal M & Zamore PD (2009) Small Silencing RNAs: an Expanding Universe. *Nat. Rev. Genet.* 10: 94-108

55. Guo P, Coban O, Snead NM, Trebley J, Hoeprich S, Guo S, & Shu Y (2010) Engineering RNA for Targeted SiRNA Delivery and Medical Application. *Advanced Drug Delivery Reviews* 62: 650-666

56. Jacque JM, Triques K, & Stevenson M (2002) Modulation of HIV-1 Replication by RNA Interference. *Nature* 418: 435-438

57. Varambally S, Dhanasekaran SM, Zhou M, Barrette TR, Kumar-Sinha C, Sanda MG, Ghosh D, Pienta KJ, Sewalt RG, Otte AP, Rubin MA, & Chinnaiyan AM (2002) The Polycomb Group Protein EZH2 Is Involved in Progression of Prostate Cancer. *Nature* 419: 624-629

58. Akinc A, Querbes W, De S, Qin J, Frank-Kamenetsky M, Jayaprakash KN, Jayaraman M, Rajeev KG, Cantley WL, Dorkin JR, Butler JS, Qin L, Racie T, Sprague A, Fava E, Zeigerer A, Hope MJ, Zerial M, Sah DW, Fitzgerald K, Tracy MA, Manoharan M, Koteliansky V, Fougerolles A, & Maier MA (2010) Targeted Delivery of RNAi Therapeutics With Endogenous and Exogenous Ligand-Based Mechanisms. *Mol. Ther.* 18: 1357-1364

59. Bora RS, Gupta D, Mukkur TK, & Saini KS (2012) RNA Interference Therapeutics for Cancer: Challenges and Opportunities (Review). *Mol. Med. Rep.* 6: 9-15

60. Bumcrot D, Manoharan M, Koteliansky V, & Sah DW (2006) RNAi Therapeutics: a Potential New Class of Pharmaceutical Drugs. *Nat Chem. Biol.* 2: 711-719

61. Chang CI, Kang HS, Ban C, Kim S, & Lee DK (2009) Dual-Target Gene Silencing by Using Long, Synthetic SiRNA Duplexes Without Triggering Antiviral Responses. *Molecules and Cells* 27: 689-695

62. Chiu YL & Rana TM (2002) RNAi in Human Cells: Basic Structural and Functional Features of Small Interfering RNA. *Mol. Cell* 10: 549-561

63. Morrissey DV, Blanchard K, Shaw L, Jensen K, Lockridge JA, Dickinson B, McSwiggen JA, Vargeese C, Bowman K, Shaffer CS, Polisky BA, & Zinnen S (2005) Activity of Stabilized Short Interfering RNA in a Mouse Model of Hepatitis B Virus Replication. *Hepatology* 41: 1349-1356

64. Behlke MA (2008) Chemical Modification of SiRNAs for in Vivo Use. *Oligonucleotides.* 18: 305-319

65. Behlke MA (2006) Progress Towards in Vivo Use of SiRNAs. *Mol Ther.* 13: 644-670

66. Gao H, Shi W, & Freund LB (2005) Mechanics of Receptor-Mediated Endocytosis. *Proc Natl Acad Sci U. S. A* 102: 9469-9474

67. Jain KK (2005) The Role of Nanobiotechnology in Drug Discovery. *Drug Discov. Today* 10: 1435-1442

68. Li W & Szoka F (2007) Lipid-Based Nanoparticles for Nucleic Acid Delivery. *Pharm. Res* 24: 438-449

69. Maeda H (2001) The Enhanced Permeability and Retention (EPR) Effect in Tumor Vasculature: the Key Role of Tumor-Selective Macromolecular Drug Targeting. *Adv. Enzyme Regul.* 41: 189-207

70. Tanaka T, Shivamoto S, Miyashita M, Fujishima Y, & Kaneo Y (2004) Tumor Targeting Based on the Effect of Enhanced Permeability and Retention (EPR) and the Mechanism of Receptor-Mediated Endocytosis (RME). *Int J Pharm.* 277: 39-61

71. Ambs S, Prueitt RL, Yi M, Hudson RS, Howe TM, Petrocca F, Wallace TA, Liu CG, Volinia S, Calin GA, Yfantis HG, Stephens RM, & Croce CM (2008) Genomic Profiling of MicroRNA and Messenger RNA Reveals Deregulated MicroRNA Expression in Prostate Cancer. *Cancer Res* 68: 6162-6170

72. Budhu A, Jia HL, Forgues M, Liu CG, Goldstein D, Lam A, Zanetti KA, Ye QH, Qin LX, Croce CM, Tang ZY, & Wang XW (2008) Identification of Metastasis-Related MicroRNAs in Hepatocellular Carcinoma. *Hepatology* 47: 897-907

73. Calin GA & Croce CM (2006) MicroRNA Signatures in Human Cancers. *Nature Reviews Cancer* 6: 857-866

74. Croce CM & Calin GA (2005) MiRNAs, Cancer, and Stem Cell Division. *Cell* 122: 6-7

75. Croce CM (2008) Oncogenes and Cancer. *N. Engl. J Med.* 358: 502-511

76. Di LG, Garofalo M, & Croce CM (2014) MicroRNAs in Cancer. *Annu. Rev. Pathol.* 9: 287-314

77. Garzon R, Marcucci G, & Croce CM (2010) Targeting MicroRNAs in Cancer: Rationale, Strategies and Challenges. *Nat Rev. Drug Discov.* 9: 775-789

78. Obad S, dos Santos CO, Petri A, Heidenblad M, Broom O, Ruse C, Fu C, Lindow M, Stenvang J, Straarup EM, Hansen HF, Koch T, Pappin D, Hannon GJ, & Kauppinen S (2011) Silencing of MicroRNA Families by Seed-Targeting Tiny LNAs. *Nat. Genet.* 43: 371-378

79. Devulapally R, Sekar NM, Sekar TV, Foygel K, Massoud TF, Willmann JK, & Paulmurugan R (2015) Polymer Nanoparticles Mediated Codelivery of AntimiR-10b and AntimiR-21 for Achieving Triple Negative Breast Cancer Therapy. *ACS Nano.* 9: 2290-2302

80. Costa PM, Cardoso AL, Custodia C, Cunha P, Pereira de AL, & Pedroso de Lima MC (2015) MiRNA-21 Silencing Mediated by Tumor-Targeted Nanoparticles Combined With Sunitinib: A New Multimodal Gene Therapy Approach for Glioblastoma. *J. Control Release* 207: 31-39

81. Shi SJ, Zhong ZR, Liu J, Zhang ZR, Sun X, & Gong T (2012) Solid Lipid Nanoparticles Loaded With Anti-MicroRNA Oligonucleotides (AMOs) for Suppression of MicroRNA-21 Functions in Human Lung Cancer Cells. *Pharm. Res.* 29: 97-109

82. Alhasan AH, Patel PC, Choi CH, & Mirkin CA (2014) Exosome Encased Spherical Nucleic Acid Gold Nanoparticle Conjugates As Potent MicroRNA Regulation Agents. *Small* 10: 186-192

83. Shu D, Li H, Shu Y, Xiong G, Carson WE, Haque F, Xu R, & Guo P (2015) Systemic Delivery of Anti-MiRNA for Suppression of Triple Negative Breast Cancer Utilizing RNA Nanotechnology. *ACS Nano* Accepted. DOI: 10.1021/acsnano.5b02471.

84. Yoo SS, Razzak R, Bedard E, Guo L, Shaw AR, Moore RB, & Roa WH (2014) Layered Gadolinium-Based Nanoparticle As a Novel Delivery Platform for MicroRNA Therapeutics. *Nanotechnology.* 25: 425102

85. Cheng CJ, Bahal R, Babar IA, Pincus Z, Barrera F, Liu C, Svoronos A, Braddock DT, Glazer PM, Engelman DM, Saltzman WM, & Slack FJ (2015) MicroRNA Silencing for Cancer Therapy Targeted to the Tumour Microenvironment. *Nature* 518: 107-110

86. Shu D, Moll WD, Deng Z, Mao C, & Guo P (2004) Bottom-Up Assembly of RNA Arrays and Superstructures As Potential Parts in Nanotechnology. *Nano Lett.* 4: 1717-1723

87. Shu D, Shu Y, Haque F, Abdelmawla S, & Guo P (2011) Thermodynamically Stable RNA Three-Way Junctions for Constructing Multifuntional Nanoparticles for Delivery of Therapeutics. *Nature Nanotechnology* 6: 658-667

88. Afonin KA, Bindewald E, Yaghoubian AJ, Voss N, Jacovetty E, Shapiro BA, & Jaeger L (2010) In Vitro Assembly of Cubic RNA-Based Scaffolds Designed in Silico. *Nat. Nanotechnol.* 5: 676-682

89. Jaeger L & Leontis NB (2000) Tecto-RNA: One Dimensional Self-Assembly Through Tertiary Interactions. *Angew. Chem Int. Ed Engl.* 39: 2521-2524

90. Leontis NB, Lescoute A, & Westhof E (2006) The Building Blocks and Motifs of RNA Architecture. *Curr Opin Struct Biol* 16: 279-287

91. Guo P (2010) The Emerging Field of RNA Nanotechnology. *Nature Nanotechnology* 5: 833-842

92. Hoeprich S, ZHou Q, Guo S, Qi G, Wang Y, & Guo P (2003) Bacterial Virus Phi29 PRNA As a Hammerhead Ribozyme Escort to Destroy Hepatitis B Virus. *Gene Ther.* 10: 1258-1267

93. Sarver NA, Cantin EM, Chang PS, Zaia JA, Ladne PA, Stephens DA, & Rossi JJ (1990) Ribozymes As Potential Anti-HIV-1 Therapeutic Agents. *Science* 24: 1222-1225

94. Liu H, Guo S, Roll R, Li J, Diao Z, Shao N, Riley MR, Cole AM, Robinson JP, Snead NM, Shen G, & Guo P (2007) Phi29 PRNA Vector for Efficient Escort of Hammerhead Ribozyme Targeting Survivin in Multiple Cancer Cells. *Cancer Biol. Ther.* 6: 697-704

95. Winkler WC, Nahvi A, Roth A, Collins JA, & Breaker RR (2004) Control of Gene Expression by a Natural Metabolite-Responsive Ribozyme. *Nature* 428: 281-286

96. Mulhbacher J, St-Pierre P, & Lafontaine DA (2010) Therapeutic Applications of Ribozymes and Riboswitches. *Curr. Opin. Pharmacol.* 10: 551-556

97. Khaled A, Guo S, Li F, & Guo P (2005) Controllable Self-Assembly of Nanoparticles for Specific Delivery of Multiple Therapeutic Molecules to Cancer Cells Using RNA Nanotechnology. *Nano Letters* 5: 1797-1808

98. Guo S, Tschammer N, Mohammed S, & Guo P (2005) Specific Delivery of Therapeutic RNAs to Cancer Cells Via the Dimerization Mechanism of Phi29 Motor PRNA. *Hum Gene Ther.* 16: 1097-1109

99. Guo S, Huang F, & Guo P (2006) Construction of Folate-Conjugated PRNA of Bacteriophage Phi29 DNA Packaging Motor for Delivery of Chimeric SiRNA to Nasopharyngeal Carcinoma Cells. *Gene Ther* 13: 814-820

100. Pegtel DM, Cosmopoulos K, Thorley-Lawson DA, van Eijndhoven MA, Hopmans ES, Lindenberg JL, de Gruijl TD, Wurdinger T, & Middeldorp JM (2010) Functional Delivery of Viral MiRNAs Via Exosomes. *Proc. Natl. Acad. Sci. U. S. A* 107: 6328-6333

101. Chen Y, Zhu X, Zhang X, Liu B, & Huang L (2010) Nanoparticles Modified With Tumor-Targeting ScFv Deliver SiRNA and MiRNA for Cancer Therapy. *Mol. Ther.* 18: 1650-1656

102. Ye X, Liu Z, Hemida MG, & Yang D (2011) Targeted Delivery of Mutant Tolerant Anti-Coxsackievirus Artificial MicroRNAs Using Folate Conjugated Bacteriophage Phi29 PRNA. *PLoS. One.* 6: e21215

103. Cantor CR, Wollenzien PL, & Hearst JE (1980) Structure and Topology of 16S Ribosomal RNA. An Analysis of the Pattern of Psoralen Crosslinking. *Nucleic Acids Res* 8: 1855-1872

104. Dunkle JA & Cate JH (2010) Ribosome Structure and Dynamics During Translocation and Termination. *Annu. Rev. Biophys.* 39: 227-244

105. Stern S, Wilson RC, & Noller HF (1986) Localization of the Binding Site for Protein S4 on 16S Ribosomal RNA by Chemical and Enzymatic Probing and Primer Extension. *J Mol Biol* 192: 101-110

106. Barta A, Steiner G, Brosius J, Noller HF, & Kuechler E (1984) Identification of a Site on 23s Ribosomal RNA Isolated at the Peptidyl Transferase Center. *Proc. Natl. Acad. Sci. USA* 81: 3607-3611

107. Bachellerie JP, Cavaille J, & Huttenhofer A (2002) The Expanding SnoRNA World. *Biochimie* 84: 775-790

108. Hertel J, Hofacker IL, & Stadler PF (2008) SnoReport: Computational Identification of SnoRNAs With Unknown Targets. *Bioinformatics* 24: 158-164

109. Jady BE & Kiss T (2001) A Small Nucleolar Guide RNA Functions Both in 2 '-O-Ribose Methylation and Pseudouridylation of the U5 Spliceosomal RNA. *EMBO J.* 20: 541-551

110. Matera AG, Terns RM, & Terns MP (2007) Non-Coding RNAs: Lessons From the Small Nuclear and Small Nucleolar RNAs. *Nature Reviews Molecular Cell Biology* 8: 209-220

111. Kiss T (2004) Biogenesis of Small Nuclear RNPs. *Journal of Cell Science* 117: 5949-+

112. Guo P, Haque F, Hallahan B, Reif R, & Li H (2012) Uniqueness, Advantages, Challenges, Solutions, and Perspectives in Therapeutics Applying RNA Nanotechnology. *Nucleic Acid Ther.* 22: 226-245

113. Abdelmawla S, Guo S, Zhang L, Pulukuri S, Patankar P, Conley P, Trebley J, Guo P, & Li QX (2011) Pharmacological Characterization of Chemically Synthesized Monomeric PRNA Nanoparticles for Systemic Delivery. *Molecular Therapy* 19: 1312-1322

114. Shu Y, Cinier M, Shu D, & Guo P (2011) Assembly of Multifunctional Phi29 PRNA Nanoparticles for Specific Delivery of SiRNA and Other Therapeutics to Targeted Cells. *Methods* 54: 204-214

115. Cerchia L, Giangrande PH, McNamara JO, & de F, V (2009) Cell-Specific Aptamers for Targeted Therapies. *Methods Mol. Biol.* 535: 59-78

116. Guo P (2005) RNA Nanotechnology: Engineering, Assembly and Applications in Detection, Gene Delivery and Therapy. *Journal of Nanoscience and Nanotechnology* 5(12): 1964-1982

117. Nakashima Y, Abe H, Abe N, Aikawa K, & Ito Y (2011) Branched RNA Nanostructures for RNA Interference. *Chem. Commun. (Camb.)* 47: 8367-8369

118. Chang CI, Lee TY, Kim S, Sun X, Hong SW, Yoo JW, Dua P, Kang HS, Kim S, Li CJ, & Lee DK (2012) Enhanced Intracellular Delivery and Multi-Target Gene Silencing Triggered by Tripodal RNA Structures. *J. Gene Med.* 14: 138-146

119. Chang CI, Lee TY, Yoo JW, Shin D, Kim M, Kim S, & Lee DK (2012) Branched, Tripartite-Interfering RNAs Silence Multiple Target Genes With Long Guide Strands. *Nucleic Acid Ther.* 22: 30-39

120. Sugimoto N, Nakano S, Katoh M, Matsumura A, Nakamuta H, Ohmichi T, Yoneyama M, & Sasaki M (1995) Thermodynamic Parameters to Predict Stability of RNA/DNA Hybrid Duplexes. *Biochemistry* 34: 11211-11216

121. Searle MS & Williams DH (1993) On the Stability of Nucleic Acid Structures in Solution: Enthalpy-Entropy Compensations, Internal Rotations and Reversibility. *Nucleic Acids Res.* 21: 2051-2056

122. Zhang H, Endrizzi JA, Shu Y, Haque F, Sauter C, Shlyakhtenko LS, Lyubchenko Y, Guo P, & Chi YI (2013) Crystal Structure of 3WJ Core Revealing Divalent Ion-Promoted Thermostability and Assembly of the Phi29 Hexameric Motor PRNA. *RNA* 19: 1226-1237

123. Haque F, Shu D, Shu Y, Shlyakhtenko L, Rychahou P, Evers M, & Guo P (2012) Ultrastable Synergistic Tetravalent RNA Nanoparticles for Targeting to Cancers. *Nano Today* 7: 245-257

124. Khisamutdinov EF, Jasinski DL, & Guo P (2014) RNA As a Boiling-Resistant Anionic Polymer Material to Build Robust Structures With Defined Shape and Stoichiometry. *ACS Nano.* 8: 4771-4781

125. Khisamutdinov E, Li H, Jasinski D, Chen J, Fu J, & Guo P (2014) Enhancing Immunomodulation on Innate Immunity by Shape Transition Among RNA Triangle, Square, and Pentagon Nanovehicles. *Nucleic Acids Res.* 42: 9996-10004

126. Jasinski D, Khisamutdinov EF, Lyubchenko YL, & Guo P (2014) Physicochemically Tunable Poly-Functionalized RNA Square Architecture With Fluorogenic and Ribozymatic Properties. *ACS Nano* 8: 7620-7629

127. Khisamutdinov EF, Bui MN, Jasinski D, Zhao Z, Cui Z, & Guo P (2015) Simple Method for Constructing RNA Triangle, Square, Pentagon by Tuning Interior RNA 3WJ Angle From 60 Degrees to 90 Degrees or 108 Degrees. *Methods Mol Biol* 1316: 181-193

128. Chworos A, Severcan I, Koyfman AY, Weinkam P, Oroudjev E, Hansma HG, & Jaeger L (2004) Building Programmable Jigsaw Puzzles With RNA. *Science* 306: 2068-2072

129. Grabow WW, Zakrevsky P, Afonin KA, Chworos A, Shapiro BA, & Jaeger L (2011) Self-Assembling RNA Nanorings Based on RNAI/II Inverse Kissing Complexes. *Nano Lett.* 11: 878-887

130. Severcan I, Geary C, VE, CA, & Jaeger L (2009) Square-Shaped RNA Particles From Different RNA Folds. *Nano Lett.* 9: 1270-1277

131. Severcan I, Geary C, Chworos A, Voss N, Jacovetty E, & Jaeger L (2010) A Polyhedron Made of TRNAs. *Nat. Chem.* 2: 772-779

132. Dibrov SM, McLean J, Parsons J, & Hermann T (2011) Self-Assembling RNA Square. *Proc. Natl. Acad. Sci. U. S. A* 108: 6405-6408

133. Ohno H, Kobayashi T, Kabata R, Endo K, Iwasa T, Yoshimura SH, Takeyasu K, Inoue T, & Saito H (2011) Synthetic RNA-Protein Complex Shaped Like an Equilateral Triangle. *Nat. Nanotechnol.* 6: 116-120

134. Shopsowitz KE, Roh YH, Deng ZJ, Morton SW, & Hammond PT (2014) RNAi-Microsponges Form Through Self-Assembly of the Organic and Inorganic Products of Transcription. *Small* 10: 1623-1633

135. Shu Y, Shu D, Diao Z, Shen G, & Guo P (2009) Fabrication of Polyvalent Therapeutic RNA Nanoparticles for Specific Delivery of SiRNA, Ribozyme and Drugs to Targeted Cells for Cancer Therapy. *IEEE/NIH Life Science Systems and Applications Workshop* 9-12

136. Li L, Liu J, Diao Z, Guo P, & Shen G (2009) Evaluation of Specific Delivery of Chimeric Phi29 PRNA/SiRNA Nanoparticles to Multiple Tumor Cells. *Molecular BioSystems* 5: 1361-1368

137. Lee TJ, Haque F, Shu D, Yoo JY, Li H, Yokel RA, Horbinski C, Kim TH, Kim S-H, Nakano I, Kaur B, Croce CM, & Guo P (2015) RNA Nanoparticles As a Vector for Targeted SiRNA Delivery into Glioblastoma Mouse Model. *Oncotarget* 6: 14766-14776

138. Cui D, Zhang C, Liu B, Shu Y, Du T, Shu D, Wang K, Dai F, Liu Y, Li C, Pan F, Yang Y, Ni J, Li H, Brand-Saberi B, & Guo P (2015) Regression of Gastric Cancer by Systemic Injection of RNA Nanoparticles Carrying Both Ligand and SiRNA. *Scientific reports* 5: 10726

139. Rychahou P, Haque F, Shu Y, Zaytseva Y, Weiss HL, Lee EY, Mustain W, Valentino J, Guo P, & Evers BM (2015) Delivery of RNA Nanoparticles into Colorectal Cancer Metastases Following Systemic Administration. *ACS Nano* 9: 1108-1116

140. Novina CD, Murray MF, Dykxhoorn DM, Beresford PJ, Riess J, Lee SK, Collman RG, Lieberman J, Shankar P, & Sharp PA (2002) SiRNA-Directed Inhibition of HIV-1 Infection. *Nat Med* 8: 681-686

141. Peer D, Zhu P, Carman CV, Lieberman J, & Shimaoka M (2007) Selective Gene Silencing in Activated Leukocytes by Targeting SiRNAs to the Integrin Lymphocyte Function-Associated Antigen-1. *Proc. Natl. Acad. Sci. U. S. A.* 104: 4095-4100

142. Huang L, Jin J, Deighan P, Kiner E, McReynolds L, & Lieberman J (2013) Efficient and Specific Gene Knockdown by Small Interfering RNAs Produced in Bacteria. *Nat Biotechnol.* 31: 350-356

143. Breslauer KJ, Frank R, Blocker H, & Marky LA (1986) Predicting Dna Duplex Stability From the Base Sequence. *Proceedings of the National Academy of Sciences of the United States of America* 83: 3746-3750

144. Santalucia J, Allawi HT, & Seneviratne A (1996) Improved Nearest-Neighbor Parameters for Predicting DNA Duplex Stability. *Biochemistry* 35: 3555-3562

145. Tinoco I, Uhlenbec O, & Levine MD (1971) Estimation of Secondary Structure in Ribonucleic Acids. *Nature* 230: 362-&

146. Freier SM, Kierzek R, Jaeger JA, Sugimoto N, Caruthers MH, Neilson T, & Turner DH (1986) Improved Free-Energy Parameters for Predictions of RNA Duplex Stability. *Proc. Natl. Acad. Sci. U. S. A* 83: 9373-9377

147. Xia TB, Santalucia J, Burkard ME, Kierzek R, Schroeder SJ, Jiao XQ, Cox C, & Turner DH (1998) Thermodynamic Parameters for an Expanded Nearest-Neighbor Model for Formation of RNA Duplexes With Watson-Crick Base Pairs. *Biochemistry* 37: 14719-14735

148. Mathews DH & Turner DH (2002) Experimentally Derived Nearest-Neighbor Parameters for the Stability of RNA Three- and Four-Way Multibranch Loops. *Biochemistry* 41: 869-880

149. Lesnik EA & Freier SM (1995) Relative Thermodynamic Stability of Dna, Rna, and Dna-Rna Hybrid Duplexes - Relationship With Base Composition and Structure. *Biochemistry* 34: 10807-10815

150. Gyi JI, Conn GL, Lane AN, & Brown T (1996) Comparison of the Thermodynamic Stabilities and Solution Conformations of DNA Center Dot RNA Hybrids Containing Purine-Rich and Pyrimidine-Rich Strands With DNA and RNA Duplexes. *Biochemistry* 35: 12538-12548

151. Conte MR, Conn GL, Brown T, & Lane AN (1997) Conformational Properties and Thermodynamics of the RNA Duplex R(CGCAAAUUUGCG)(2): Comparison With the DNA Analogue D(CGCAAATTTGCG)(2). *Nucleic Acids Res.* 25: 2627-2634

152. Gyi JI, Gao DQ, Conn GL, Trent JO, Brown T, & Lane AN (2003) The Solution Structure of a DNA Center Dot RNA Duplex Containing 5-Propynyl U and C; Comparison With 5-Me Modifications. *Nucleic Acids Res.* 31: 2683-2693

153. Rauzan B, McMichael E, Cave R, Sevcik LR, Ostrosky K, Whitman E, Stegemann R, Sinclair AL, Serra MJ, & Deckert AA (2013) Kinetics and Thermodynamics of DNA, RNA, and Hybrid Duplex Formation. *Biochemistry* 52: 765-772

154. Zuker M & Stiegler P (1981) Optimal Computer Folding of Large RNA Sequences Using Thermodynamics and Auxiliary Information. *Nucleic Acids Res.* 9: 133-148

155. Markham NR & Zuker M (2008) UNAFold: Software for Nucleic Acid Folding and Hybridization. *Methods Mol. Biol.* 453: 3-31

156. Hofacker IL, Fontana W, Stadler PF, Bonhoeffer LS, Tacker M, & Schuster P (1994) Fast Folding and Comparison of Rna Secondary Structures. *Monatshefte fur Chemie* 125: 167-188

157. Leontis NB & Westhof E (2003) Analysis of RNA Motifs. *Curr. Opin. Struct. Biol.* 13: 300-308

158. Westhof E, Masquida B, & Jaeger L (1996) RNA Tectonics: Towards RNA Design. *Folding & Design* 1: R78-R88

159. Lescoute A & Westhof E (2006) Topology of Three-Way Junctions in Folded RNAs. *RNA.* 12: 83-93

160. Jossinet F, Ludwig TE, & Westhof E (2007) RNA Structure: Bioinformatic Analysis. *Current Opinion in Microbiology* 10: 279-285

161. Leontis NB & Westhof E (2001) Geometric Nomenclature and Classification of RNA Base Pairs. *RNA.* 7: 499-512

162. Leontis NB & Westhof E (2002) The Annotation of RNA Motifs. *Comp Funct. Genomics* 3: 518-524

163. Xin Y, Laing C, Leontis NB, & Schlick T (2008) Annotation of Tertiary Interactions in RNA Structures Reveals Variations and Correlations. *RNA* 14: 2465-2477

164. Lilley DM (1999) Structure, Folding and Catalysis of the Small Nucleolytic Ribozymes. *Curr. Opin. Struct. Biol* 9: 330-338

165. McKinney SA, Declais AC, Lilley DMJ, & Ha T (2003) Structural Dynamics of Individual Holliday Junctions. *Nature Structural Biology* 10: 93-97

166. Schroeder KT, McPhee SA, Ouellet J, & Lilley DM (2010) A Structural Database for K-Turn Motifs in RNA. *RNA.* 16: 1463-1468

167. Ouellet J, Melcher S, Iqbal A, Ding Y, & Lilley DM (2010) Structure of the Three-Way Helical Junction of the Hepatitis C Virus IRES Element. *RNA.* 16: 1597-1609

168. Bindewald E, Grunewald C, Boyle B, O'Connor M, & Shapiro BA (2008) Computational Strategies for the Automated Design of RNA Nanoscale Structures From Building Blocks Using NanoTiler. *Journal of Molecular Graphics & Modelling* 27: 299-308

169. Bindewald E, Hayes R, Yingling YG, Kasprzak W, & Shapiro BA (2008) RNAJunction: a Database of RNA Junctions and Kissing Loops for Three-Dimensional Structural Analysis and Nanodesign. *Nucleic Acids Res.* 36: D392-D397

170. Petrov AI, Zirbel CL, & Leontis NB (2013) Automated Classification of RNA 3D Motifs and the RNA 3D Motif Atlas. *Rna-A Publication of the Rna Society* 19: 1327-1340

171. Berman HM, Olson WK, Beveridge DL, Westbrook J, Gelbin A, Demeny T, Hsieh SH, Srinivasan AR, & Schneider B (1992) The Nucleic Acid Database. A Comprehensive Relational Database of Three-Dimensional Structures of Nucleic Acids. *Biophys. J.* 63: 751-759

172. Ye X, Hemida M, Zhang HM, Hanson P, Ye Q, & Yang D (2012) Current Advances in Phi29 PRNA Biology and Its Application in Drug Delivery. *Wiley. Interdiscip. Rev. RNA.* 3(4): 469-481

173. Afonin KA, Danilov EO, Novikova IV, & Leontis NB (2008) TokenRNA: A New Type of Sequence-Specific, Label-Free Fluorescent Biosensor for Folded RNA Molecules. *Chembiochem* 9: 1902-1905

174. Jaeger L & Chworos A (2006) The Architectonics of Programmable RNA and DNA Nanostructures. *Curr Opin Struct Biol.* 16: 531-543

175. Bindewald E, Afonin K, Jaeger L, & Shapiro BA (2011) Multistrand RNA Secondary Structure Prediction and Nanostructure Design Including Pseudoknots. *ACS Nano.* 5: 9542-9551

176. Shu D, Huang L, Hoeprich S, & Guo P (2003) Construction of Phi29 DNA-Packaging RNA (PRNA) Monomers, Dimers and Trimers With Variable Sizes and Shapes As Potential Parts for Nano-Devices. *J. Nanosci. Nanotechnol.* 3: 295-302

177. Shu Y, Haque F, Shu D, Li W, Zhu Z, Kotb M, Lyubchenko Y, & Guo P (2013) Fabrication of 14 Different RNA Nanoparticles for Specific Tumor Targeting Without Accumulation in Normal Organs. *RNA* 19: 766-777

178. Afonin KA, Grabow WW, Walker FM, Bindewald E, Dobrovolskaia MA, Shapiro BA, & Jaeger L (2011) Design and Self-Assembly of SiRNA-Functionalized RNA Nanoparticles for Use in Automated Nanomedicine. *Nat. Protoc.* 6: 2022-2034

179. Severcan I, Geary C, Jaeger L, Bindewald, E., Kasprzak, W., and Shapiro, B. A. (2009) Computational and Experimental RNA Nanoparticle Design. In Alterovitz, G. and Ramoni, M., editors. *Automation in Genomics and Proteomics: An Engineering Case-Based Approach*, Wiley, Boston, MA,

180. Tabernero J, Shapiro GI, Lorusso PM, Cervantes A, Schwartz GK, Weiss GJ, Paz-Ares L, Cho DC, Infante JR, Alsina M, Gounder MM, Falzone R, Harrop J, Seila White AC, Toudjarska I, Bumcrot D, Meyers RE, Hinkle G, Svrzikapa N, Hutabarat RM, Clausen VA, Cehelsky J, Nochur SV, Gamba-Vitalo C, Vaishnaw AK, Sah DW, Gollob JA, &

Burris HA, III (2013) First-in-Man Trial of an RNA Interference Therapeutic Targeting VEGF and KSP in Cancer Patients With Liver Involvement. *Cancer Discov.* 3: 406-417

181. Yingling YG & Shapiro BA (2007) Computational Design of an RNA Hexagonal Nanoring and an RNA Nanotube. *Nano Letters* 7: 2328-2334

182. Delebecque CJ, Silver PA, & Lindner AB (2012) Designing and Using RNA Scaffolds to Assemble Proteins in Vivo. *Nat. Protoc.* 7: 1797-1807

183. Maeda H, Nakamura H, & Fang J (2013) The EPR Effect for Macromolecular Drug Delivery to Solid Tumors: Improvement of Tumor Uptake, Lowering of Systemic Toxicity, and Distinct Tumor Imaging in Vivo. *Adv. Drug Deliv. Rev.* 65: 71-79

184. Privalov PL & Filiminov VV (1978) Thermodynamic Analysis of Transfer RNA Unfolding. *J. Mol. Biol.* 122: 447-464

185. Jaeger JA, SantaLucia JJ, & Tinoco IJ (1993) Determination of RNA Structure and Thermodynamics. *Annu. Rev. Biochem.* 62: 255-285

186. Kawasaki AM, Casper MD, Freier SM, Lesnik EA, Zounes MC, Cummins LL, Gonzalez C, & Cook PD (1993) Uniformly Modified 2'-Deoxy-2'-Fluoro Phosphorothioate Oligonucleotides As Nuclease-Resistant Antisense Compounds With High Affinity and Specificity for RNA Targets. *J. Med. Chem.* 36: 831-841

187. Diamond JM, Turner DH, & Mathews DH (2001) Thermodynamics of Three-Way Multibranch Loops in RNA. *Biochemistry* 40: 6971-6981

188. Brunel C, Marquet R, Romby P, & Ehresmann C (2002) RNA Loop-Loop Interactions As Dynamic Functional Motifs. *Biochimie* 84: 925-944

189. Liu J, Guo S, Cinier M, Shlyakhtenko LS, Shu Y, Chen C, Shen G, & Guo P (2011) Fabrication of Stable and RNase-Resistant RNA Nanoparticles Active in Gearing the Nanomotors for Viral DNA Packaging. *ACS Nano* 5: 237-246

190. Walter AE, Turner DH, Kim J, Lyttle MH, Muller P, Mathews DH, & Zuker M (1994) Coaxial Stacking of Helixes Enhances Binding of Oligoribonucleotides and Improves Predictions of RNA Folding. *Proc. Natl. Acad. Sci. U. S. A* 91: 9218-9222

191. Marky LA & Breslauer KJ (1987) Calculating Thermodynamic Data for Transitions of Any Molecularity From Equilibrium Melting Curves. *Biopolymers* 26: 1601-1620

192. Zhang CL, Lee C-S, & Guo P (1994) The Proximate 5' and 3' Ends of the 120-Base Viral RNA (PRNA) Are Crucial for the Packaging of Bacteriophage Φ29 DNA. *Virology* 201: 77-85

193. Reid RJD, Bodley JW, & Anderson D (1994) Characterization of the Prohead-PRNA Interaction of Bacteriophage Phi29. *J Biol Chem* 269: 5157-5162

194. Guo P, Schwartz C, Haak J, & Zhao Z (2013) Discovery of a New Motion Mechanism of Biomotors Similar to the Earth Revolving Around the Sun Without Rotation. *Virology* 446: 133-143

195. de PD, Bentley MV, & Mahato RI (2007) Hydrophobization and Bioconjugation for Enhanced SiRNA Delivery and Targeting. *RNA.* 13: 431-456

196. Novikova IV, Hassan BH, Mirzoyan MG, & Leontis NB (2010) Engineering Cooperative Tecto-RNA Complexes Having Programmable Stoichiometries. *Nucleic Acids Res.* 39(7): 2903-2917

197. Berdalet E, Roldan C, Olivar MP, & Lysnes K (2005) Quantifying RNA and DNA in Planktonic Organisms With SYBR Green II and Nucleases. Part A. Optimisation of the Assay. *Scientia Marina* 69: 1-16

198. Reif R, Haque F, & Guo P (2013) Fluorogenic RNA Nanoparticles for Monitoring RNA Folding and Degradation in Real Time in Living Cells. *Nucleic Acid Ther.* 22(6): 428-437

199. Pallan PS, Greene EM, Jicman PA, Pandey RK, Manoharan M, Rozners E, & Egli M (2011) Unexpected Origins of the Enhanced Pairing Affinity of 2 '-Fluoro-Modified RNA 7. *Nucleic Acids Res.* 39: 3482-3495

200. Chadalavada DM & Bevilacqua PC (2009) Analyzing RNA and DNA Folding Using Temperature Gradient Gel Electrophoresis (TGGE) With Application to in Vitro Selections. *Methods Enzymol.* 468: 389-408

201. Hecker R, Wang ZM, Steger G, & Riesner D (1988) Analysis of RNA Structures by Temperature-Gradient Gel Electrophoresis: Viroid Replication and Processing. *Gene* 72: 59-74

202. Petersheim M & Turner DH (1983) Base-Stacking and Base-Pairing Contributions to Helix Stability: Thermodynamics of Double-Helix Formation With CCGG, CCGGp, CCGGAp, ACCGGp, CCGGUp, and ACCGGUp. *Biochemistry* 22: 256-263

203. Watts JK, Martin-Pintado N, Gomez-Pinto I, Schwartzentruber J, Portella G, Orozco M, Gonzalez C, & Damha MJ (2010) Differential Stability of 2 ' F-ANA.RNA and ANA.RNA Hybrid Duplexes: Roles of Structure, Pseudohydrogen Bonding, Hydration, Ion Uptake and Flexibility. *Nucleic Acids Res.* 38: 2498-2511

204. Baugh C, Grate D, & Wilson C (2000) 2.8 A Crystal Structure of the Malachite Green Aptamer. *J. Mol. Biol.* 301: 117-128

205. Babendure JR, Adams SR, & Tsien RY (2003) Aptamers Switch on Fluorescence of Triphenylmethane Dyes. *J. Am. Chem. Soc.* 125: 14716-14717

206. Lee T, Yagati AK, Pi F, Sharma A, Choi J-W, & Guo P (2015) Construction of RNA-Quantum Dot Chimera for Nanoscale Resistive Biomemory Application. *ACS Nano* 9: 6675-6682

207. Qiu M, Khisamutdinov E, Zhao Z, Pan C, Choi J, Leontis N, & Guo P (2013) RNA Nanotechnology for Computer Design and *in Vivo* Computation. *Phil Trans R Soc A* 371(2000): 20120310

208. Shu D, Khisamutdinov E, Zhang L, & Guo P (2013) Programmable Folding of Fusion RNA Complex Driven by the 3WJ Motif of Phi29 Motor PRNA. *Nucleic Acids Res.* 42: e10

209. Benenson Y (2009) RNA-Based Computation in Live Cells. *Curr. Opin. Biotechnol.* 20: 471-478

210. Rinaudo K, Bleris L, Maddamsetti R, Subramanian S, Weiss R, & Benenson Y (2007) A Universal RNAi-Based Logic Evaluator That Operates in Mammalian Cells. *Nature Biotechnology* 25: 795-801

211. Xie Z, Liu SJ, Bleris L, & Benenson Y (2010) Logic Integration of MRNA Signals by an RNAi-Based Molecular Computer. *Nucleic Acids Res.* 38: 2692-2701

212. Xie Z, Wroblewska L, Prochazka L, Weiss R, & Benenson Y (2011) Multi-Input RNAi-Based Logic Circuit for Identification of Specific Cancer Cells. *Science* 333: 1307-1311

213. Breaker RR (2008) Complex Riboswitches. *Science* 319: 1795-1797

214. Win MN & Smolke CD (2008) Higher-Order Cellular Information Processing With Synthetic RNA Devices. *Science* 322: 456-460

215. Chen Z, Penet MF, Nimmagadda S, Li C, Banerjee SR, Winnard PT, Jr., Artemov D, Glunde K, Pomper MG, & Bhujwalla ZM (2012) PSMA-Targeted Theranostic Nanoplex for Prostate Cancer Therapy. *ACS Nano* 6: 7752-7762

216. Calzada V, Zhang X, Fernandez M, az-Miqueli A, Iznaga-Escobar N, Deutscher SL, Balter H, Quinn TP, & Cabral P (2012) A Potencial Theranostic Agent for EGF-R Expression Tumors: (177)Lu-DOTA-Nimotuzumab. *Curr. Radiopharm.* 5: 318-324

217. Paige JS, Nguyen-Duc T, Song W, & Jaffrey SR (2012) Fluorescence Imaging of Cellular Metabolites With RNA. *Science* 335: 1194

218. Kellenberger CA, Wilson SC, Sales-Lee J, & Hammond MC (2013) RNA-Based Fluorescent Biosensors for Live Cell Imaging of Second Messengers Cyclic Di-GMP and Cyclic AMP-GMP. *J. Am. Chem. Soc.* 135: 4906-4909

219. Noy A (2011) Bionanoelectronics. *Adv. Mater.* 23: 807-820

220. Pieken WA, Olsen DB, Benseler F, Aurup H, & Eckstein F (1991) Kinetic Characterization of Ribonuclease-Resistant 2'-Modified Hammerhead Ribozymes. *Science* 253: 314-317

221. Czauderna F, Fechtner M, Dames S, Aygun H, Klippel A, Pronk GJ, Giese K, & Kaufmann J (2003) Structural Variations and Stabilising Modifications of Synthetic SiRNAs in Mammalian Cells. *Nucleic Acids Res.* 31: 2705-2716

222. Kaur H, Arora A, Wengel J, & Maiti S (2006) Thermodynamic, Counterion, and Hydration Effects for the Incorporation of Locked Nucleic Acid Nucleotides into DNA Duplexes. *Biochemistry* 45: 7347-7355

223. Binzel DW, Khisamutdinov EF, & Guo P (2014) Entropy-Driven One-Step Formation of Phi29 PRNA 3WJ From Three RNA Fragments. *Biochemistry* 53: 2221-2231

224. Seeman NC (1998) DNA Nanotechnology: Novel DNA Constructions. *Annu. Rev. Biophys. Biomol. Struct.* 27:225-48.: 225-248

225. Seeman NC (2010) Nanomaterials Based on DNA. *Annu. Rev. Biochem.* 79: 65-87

226. Seeman NC (2001) DNA Nicks and Nodes and Nanotechnology. *Nano Letters* 1: 22-26

227. Pinheiro AV, Han DR, Shih WM, & Yan H (2011) Challenges and Opportunities for Structural DNA Nanotechnology. *Nature Nanotechnology* 6: 763-772

228. Bellini M, Mazzucchelli S, Galbiati E, Sommaruga S, Fiandra L, Truffi M, Rizzuto MA, Colombo M, Tortora P, Corsi F, & Prosperi D (2014) Protein Nanocages for Self-Triggered Nuclear Delivery of DNA-Targeted Chemotherapeutics in Cancer Cells. *Journal of Controlled Release* 196: 184-196

229. Shu Y, Pi F, Sharma A, Rajabi M, Haque F, Shu D, Leggas M, Evers BM, & Guo P (2014) Stable RNA Nanoparticles As Potential New Generation Drugs for Cancer Therapy. *Adv. Drug Deliv. Rev.* 66C: 74-89

230. Horoszewicz JS, Leong SS, Kawinski E, Karr JP, Rosenthal H, Chu TM, Mirand EA, & Murphy GP (1983) Lncap Model of Human Prostatic-Carcinoma. *Cancer Research* 43: 1809-1818

231. Pettaway CA, Pathak S, Greene G, Ramirez E, Wilson MR, Killion JJ, & Fidler IJ (1996) Selection of Highly Metastatic Variants of Different Human Prostatic Carcinomas Using Orthotopic Implantation in Nude Mice. *Clin. Cancer Res* 2: 1627-1636

232. Israeli RS, Powell CT, Corr JG, Fair WR, & Heston WDW (1994) Expression of the Prostate-Specific Membrane Antigen. *Cancer Research* 54: 1807-1811

233. Friedrich M, Raum T, Lutterbuese R, Voelkel M, Deegen P, Rau D, Kischel R, Hoffmann P, Brandl C, Schuhmacher J, Mueller P, Finnern R, Fuergut M, Zopf D, Slootstra JW, Baeuerle PA, Rattel B, & Kufer P (2012) Regression of Human Prostate

Cancer Xenografts in Mice by AMG 212/BAY2010112, a Novel PSMA/CD3-Bispecific BiTE Antibody Cross-Reactive With Non-Human Primate Antigens. *Molecular Cancer Therapeutics* 11: 2664-2673

234. Wu X, Ding B, Gao J, Wang H, Fan W, Wang X, Zhang W, Wang X, Ye L, Zhang M, Ding X, Liu J, Zhu Q, & Gao S (2011) Second-Generation Aptamer-Conjugated PSMA-Targeted Delivery System for Prostate Cancer Therapy. *Int. J. Nanomedicine* 6: 1747-1756

235. Dassie JP, Liu XY, Thomas GS, Whitaker RM, Thiel KW, Stockdale KR, Meyerholz DK, McCaffrey AP, McNamara JO, & Giangrande PH (2009) Systemic Administration of Optimized Aptamer-SiRNA Chimeras Promotes Regression of PSMA-Expressing Tumors. *Nat Biotechnol.* 27: 839-849

236. Conway RE, Petrovic N, Li Z, Heston W, Wu D, & Shapiro LH (2006) Prostate-Specific Membrane Antigen Regulates Angiogenesis by Modulating Integrin Signal Transduction. *Mol Cell Biol* 26: 5310-5324

237. Yao V & Bacich DJ (2006) Prostate Specific Membrane Antigen (PSMA) Expression Gives Prostate Cancer Cells a Growth Advantage in a Physiologically Relevant Folate Environment in Vitro. *Prostate* 66: 867-875

238. Silver DA, Pellicer I, Fair WR, Heston WD, & Cordon-Cardo C (1997) Prostate-Specific Membrane Antigen Expression in Normal and Malignant Human Tissues. *Clin. Cancer Res.* 3: 81-85

239. Jansson MD & Lund AH (2012) MicroRNA and Cancer. *Molecular Oncology* 6: 590-610

240. Sassen S, Miska EA, & Caldas C (2008) MicroRNA - Implications for Cancer. *Virchows Archiv* 452: 1-10

241. Lee YS & Dutta A (2009) MicroRNAs in Cancer. *Annual Review of Pathology-Mechanisms of Disease* 4: 199-227

242. Gong AY, Eischeid AN, Xiao J, Zhao J, Chen DQ, Wang ZY, Young CYF, & Chen XM (2012) MiR-17-5p Targets the P300/CBP-Associated Factor and Modulates Androgen Receptor Transcriptional Activity in Cultured Prostate Cancer Cells. *BMC Cancer* 12:

243. Pang YX, Young CYF, & Yuan HQ (2010) MicroRNAs and Prostate Cancer. *ACTA BIOCHIMICA ET BIOPHYSICA SINICA* 42: 363-369

244. Li T, Li D, Sha J, Sun P, & Huang Y (2009) MicroRNA-21 Directly Targets MARCKS and Promotes Apoptosis Resistance and Invasion in Prostate Cancer Cells. *Biochem. Biophys. Res Commun.* 383: 280-285

245. Meng FY, Henson R, Wehbe-Janek H, Ghoshal K, Jacob ST, & Patel T (2007) MicroRNA-21 Regulates Expression of the PTEN Tumor Suppressor Gene in Human Hepatocellular Cancer. *Gastroenterology* 133: 647-658

246. Scherr M, Elder A, Battmer K, Barzan D, Bomken S, Ricke-Hoch M, Schroder A, Venturini L, Blair HJ, Vormoor J, Ottmann O, Ganser A, Pich A, Hilfiker-Kleiner D, Heidenreich O, & Eder M (2014) Differential Expression of MiR-17 Similar to 92 Identifies BCL2 As a Therapeutic Target in BCR-ABL-Positive B-Lineage Acute Lymphoblastic Leukemia. *Leukemia* 28: 554-565

247. Gabriely G, Wurdinger T, Kesari S, Esau CC, Burchard J, Linsley PS, & Krichevsky AM (2008) MicroRNA 21 Promotes Glioma Invasion by Targeting Matrix Metalloproteinase Regulators. *Mol Cell Biol* 28: 5369-5380

248. Wickramasinghe NS, Manavalan TT, Dougherty SM, Riggs KA, Li Y, & Klinge CM (2009) Estradiol Downregulates MiR-21 Expression and Increases MiR-21 Target Gene Expression in MCF-7 Breast Cancer Cells. *Nucleic Acids Res.* 37: 2584-2595

249. Schwartz C & Guo P (2013) Ultrastable PRNA Hexameric Ring Gearing Hexameric Phi29 DNA-Packaging Motor by Revolving Without Rotating and Coiling. *Current Opinion in Biotechnology* 24(4): 581-590

250. Trottier M, Garver K, Zhang C, & Guo P (1997) DNA-Packaging PRNA As Target for Complete Inhibition of Viral Assembly in Vitro and in Vivo. *Nucleic Acids Symposium Series* 36: 187-189

251. Reid RJD, Bodley JW, & Anderson D (1994) Identification of Bacteriophage Phi29 Prohead RNA (PRNA) Domains Necessary for *in Vitro* DNA-Gp3 Packaging. *J. Biol. Chem.* 269: 9084-9089

252. Guo P & Trottier M (1994) Biological and Biochemical Properties of the Small Viral RNA (PRNA) Essential for the Packaging of the Double-Stranded DNA of Phage Φ29. *Seminars in Virology* 5: 27-37

253. Lupold SE, Hicke BJ, Lin Y, & Coffey DS (2002) Identification and Characterization of Nuclease-Stabilized RNA Molecules That Bind Human Prostate Cancer Cells Via the Prostate-Specific Membrane Antigen. *Cancer Res.* 62: 4029-4033

254. Rockey WM, Hernandez FJ, Huang SY, Cao S, Howell CA, Thomas GS, Liu XY, Lapteva N, Spencer DM, McNamara JO, Zou X, Chen SJ, & Giangrande PH (2011) Rational Truncation of an RNA Aptamer to Prostate-Specific Membrane Antigen Using Computational Structural Modeling. *Nucleic Acid Ther.* 21: 299-314

255. Gregor PD, Wolchok JD, Turaga V, Latouche JB, Sadelain M, Bacich D, Heston WDW, Houghton AN, & Scherl HI (2005) Induction of Autoantibodies to Syngeneic Prostate-Specific Membrane Antigen by Xenogeneic Vaccination. *International Journal of Cancer* 116: 415-421

256. Ghosh A, Wang YN, Klein E, & Heston WDW (2005) Novel Role of Prostate-Specific Membrane Antigen in Suppressing Prostate Cancer Invasiveness. *Cancer Research* 65: 727-731

257. Meller B, Bremmer F, Sahlmann CO, Hijazi S, Bouter C, Trojan L, Meller J, & Thelen P (2015) Alterations in Androgen Deprivation Enhanced Prostate-Specific Membrane Antigen (PSMA) Expression in Prostate Cancer Cells As a Target for Diagnostics and Therapy. *Ejnmmi Research* 5:

258. Ben Jemaa A, Bouraoui Y, Sallami S, Banasr A, Ben Rais N, Ouertani L, Nouira Y, Horchani A, & Oueslati R (2010) Co-Expression and Impact of Prostate Specific Membrane Antigen and Prostate Specific Antigen in Prostatic Pathologies. *Journal of Experimental & Clinical Cancer Research* 29:

259. Sweat SD, Pacelli A, Murphy GP, & Bostwick DG (1998) Prostate-Specific Membrane Antigen Expression Is Greatest in Prostate Adenocarcinoma and Lymph Node Metastases. *Urology* 52: 637-640

260. Wright GL, Grob BM, Haley C, Grossman K, Newhall K, Petrylak D, Troyer J, Konchuba A, Schellhammer PF, & Moriarty R (1996) Upregulation of Prostate-Specific Membrane Antigen After Androgen-Deprivation Therapy. *Urology* 48: 326-334

261. Ribas J, Ni XH, Haffner M, Wentzel EA, Salmasi AH, Chowdhury WH, Kudrolli TA, Yegnasubramanian S, Luo J, Rodriguez R, Mendell JT, & Lupold SE (2009) MiR-21: An Androgen Receptor-Regulated MicroRNA That Promotes Hormone-Dependent and Hormone-Independent Prostate Cancer Growth. *Cancer Research* 69: 7165-7169

262. Schramedei K, Morbt N, Pfeifer G, Lauter J, Rosolowski M, Tomm JM, von Bergen M, Horn F, & Brocke-Heidrich K (2011) MicroRNA-21 Targets Tumor Suppressor Genes ANP32A and SMARCA4. *Oncogene* 30: 2975-2985

263. Yang XL, Du WW, Li HR, Liu FQ, Khorshidi A, Rutnam ZJ, & Yang BB (2013) Both Mature MiR-17-5p and Passenger Strand MiR-17-3p Target TIMP3 and Induce Prostate Tumor Growth and Invasion. *Nucleic Acids Res.* 41: 9688-9704

264. Lee H, Lytton-Jean AK, Chen Y, Love KT, Park AI, Karagiannis ED, Sehgal A, Querbes W, Zurenko CS, Jayaraman M, Peng CG, Charisse K, Borodovsky A, Manoharan M, Donahoe JS, Truelove J, Nahrendorf M, Langer R, & Anderson DG (2012) Molecularly Self-Assembled Nucleic Acid Nanoparticles for Targeted in Vivo SiRNA Delivery. *Nat. Nanotechnol.* 7: 389-393

265. Wheeler LA, Vrbanac V, Trifonova R, Brehm MA, Gilboa-Geffen A, Tanno S, Greiner DL, Luster AD, Tager AM, & Lieberman J (2013) Durable Knockdown and Protection From HIV Transmission in Humanized Mice Treated With Gel-Formulated CD4 Aptamer-SiRNA Chimeras. *Molecular Therapy* 21: 1378-1389

266. Afonin KA, Viard M, Koyfman AY, Martins AN, Kasprzak WK, Panigaj M, Desai R, Santhanam A, Grabow WW, Jaeger L, Heldman E, Reiser J, Chiu W, Freed EO, & Shapiro BA (2014) Multifunctional RNA Nanoparticles. *Nano Lett.* 14: 5662-5671

267. Shu Y, Shu D, Haque F, & Guo P (2013) Fabrication of PRNA Nanoparticles to Deliver Therapeutic RNAs and Bioactive Compounds into Tumor Cells. *Nat Protoc.* 8: 1635-1659

268. Jasinski D, Schwartz C, Haque F, & Guo P (2015) Large Scale Purification of RNA Nanoparticles by Preparative Ultracentrifugation. *Methods in Molecular Biology* 1297: 67-82

Vita

Daniel William Binzel

Educational Institutions

Miami University	2006 – 2010	Bachelors of Engineering	Chemical Engineering
University of Cincinnati	2010 – 2011	PhD Student	Biomedical Engineering
University of Kentucky	2012 - 2016	PhD Candidate	Pharmaceutical Sciences

Professional Publications

(1) P. Guo, Y. Shu, D.W. Binzel, M. Cinier. **"Synthesis, Conjugation, and Labeling of Multifunctional pRNA Nanoparticles for Specific Delivery of siRNA, Drugs, and Other Therapeutics to Target Cells."** *Methods in Molecular Biology.* 928: 197 – 219 (Aug. 2012).

(2) B. Guo, D.W. Binzel. **"MicroRNAs: Biology and Role in RNA Nanotechnology."** *RNA Nanotechnology and Therapeutics*. (July 2013).

(3) D.W. Binzel, E.F. Khisamutdinov, P. Guo. **"Entropy-Driven One-Step Formation of Phi29 pRNA 3WJ from Three RNA Fragments."** *Biochemistry*. 53(14): 2221 – 2231 (Apr. 2014).

(4) D.W. Binzel, Y. Shu, D. Shu, P. Guo. **"Specific Delivery of miRNA for High Efficient Inhibition of Prostate Cancer by RNA nanotechnology."** *Molecular Therapy*. In press, 2016.

(5) F. Haque, D.W. Binzel, D.L. Jasinski, F. Storici, S.J. Chen, P. Guo. **"RNA as an Elastic Thermostable Material for Fabricating RNA Nanoarchitectures."** *WIREs RNA.* In submission.

(6) D.W. Binzel, E.F. Khisamutdinov, J Ortega, G.M. Li, P.Guo. **"Kinetics of Three-Component Collision of the Ultra Stable pRNA Three-way Junction of Phi29 DNA Motor."** *Journal of Biological Chemistry.* In submission.

(7) F. Pi, H. Li, M. Sun, F. Haque, D.W. Binzel, S. Wang, B. Guo, B.M. Evers, P. Guo "RNA Ligand-Displaying Exosomes for Specific Delivery of siRNA with Unusually-high Efficiency in Cancer Inhibition." *Nature Medicine*. In submission.

Scholastic and Professional Honors

Kemira Chemicals Award	2006 – 2007
Miami University Paper Science and Engineering Foundation Scholarship	2007
Engineering Intern, Ohio Professional Engineers and Surveyors Board	2010
Cancer Nanotechnology Training Center Fellowship	2014 – 2015